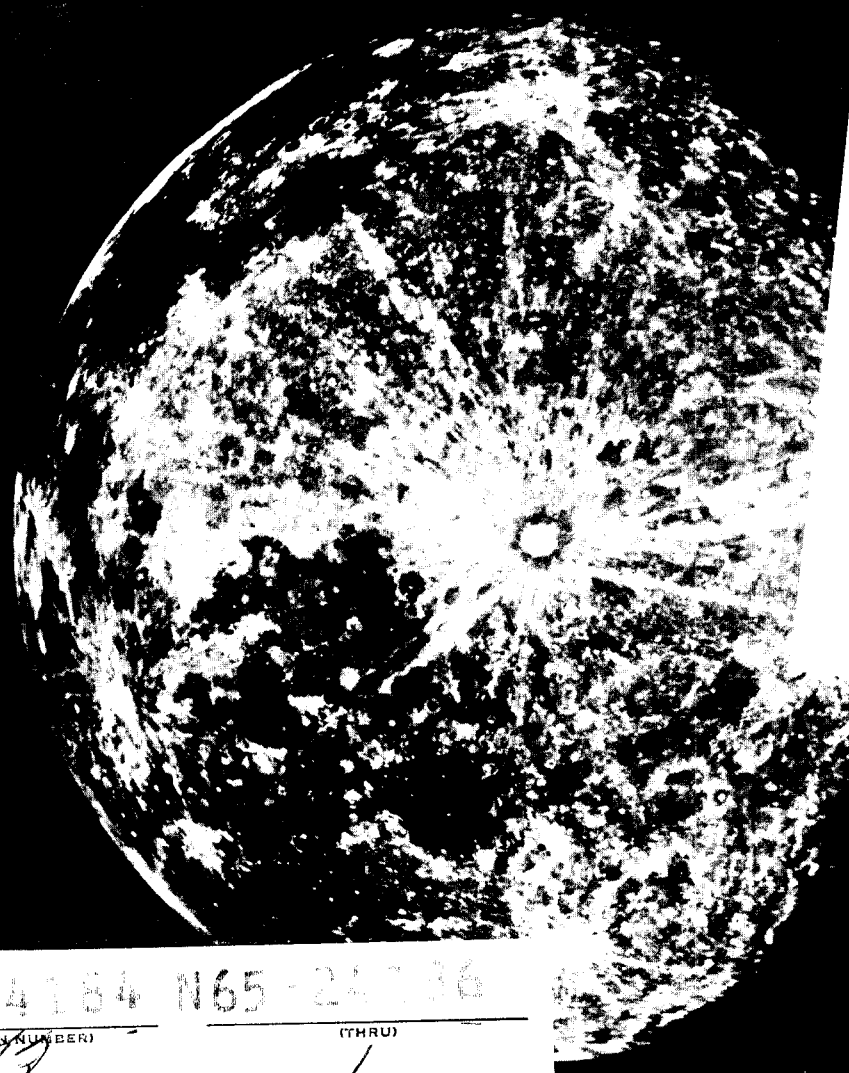
Communications of the LUNAR AND PLANETARY LABORATORY

Volume 2 Numbers 36–39



GPO PRICE $
OTS PRICE(S) $
Hard copy (HC)
Microfiche (MF)

FACILITY FORM 602
N65-24184 N65-24216
(ACCESSION NUMBER)
73
(PAGES)
CR-62820
(NASA CR OR TMX OR AD NUMBER)
(THRU)
1
(CODE)
30
(CATEGORY)

THE UNIVERSITY OF ARIZONA

Communications of the LUNAR AND PLANETARY LABORATORY

Volume 2 Numbers 36–39

THE UNIVERSITY OF ARIZONA

1964

Communications of the Lunar and Planetary Laboratory

These *Communications* contain the shorter publications and reports by the staff of the Lunar and Planetary Laboratory. They may be either original contributions, reprints of articles published in professional journals, preliminary reports, or announcements. Tabular material too bulky or specialized for regular journals is included if future use of such material appears to warrant it. The *Communications* are issued as separate numbers, but they are paged and indexed by volumes.

The *Communications* are mailed to observatories and to laboratories known to be engaged in planetary, interplanetary or geophysical research in exchange for their reports and publications. The University of Arizona Press can supply at cost copies to other libraries and interested persons.

The University of Arizona
Tucson, Arizona

GERARD P. KUIPER, *Director*
Lunar and Planetary Laboratory

Published with the support of the National Aeronautics and Space Administration

Library of Congress Catalog Number 62-63619

TABLE OF CONTENTS

No. 36 Radial Structures Surrounding Lunar Basins, II: Orientale and Other Systems; Conclusions 175
by William K. Hartmann

No. 37 Comparison of the Infrared Spectrum of Mars with the Spectra of Selected Terrestrial Rocks and Minerals 193
by Alan B. Binder and Dale P. Cruikshank

No. 38 On the Distribution of Lunar Crater Diameters 197
by William K. Hartmann

No. 39 Analysis of Lunar Lineaments, I: Tectonic Maps of the Moon 205
by Robert G. Strom

NO. 36. RADIAL STRUCTURES SURROUNDING LUNAR BASINS, II: ORIENTALE AND OTHER SYSTEMS; CONCLUSIONS

by WILLIAM K. HARTMANN

June 20, 1964

N65-24185

ABSTRACT

A new analysis of mare basins begun by Hartmann (1963) is concluded with this paper. The radial systems of the oldest basins are the least developed, while those of the young basins — Mare Imbrium and Mare Orientale — are the most prominent. It is therefore hypothesized that conditions for producing radial lineaments were optimum during the relatively short period when the mare basins were flooded. Many lineaments are spatially associated with this flooding. The basins are probably the sites of great impacts which were accompanied by radiating fractures. Most lineaments are interpreted as the expressions of tectonic adjustments in the stressed crust along these fractures as a result of heating of the subsurface. Most of the adjustment appears to be by vertical motion. There is little evidence for horizontal motion or for gouging of radial valleys by flying fragments. The discussion includes reviews of the nonradial grid patterns and of the small radial systems around some recent craters.

Author

1. Introduction

This paper completes a new and independent study of radial basin systems, founded largely upon rectified photography. The Imbrium system was surveyed in Part I (*LPL Comm.* No. 24, 1963). In Part II the discussion is extended to other basin systems and further suggestions are offered as to their significance. Astronautical directions are used, as before. For each basin, the surroundings are described under subheading (*a*) and interpretations under (*b*).

2. The Orientale System

(a) Morphology

Plates 36.1 through 36.6 show the Orientale System radial structures. With the sunrise terminator near longitude 80° W (good sunset pictures are lacking at the narrow crescent phase), a major family of linear features is seen NW of Wargentin. This aspect is shown in Plate 36.1. Rectified photography at once reveals the convergence of the linear features. Plate 36.6*a*, centered over Orientale, reveals the concentric scarp system and confirms that the convergence is toward the Orientale inner basin. It is clear that the Orientale basin, second only to the Imbrium basin in the magnitude of its concentric ring system (Hartmann and Kuiper, 1962), is also second only to Imbrium in the prominence and extent of its radial system. Plates 36.1 and 36.2, taken with low lighting, demonstrate the great extent of the Orientale radial family toward Wargentin.

Comparison of Plates 36.2 (low lighting) and 36.3 (high lighting) shows, as did 24.14 and 24.18 for the Imbrium system, that there is no prominent ray system radial to Orientale, and that the radial system is structural, not surficial. Plate 36.3 also reveals the small mare at the center of the basin system.

No radial structure is found inside the Eichstadt ring. Outside this ring, running to the SE, are several shallow valleys, some 30 km across. These valleys merge to the S with arcs of the SE limb basin system (Hartmann and Kuiper, 1962, p. 57, Pl. 12.45). In this same region, and out as far as Inghirami, the

mountainous uplands have a pronounced radial and concentric, nearly orthogonal, pattern. Some of the radial structures, such as those running toward the NE rim of Inghirami (best shown in Pls. 36.1 and 36.2) are clearly neither narrow valleys nor mountain ridges, but scarps, probably bounding broad depressions. The whole region gives the impression of a crustal mass fractured along nearly orthogonal lines.

Further out, beyond Inghirami and near Bailly, are curious structures formed by 10–20 km craters with narrow valleys running SE out of them away from Orientale. They can be seen clearly in Plate 36.2, and some may be seen under the very low lighting and high resolution of Plate 36.4. The valleys are on the order of 10 km across and have slightly-raised rims (see Pl. 36.4). On the floor of Schickard may be seen some further examples which appear to be buried by the mare material in that crater.

To the E and NE of the Orientale basin the radial structure is not nearly so pronounced. None is prominent in the region due east of Mare Orientale (see Pls. 36.5, 12.32–12.34). In Plate 36.5, showing the northeastern regions from above Grimaldi, we find such structures just outside the Eichstadt ring. It is remarkable that so many of these lineaments show in spite of being oriented nearly perpendicular to the terminator. Here again in the rough uplands is distinguishable a nearly-orthogonal pattern symmetric with Orientale. Locally, e.g., NE of Schlüter, the pattern resembles a Cartesian grid rather than a radial fan, though the relationship to Orientale is clear from the grid orientation.

Just ENE of Schlüter there occurs a pair of striking grooves, typical of radial structure, but not aligned with Orientale. These and several other lineaments are much more closely aligned with Imbrium (see Pl. 36.6 *b*) and may be outlying members of that system. All prominent lineaments in the regions so far considered appear to be attributable to either Orientale or Imbrium.

The radial structure of the Orientale basin system is summarized in an overlay on Plate 36.6*b*. Comparison of the Orientale system with the Imbrium system shows the Orientale radial structures to be profuse as far as 48° selenocentric SSE of the basin, while the comparable figure for the Imbrium system is at least 80° selenocentric. Thus the ratio of the sizes of the radial systems is roughly 0.6. The Orientale structure begins just outside the Eichstadt ring, which is therefore analogous to Imbrium's Apennine ring. The ratio of diameters of these rings is roughly 0.7. We may therefore consider the Orientale radial and concentric system to be two-thirds the size of the Imbrium system.

Imbrium is flooded up to and beyond its Apennine ring (diameter 1340 km); Orientale is flooded only inside its innermost ring (diameter 320 km) and in arcuate patches along the base of the Eichstadt ring and its inner companion.

There are also differences in the forms of the major radial structures. The well-known Imbrium gashes, characteristic of the Ptolemaeus region, are rare in the Orientale system. The valleys near Schickard (Pl. 36.4) are their closest analogue. The Imbrium structures, which in Part I were associated with *flooding*, e.g., broken crater walls, split mountain masses, mountain ridges, etc., are absent here. On the other hand, the local orthogonal patterns present in Orientale are not so characteristic of Imbrium.

The Orientale system shows more asymmetry in azimuth than does the Imbrium system. It has often been stated that the Imbrium radial system is highly asymmetric, being concentrated in the sector from the Haemus Mountains to Ptolemaeus. However, it must be noted that this is the only well-observed region of old upland surface close to Imbrium and that radial systems are well seen only on such a surface. Other upland regions around Imbrium are either small or near the N limb. Plate 24.40 shows that some radial structure is found on uplands in all directions from Imbrium, although the greatest density is indeed in the Ptolemaeus direction. The Imbrium radial system is thus only slightly asymmetric. In the case of Orientale, on the other hand, the basin is bordered by uplands on *all* visible sides, and it is clear that the radial structure is asymmetric and highly concentrated toward the SE.

In interpreting these photographs one must bear in mind the distortions inherent in rectification. In any depression near the W limb, the W inner wall is seen, but the E inner wall is mostly hidden; thus the rectified photographs cannot reveal the whole interior.

(b) Interpretation

The Orientale radial and concentric system is second in magnitude only to that of the Imbrium basin, but it shows significant differences in appearance. If the various lunar basins were caused similarly, the question arises how one can account for these differences. The most promising hypothesis is

that they were formed during different stages of lunar evolution. Evidence was summarized in Part I that the Imbrium event occurred near a period of maximum surface heating, when the crust was already subject to subsidence into softer subsurface layers, and when the dark mare material had its maximum accessibility to the surface. Hartmann and Kuiper (1962) pointed out that the Orientale basin is a relatively recent feature. Its ring system has a fresh appearance. Its radial system is superimposed on the SE limb basin, and cuts the floors of Schickard and Bailly. The distribution of mare material is explained if the subsurface was already cooling and material could reach the surface from depth only in the highly-disturbed center and along concentric scarps. For these various reasons the Orientale basin is supposed to have originated *late* in the period of mare formation.

The orthogonal appearance of the unflooded uplands toward Inghirami appears to be due to block faulting. It is a different pattern from the orthogonality noted in parts of the Imbrium system, which was related to modification during flooding. It does not seem possible to explain either this orthogonality or the structural differences with Imbrium under the hypothesis of sculpture by projectiles from a central explosion. The hypothesis of tectonic activity allows a greater range in structures. If the late-mare crust of the Orientale region were less plastic than the late pre-mare crust near the Imbrium impact, the Orientale system would show more of a shatter pattern than the Imbrium system, as it actually does.

The craters with trailing valleys (shown in Plates 36.2 and 36.4), farther away from Mare Orientale, may be impact sites of flying fragments. They are similar to some very small Imbrium valleys, shown on USAF-NASA chart LAC-77 (1963). The discussion in Part I (p. 7) shows that the larger Imbrium radial valleys tend to have crâterform segments, but not preferentially at one end. An example of nonimpact craters at the ends of rille-like valleys is seen NE of Aristarchus in Plate 36.23*d*.

We have seen that the Orientale radial system is highly asymmetric in azimuth. This phenomenon has been attributed to nonisotropic stresses from a nonvertical impact (Urey, 1961). In this case the crust may have been compressed and broken to the SE when a large body impacted in the present inner ring from the NW at a low angle. Why, however, is the concentric ring system so much more isotropic than the radial system? Possibly, the concentric ring system is due primarily to the isotropic shock waves from a central explosion, while the radial structures are caused primarily by the horizontal component of the momentum imparted to the crust by the impacting body. Hartmann and Kuiper (1962, pp. 62–63) consider both (1) faulting along concentric fractures which were caused by the impact, and (2) crustal compression from horizontal momentum components as possible causes of concentric arcs. Alternative suggestions are Baldwin's (1963, p. 317), that the arcs are frozen shock waves; and Fielder's (1963*a*), that basin systems are internally produced through faulting and not related to impacts.

3. *The Nectaris System*

(a) Morphology

Plates 36.7 through 36.12 show regions near Mare Nectaris. Plate 36.12, centered over Nectaris, is best for an overall view of the system.

In the arc from S to NW of the Nectaris basin lies an expanse of upland where one would expect to find radial structures analogous to those of the Imbrium and Orientale systems. However, no prominent Nectaris radial system is found there in spite of the fact that the concentric system finds its most prominent expression — the Altai scarp — in this direction. R. G. Strom (1964) has pointed out some minor lineaments SW and NW of the basin, which are part of a more general global pattern.

Also, as might be expected from the Imbrium discussion, there are no radial structures on the mare surfaces NW to NE of Nectaris. The small upland area near Capella and Isidorus, N of Nectaris, shows few prominent Nectaris radial structures. The single prominent valley cuts through Capella and is nearly aligned with Imbrium (see Pl. 12.3).

In the arc from E to S of the Nectaris basin is found a whole family of linear valleys. The three most prominent of these are the Rheita Valley (defined in the IAU catalogue of Blagg and Müller, 1935, to extend from near Rheita to Young); the narrow valley extending S from Young through Mallet, called here the Mallet Valley (sometimes incorrectly taken to be a part of the Rheita Valley); and the long valley running through Snellius, called here the Snellius Valley (see Pl. 36.12). In the following paragraphs, some characteristics of these three are enumerated.

(1) The approximate dimensions are: Rheita Valley, 25 by 330 km; Mallet Valley, 12 by 190 km; Snellius Valley, 23 by 800 km.

(2) Each of these valleys is broken by relatively recent craters (e.g., Rheita), but each disturbs older craters (e.g., Young, whose walls and floor are broken).

(3) The two larger valleys (Rheita and Snellius) exhibit craterform segments. In the Rheita Valley these are separated by parallel transverse ridges, and the segments so defined do not resemble the normal craterlets of the surrounding uplands. The Snellius Valley most clearly shows craterform segments and its western part strongly resembles a crater chain.

(4) The three valleys have rims which are very slightly raised relative to the surroundings (e.g., see Pls. 36.7, 36.10*a*, and 36.11).

(5) The interior of the Rheita Valley displays considerable detail in the form of minor ridges and valleys (in addition to the transverse ridges) and the Snellius Valley is even more broken. The Mallet Valley appears to be more regular.

(6) The Mallet Valley departs by about 12° from the direction of the Rheita Valley. Because of this and the differences in form, it should not be assumed that these form a single structural unit.

(7) The Snellius Valley displays an *en échelon* pattern, especialy clear at its E end (see Pl. 36.10).

(8) The Mallet Valley is quite accurately radial to the Nectaris inner basin, but the Rheita Valley is nearly tangential to it. The Snellius Valley's *en échelon* pattern defines a parallel family whose central member is approximately radial to the Nectaris inner basin.

In addition to these major valleys there are a great number of smaller valleys, especially near the Rheita Valley, E of Janssen. This area is well shown on the matching Plates 36.8 and 36.9 (sunrise and sunset views, respectively). The valleys converge approximately toward the center of the Nectaris basin. Of the three larger valleys discussed above, they most nearly resemble the Mallet Valley. They do not exhibit such clear craterform segments as the Rheita and Snellius Valleys. They do have slightly raised rims. They are close to the limb and difficult to interpret adequately, but bear some resemblance to the Imbrium valleys near Ptolemaeus.

A pair of linear scarps runs from Janssen toward the Nectaris inner basin. They are well seen on Plates 36.8 and 36.9. The E side of each scarp is the higher. The eastern scarp is about 300 km long; the western, at least 120 km. The N end of the eastern scarp terminates abruptly where it touches the Altai ring just E of Piccolomini. In its central parts can be seen a resemblance to a valley with craterform segments. Both scarp directions are nearly tangent to the inner basin (see Pl. 36.9).

All of the structures discussed so far lie outside the outer ring of the Nectaris basin system. The only prominent radial pattern to be found within the Altai ring is best shown in Plate 36.7, where a radial trend can be detected in the mountain masses in the arc from S to E of the inner basin. This trend continues outside the Altai ring and it is in this same direction that the major valleys are found still further out.

The system of valleys and scarps described above is identified here as a Nectaris system because most of the structures converge toward the Nectaris inner basin. Gilbert (1893) and others have attributed the major valleys to the Imbrium system. Plate 36.12, centered over Nectaris, also shows part of Imbrium's Apennine arc, and one sees that the valley system is more nearly symmetric to Nectaris. Nonetheless, the region is marked by many outlying members of the Imbrium system.

The degree of convergence of the Nectaris system is not as great as in the Imbrium or Orientale systems, but the rule still applies that the trends of the structures pass within or are tangent to the inner ring of the basin system. This system, with its many valleys, resembles the Imbrium system more closely than it does the Orientale system; yet it is analogous to the Orientale system in its nonuniform distribution in azimuth.

Comparing the extent of Nectaris and Imbrium systems, we find that the Nectaris radial system can be traced as far as 42° selenocentric from the basin center, 53% of the comparable distance in Imbrium. The structures begin at the Altai ring, which has a radius 63% of that of the comparable Apennine ring of Imbrium. Similarly, the ratio of inner basin diameters is 0.60. The scale of the Nectaris basin system is thus about 0.6 that of the Imbrium system.

(b) Interpretation

Although the features discussed do not all show precise convergence toward the center of the Nectaris inner basin, they do define a pattern associated with Nectaris.

The Nectaris radial system appears to be of an intermediate pre-mare age, based on the observation that the system cuts and is cut by many craters. Because of the large number of superimposed craters we conclude that the Nectaris radial system is older than the Imbrium and Orientale systems. The same is true of the concentric system. These results agree

with independently assigned ages based on pre-mare crater densities in the systems, as described by Hartmann and Kuiper (1962, pp. 52–53).

Regarding the formation of the valleys, we may rule out a simple splitting-apart of the crust, suggested for the Alpine Valley of the Imbrium system (see the review of literature in Hartmann, 1963, pp. 2, 4). This hypothesis would not account for (1) the circular outline of Young (not deformed though the Rheita Valley cuts its floor and walls), (2) the transverse ridges, (3) the slightly-raised rims, and (4) craterform segments within these valleys. Apparently there have been no horizontal shifts in forming the valleys.

Gouging by flying fragments does not satisfactorily explain (1) the transverse ridges, and (2) the craterform segments. Fielder (1961, p. 184) also lists arguments against an external origin.

Some sort of tectonic activity and subsidence along major faults accords with the observations. The observed *en échelon* pattern of the Snellius Valley is a known characteristic of terrestrial fault structures. DeSitter (1956, p. 157) states that "normal faulting often shows an *en échelon* arrangement" and that among wrench faults (p. 174), "an *en échelon* arrangement is not common, but in general the wrench-faults are accompanied by many smaller parallel faults of the same character." Although subsidence *alone* does not account for the raised rims, subsidence does appear involved. The craterform segments do not conflict with this interpretation, for evidence was cited in Part I, p. 7 relating crater chains with graben-like features. Furthermore, other authors (e.g., Shoemaker, 1962, pp. 298–303; Rittmann, 1962, pp. 88–92; and Fielder, 1961, pp. 210–216) have discussed the development of lunar and terrestrial craters and graben along deep-seated faults. The two scarps N of Janssen may mark faults along which full-fledged valleys never developed.

Because even the terrestrial examples are not completely understood, it is not profitable to try to describe in further detail the processes which occurred along the hypothetical deep-seated lunar faults.

There are fundamental differences in form among the various rilles, crater chains, graben, and radial valleys of the lunar lineaments. The writer suggests that these are due in part to differences in depth of the underlying faults and in the accessibility of magma and gas to the surface. These differences may in turn be due to the different epochs during which the particular basin systems formed, as suggested above. The evidence already cited that the Nectaris system formed before Imbrium and Orientale would thus be in accord with the differences in form of these systems.

Nectaris shows evidence that the development of the radial and concentric systems occupied an extended period of time. The inner basin itself is old and pre-mare, as evidenced by the many superimposed, post-basin, pre-mare craters; and the radial valleys appear to be pre-mare on similar grounds. However, the Altai scarp must have formed later and may even be post-mare, judging by its fresher appearance and the relative lack of major craters along its length. Such a difference in appearance (and presumably age) within a single ring system is inconsistent with Baldwin's (1963, p. 317) interpretation that the concentric rings are frozen shock waves.

4. The Humorum System

(a) Morphology

Plates 36.13 through 36.16 show the region of Mare Humorum. As expected, no radial pattern is visible in the maria N and E of the Humorum basin, although Plate 36.16 shows lineaments in the Riphaeus Mountains in neighboring peaks.

SE of the basin, as shown in Plate 36.13, aligned ridges are found. Study of the plate reveals a family of parallel structures, most prominent near the center, and on a line radial to Humorum. There is a resemblance to the Imbrium system in the sense that many of the ridges in this partly-flooded region mark portions of older damaged craters.

The same description applies S of the basin. The parallelism here is aligned in a different direction from that of Plate 36.13, but again it is most prominent near the line radial to the basin.

SW of the basin is found a very striking orthogonal pattern of ridges and broken-down craters. This is shown in matching Plates 36.14 and 36.15 (morning and evening, respectively). Most of the structural lines are associated with old craters which have been modified, and there is some localized flooding (cf. Pl. 36.3). In these respects the region is similar to the Haemus Mountains in the Imbrium system (cf. the square crater Auwers, Pls. 24.6 and 24.7, and portions of the Orientale system, Pl. 36.5). This part of the Humorum lineament system is parallel, not radial. The width of the region of local parallelism is roughly equal to the diameter of the inner

basin and in the center of the region the direction is radial to the basin. There are two predominant directions of trend, NE-SW and NW-SE. The line of symmetry is directed to the center of Mare Humorum.

(b) Interpretation

The Humorum basin is accompanied by several families of nearly-parallel lineaments; the members of each family are strongest where the direction is strictly radial. Together, these families define a radial system and therefore are related to the basin. The structures of this radial system exhibit both differences and similarities to structures of previously discussed systems. The Humorum system exhibits no major valleys but, rather, a system of ridges and oriented crater-wall remnants in regions of local flooding. The Nectaris system, on the other hand, consists primarily of valleys. Imbrium shows both types of structure. The most prominent feature of the Orientale radial system is a pattern of nearly-orthogonal faults, whereas flooding is very limited and with it, the process of crater destruction.

We have already suggested that these differences reflect varying ages of the basins. The observations of the Humorum basin suggest this structure is of intermediate pre-mare age. In view of the fact that the major valley systems of Imbrium and Nectaris occur in the unflooded uplands while the ridge systems of Imbrium and Humorum occur in partially-flooded regions, it appears that the nature of the radial structure is correlated with the degree of local flooding.

Fielder's recent study (1963) of the grid system includes a discussion of Humorum. He lists a number of structures in the Humorum system which must have been *internally* produced, including faults along the mare edge, concentric rilles, and wrinkle ridges. In this respect Fielder and the writer are in close accord: the evidence indicates extensive tectonic activity. But he continues (p. 83),

> "All these features are characteristic of the rudely circular type of lunar mare. The conclusion that Mare Humorum is a sink, like Mare Imbrium, is inescapable."
> "... other maria — in particular, Mare Nectaris, which is also obviously an igneous sink — might have been chosen to illustrate many of these points."

Fielder's argument apparently is that if many structures intimately associated with a basin are internally produced, then the basin itself must have been internally produced. The writer has endeavored to show in Part I and here that, on the contrary, the coupling of the impact hypothesis of basin formation with the hypothesis of extensive tectonic activity allows explanation of the various observed features. It provides for the radial fractures along which activity occurs; it also explains the varying time lags between basin formation and mare formation, which are not predicted by the sink hypothesis.

5. The Crisium System

(a) Morphology

Near the Crisium basin, shown in Plates 36.17–36.19, there are very clear examples of lineaments forming orthogonal patterns. A plot of these reveals symmetry with the basin, as seen in Plate 36.19. Reference is made to Fields 14 and 15 in the *Rectified Lunar Atlas* (Whitaker, *et. al.* 1963) for further illustrations.

The clearest examples are found NW of the basin, toward Posidonius. In the depressed, partly-flooded zone, between the inner ring and the outer scarps, are ridges and rectilinear outlines of flooded depressions (see Pl. 36.17). The lineaments are more nearly parallel than radial, but the pattern is strongest where the common direction is radial to the basin, as was found with other basins. There is a remarkable resemblance between this area and the rectilinear structures of the depressed, partly-flooded zone of the Imbrium system just inside the Apennine ring (see Pls. 12.26 and 12.27, and bottoms of Pls. 24.8–24.10).

The same rectilinear pattern can be traced on other sides of the basin, particularly on the SW, where one of its directions is again radial. This is seen in Plate 36.18 where the SW arc of the basin wall consists of a step-like pattern of lineaments. The overlay of Plate 36.19 maps the pattern, showing its presence also in the NE.

Additional lineaments can be seen in Plates 36.18 through 36.19. Many flooded depressions to the SE are bounded by straight sides radial to the Crisium center, and other linear structures can be found in the uplands by careful study of various photographs, not all reproduced here. They are mapped in Plate 36.19. Near the limb, the interpretation of structure is difficult, but ridges and scarps appear to be the most common.

More than any other basin, Crisium exhibits local parallelism of lineaments. West of Crisium the predominant lineaments are not radial but continue the orthogonal pattern which is more clearly seen in the NW and SW. The Crisium basin resembles the Humorum basin in the degree of local flooding, in

the parallelism of nearby lineaments, and in the absence of major valleys.

(b) Interpretation

As with the basins discussed above, it is concluded that the lineament pattern near the Crisium basin is causally related to it. Fielder, examining the grid system (1961, p. 177) states that

> "... careful examinations reveal that [near both Mare Humorum and Mare Crisium] these localized ridges and valleys are specially placed components of a more general family of parallel striations. Clearly, some components of any family of parallel lines which intersect a circle will run along radii of the circle, and it would seem that the two cases cited would be examples of this situation."

The present study shows that there are prominent lineament systems genetically related to neighboring basins; these are not chance juxtapositions of a global grid system and the circular basins. The supporting evidence may be summarized as follows: (1) the indisputable presence of accurately-radial systems around several major basins, e.g., Imbrium and Orientale; (2) the greater prominence of parallel families where the direction of parallelism coincides with the radial direction; (3) the close resemblance in "fine structure" of some of the members of the Crisium and Humorum families with members of the Imbrium system (cf. Plate 36.25, below); (4) the presence of local parallelism within the radial systems of craters like Aristillus (see Sec. 8).

Yet the continuity of the orthogonal pattern, even in places where it is not radially symmetric with a basin, is evidence for the existence of a more widespread grid system, especially in the vicinity of the Crisium basin. Other influences, such as crustal stresses, must have caused such a wider grid system. Lines on Plate 36.19 indicate the directions to the center of the Imbrium basin system. The lineaments under review do not follow the Imbrium direction.

All of these facts are consistent with the concepts that (1) the radial systems are the expressions of fractures created at the times of formation of the basins; (2) the basins are of different ages, mostly pre-mare; (3) the fractures of the grid pattern were superimposed on the radial fractures; and (4) virtually all of the visible lineament structure evolved along these fractures before and during the period of mare formation.

6. Other Basins

The Mare Humboldtianum basin is seen in Plates 36.20 and 36.21. Accurately radial to the inner basin, and extending roughly 140 km between the inner and outer scarps toward the SW, is an unusually straight scarp, revealed by its shadow on Plate 36.21. Comparison of the opposite-lighting views of 36.20*a* and 36.21 indicates a row of hills on this line, with the scarp facing SE. Plate 36.20*b* shows patchy flooding along the lineament. Our interpretation is that we see a fault scarp with lava extruded along its base. This interpretation was also given to the Orientale scarps along which one finds flooding (Hartmann and Kuiper, 1962, p. 57).

Between Humboldtianum and Crisium are several linear features, well shown in Plates 36.20*a* and 36.21. The clearest example is a scarp facing E, curiously smoothed, not sharp, as is the Straight Wall. It might be termed a "ghost scarp." Its surroundings are smooth but bright, neither rugged upland nor mare. Other minor structures, mostly scarps and ridges, in an area of partial flooding SW of Humboldtianum, appear to form a radial pattern. However, identification and interpretation is difficult so close to the limb.

Grimaldi, Janssen, and a basin near Schiller are remaining multi-ring systems discussed in *Communications* No. 12. None of these shows clear radial structure. Judging by subsequent damage, we conclude they are early pre-mare structures.

Other mare basins which give little or no evidence of radial structure include Serenitatis, Nubium, Smythii, Marginus, and the basin on the limb NW of Bailly. Significantly, none but the latter shows well-defined concentric structure. All of these give the impression of being relatively old basins, judging by sharpness of the walls and extent of subsequent damage. The term basin is applied because of the size of the circular bounding walls, which can only be partially traced in most cases.

It is seen that as one proceeds from the youngest basins, dating from the mare epoch, back through the older pre-mare basins, the radial systems become harder to trace, and generally become subordinate to weak local grid patterns. To a lesser extent, the concentric scarps also become harder to trace but they are less clearly related to the local grid directions. Similar observations apply as one proceeds from larger basins through smaller basins to crater-sized objects.

Figure 1 summarizes the observations of all of the radial systems discussed so far, based on an unrectified full-moon photo. The Imbrium system shown here is based on Plate 24.40 in Part I. Some lineament patterns not clearly related to basin sys-

tems are shown by dotted lines. They were noted during the preparation of this paper, but no attempt was made to map all of them.

7. *Grid Systems*

The term "grid" was apparently first applied by Spurr (1948), who used it to refer to a global system of fractures. Spurr spoke primarily of a polar-grid fracture system, most prominent near the poles, and with nearly-meridional members. He suggested symmetry with respect to the moon's equator and central meridian. Spurr (1948, p. 101) proposed that the polar grids were older than the Imbrium system and that they arose when the moon's rotation became synchronous with its revolution.

The concept of a grid system defined by lineaments has aroused wide interest in the past 15 years. Fielder (1961, pp. 180–195) gives an excellent review of the work done, and reproduces charts by various authors. He includes the polygonal shape of some craters as part of the grid concept, and traces such discussions back more than 50 years (Fielder 1961, p. 180).

There is some ambiguity in the use of the term "grid system." Virtually every author who recognizes the validity of the term considers the systems to be tectonic, internally-produced phenomena. Further, it is usually implied that local grid patterns can be combined into one global system which had its origin in a global phenomenon such as a change in rotation rate, shift in polar position, contraction, or expansion. Nevertheless, all of the grid system charts reproduced by Fielder (1961) include the Imbrium radial system, which is definitely a local system. The present paper shows that systems of lineaments accompany other major basins as well. Therefore, if "grid system" is to refer to a single global pattern only, the local radial systems should be excluded, except insofar as they show systematic asymmetries.

Baldwin (1963, p. 385) makes the additional criticism that merely mapping linear formation is not sufficient for grid-system analysis because the resulting charts will mix old and young features of different types, such as wrinkle ridges, valleys, and sections of crater walls. This mixing has in fact occurred as can be seen from the charts reproduced by Fielder.

The following additional points are made regarding the grid systems:

(*a*) The writer defines as a *grid system any background pattern of lineaments not clearly related to any individual basin*. Therefore, symmetric radial systems must be subtracted before a study of a grid system is made, although asymmetry in density or direction of radial structures may be related to grid systems. In fact, there *appears to be a preference for radial structures extending SE from basin centers.* In these radial systems there is a tendency to favor SE-NW strikes, and to a lesser extent SW-NE strikes, producing a pattern not unlike that predicted by Vening Meinesz (1947) to result from a change in the planetary rotation axis. This diagonal preference around basins is probably related to the diagonal global network noted by Fielder (1963, pp. 72–75).

(*b*) The lineaments defining the grid systems are, for the most part, less prominent than those in radial systems.

(*c*) Evidence has been found for *localized manifestations of grid systems.* We have already seen that in the older basins, the radial pattern is characterized by families of locally-parallel lineaments. The identity of these families is maintained even where their dominant direction is nonradial. Second, there are lineament families not radial to any nearby basins. An example is the well-known lattice pattern near Arzachel, mapped in Plates 24.20 and 24.21 of Part I. This system appears to be very old. Neither Nubium, Serenitatis, Tranquillitatis, nor Nectaris is in a symmetric position to this pattern, and it does not increase in prominence toward any of them. A more unusual example is the well-defined lineament pattern which includes the Ariadaeus Rille, the parallel branch of the Hyginus Rille, and an *en échelon* extension of the Hyginus Rille westward. This family differs from most in being quite young.

(*d*) The local grids consist of structures similar to those forming the radial systems. Both classes of structure probably have tectonic origins.

(*e*) In addition to local grid systems, there is evidence for one or more global grid systems. These are not discussed here but are being studied by R. G. Strom (1964) of this Laboratory.

8. *Radial Systems Around Craters*

Many craters display radial patterns. This is best seen around young craters on the nearly featureless mare surfaces. Here, one observes a coarse radial pattern in the hummocky raised rim, grading into a pattern of fine ridges and valleys, from a few kilometers width on down, on the surrounding mare. It is well known that these systems exhibit a local parallelism similar to that described here in the radial systems of basins (See Warner, 1961, pp.



Fig. 1. Schematic diagram of lunar basin systems. Each line marks a concentric or relatively prominent radial lineament and each is drawn to proper scale and orientation. Dotted lines give examples of some prominent local grid patterns, not related to basin systems.

391–392). Some examples are shown in Plates 36.22 and 36.23.

Baldwin (1949, p. 208), proposing that the sequence from small crater pits to the large mare basins represents only a size range in a single family of impact structures, described the radial systems of craters simply as reduced versions of the basin radial systems. The writer regards this description as valid only in a limited sense for the reasons which follow.

The coarse radial structures in the rough rims of these fresh craters indeed resemble the coarse pattern observed in the Apennine rim of Imbrium and perhaps in the rim of the Orientale basin. We have already identified these basins as relatively recent, and commented on the lack of flooding in the Apennines and Orientale region. Therefore, this type of radial structure can be regarded as the immediate and unaltered result of buckling of the crust on impact and emplacement of debris on the outer rim. Its presence in both well-preserved craters and basins supports Baldwin's conclusion that craters and basins are of similar origin.

However, the many other radial structures in large basin systems, e.g., pre-existing mountainous areas broken into ridges, damaged craters, and troughlike structures, find no counterpart in the radial systems of fresh craters. Yet this is in accord with the ideas here presented, as these structures have been attributed to tectonic processes along fractures and related to the high-temperature mare epoch. The craters recent enough to be well preserved are post-mare. Furthermore, it is likely that crater-sized objects are too small to provide suitable conditions for the development of tectonic radial structure.

The most delicate lineaments, e.g., those which radiate at least 160 km from the center of Aristillus, have no known counterparts in the basin systems because they would lie in the rugged uplands where their fineness would prevent detection. Available photos lack sufficient resolution to prove whether these ripples represent fracturing or buckling of the crust, or grooving by fragments blown out by impact. D. W. G. Arthur (private communication, 1963) favors the latter view on the basis of high-resolution visual studies.

There remain important differences between craters and basins. The preference of the mare material for the large basins is easily explained if this material is lava. Because of greater damage to the lunar crust at the largest impact sites, lava had easier access to the surface. The most puzzling difference is the presence of the concentric rings around the basins, with no trace of them around either the recent craters with radial structures, or around some pre-mare craters of basin dimensions. To explain this, one may have to appeal to differences in impact velocity or possible differences in the impacted crust.

9. *Conclusions and Summary*

The primary result of this paper is the conclusion that a system of radially-oriented lineaments is an integral part of the typical mare basin system. The radial structure can be traced, in some cases, as far as seven times the radius of the innermost ring of the concentric ring systems of these basins. This concept of a basin system with radial and concentric structure has been heavily influenced by study of the best-preserved and largest examples, Imbrium and Orientale.

The basins are of varying ages, but the mare surfaces stem more nearly from one epoch. This has been well documented by Baldwin (1949, pp. 211–212; 1963, pp. 304–309), Shoemaker, Hackman, and Eggleton (1962, Table 2), and Hartmann and Kuiper (1962, pp. 62, 65). The basins can be placed in an age sequence by consideration of: (*a*) sharpness of concentric walls, (*b*) density of post-basin, pre-mare craters, and (*c*) extent of flooding. When the basins are considered in this sequence, it is found that with increasing age the radial systems become less well defined. The basins are tentatively classed by increasing age as follows: Orientale, late-mare; Imbrium, late pre-mare or early-mare; Humboldtianum, Nectaris, Crisium, Humorum, Serenitatis and the smaller basins, pre-mare.

Numerous observations of special interest have resulted from this survey of the radial systems:

(*a*) No known radial system is post-mare. A few scattered individual features such as the Straight Wall and Cauchy scarp are probably post-mare.

(*b*) The bulk of the structures cannot be accounted for by the grooving action of flying fragments. Most of the structures form nearly-orthogonal patterns of ridges and depressed, often-flooded zones. Major valleys, which have been considered the prime evidence for grooving, are confined mostly to the upland parts of the Imbrium and Nectaris systems. Their characteristics — craterform segments, transverse ridges and other structures on their floors, darkness of their floors, *en échelon* patterns (e.g., Snellius

Valley), etc. — indicate that not even they originated by grooving.

(*c*) No horizontal motion has been found in the study of the radial systems (cf. also Baldwin, 1963, p. 375, and others) and the Rheita Valley shows definite evidence against horizontal displacement. Vertical motion must dominate. This finding differs from Fielder's (1963, p. 87) conclusion from a study of the grid system that "strike-slip faults are of even greater importance on the moon than are normal faults."

(*d*) The *en échelon* pattern of the Snellius Valley strongly suggests faulting.

(*e*) Repeated evidence is found in various localized regions that the structures of the crust have been modified in some cases to the extent of complete destruction (see also Hartmann, 1963, p. 10). Best evidence for this is found among structures of the Imbrium and Crisium systems. Near mare surfaces there is often a clear association of this phenomenon with the mare material, but examples can also be found in unflooded upland regions.

(*f*) Some radial systems show an asymmetric distribution in azimuth, even after allowance for disappearance by flooding. This is most clearly seen in the uplands around Orientale and Nectaris. It is not so definitely known in the case of Imbrium, because of the extent of flooding, but there is probably a concentration toward the SE. In both Orientale and Nectaris, the concentric system is more uniform in azimuth than the radial system.

(*g*) In the typical basin system, most of the radial structure lies beyond the outermost concentric ring. The pattern found within the concentric ring system is usually limited to flooded regions of subsidence.

(*h*) A certain unity exists among the different radial systems, as may be seen by noting the similarity of radial lineaments in different parts of the moon. Plates 36.24 and 36.25 give such a comparison at uniform scale. In plate 36.24, valleys from widely separated points on the moon are compared. Plate 36.25 gives 3 examples each of (1) flooded regions showing orthogonality, (2) scarps, and (3) craters broken into linear segments. The form of the predominant lineaments may nonetheless vary from one basin system to another.

(*i*) Independent of the radial systems, there exist patterns of lineaments which define local "grid systems." Study of these is beyond the scope of this paper. A consideration of grid systems as a global phenomenon must take into account the presence of independent radial systems around basins.

Having listed the chief observations, we now attempt to fit them systematically into a hypothesis of the development of the lunar surface. On the basis of telescopic observations alone, one is led to the conviction that there was a period of extensive tectonic activity during which many pre-existing structures were damaged and the mare material was deposited. Reference to theoretical work of the last decade suggests that this was the period of maximum radioactive heating at the surface. This period conveniently divides lunar history and is called here the *mare epoch*. The following model is believed consistent with all of the observed facts.

In the pre-mare period most of the craters formed. The basins either are unusually large examples of these ordinary craters, or represent a separate class of objects. In support of the first interpretation, the distribution of crater diameters D with respect to number of craters n is given by $n = cD^{-2.1}$ where c is a constant (Hartmann, 1964). Thus, the basins may represent one extreme of this distribution. It should be possible to check this quantitatively when a larger sample of craters has been measured. In support of the latter interpretation are the differences in form between basins (with their concentric and radial patterns) and ordinary craters. Both craters and basins are probably impact features. As each basin formed, it probably acquired some radial structure around its walls, analogous to that seen in recent crater rims. But, just as importantly, many radiating fractures were formed. The direction and velocity of fall, and the presence of any pre-existing stresses in the surface were probably important factors in determining the distribution of these fractures. The nature of the surface, the presence of local stresses, the time interval from basin formation to maximum heating, and the degree of local heating were probably important factors in the development of tectonic adjustments along these fractures.

These developments must have occurred throughout the interval between basin formation and the close of the mare epoch, in view of the following observations: (*a*) coarse radial patterns are thought to be original features of the basin rims; (*b*) some structures appear to be pre-mare (e.g., valleys in the Nectaris system); (*c*) other structures in the same systems appear to be younger than those under (*b*) (e.g., Altai scarp); (*d*) even in older basin systems, there is a correlation between the degree of local flooding and the presence of certain types of radial structure (e.g., partially destroyed craters in Im-

brium and Humorum systems), suggesting that these particular structures formed during the mare epoch; (*e*) the mare surfaces are virtually never broken by post-mare radial structure.

We have noted that radial systems of the older basins are less clearly defined than those of the younger basins. Not all the differences are due to erosion alone, and the following statement holds approximately: The more nearly coincident the basin-forming impact was with the mare epoch, the more pronounced was the resulting radial system. The period leading into the mare epoch was the optimum period for tectonic activity, because (*a*) temperatures were maximal in subsurface layers, (*b*) the viscosity was correspondingly lowered in these layers, (*c*) the surface was stressed due to the expansion prior to the mare epoch (MacDonald, 1961), (*d*) the surface should have been unstable if there was extensive melting below (Urey, 1955). The first two reasons allowed tectonic adjustments to occur; the last two caused them to occur. The observations are thus compatible with theory. The observations indicate that if the interval between basin formation and mare epoch was long, the likelihood of tectonic activity along radial lines during the mare epoch was lessened.

The origin of the grid systems and of asymmetry and parallelism in the radial systems remains puzzling. They must relate to stress patterns not associated with the basin systems. The most important conclusion reached here in this connection is that the radial systems themselves are independent of the proposed global grid system except for possible local modifications of the former by the latter. This fact is most clearly shown by Orientale and Imbrium. Therefore, lineaments of a symmetric radial pattern centered on basins should be disregarded in discussions of lunar grids and global stresses. Most such discussions to date have ignored this aspect; exceptions are Fielder's recent paper (1963) and the work of Strom (1964). The author agrees with the often-expressed view that the lunar lineaments are internally produced.

During the mare epoch, magma reached the surface in most of the highly-disturbed basins and their fracture systems, and in some other localized areas. Much damage was done to pre-existing surface structures. In view of this hypothesis of an era of strong tectonic activity, also described in Part I (Hartmann, 1963), the following remarks by Dunbar (1963) on pre-Cambrian activity on the earth are of great interest.

> ". . . contemplate the 2,000,000 square miles of granite gneiss that floors the Canadian Shield, and realize that it all came into place as fluid magma, which congealed beneath a cover of older rocks now long since removed by erosion. The relatively small areas of sedimentary formations that lie infolded among these bathyliths, as remnants of their former cover, convey the impression that during these primeval eras, *the crust of the Earth was repeatedly broken and largely engulfed in upwellings of molten material that dwarf all post-Cambrian igneous activity.*" [Italics by W. K. H.]

It is doubtful that this represents a true mare epoch on earth, but the analogy to the hypothesized lunar processes is obvious. The rate of crater production did not change much during the mare epoch, as evidenced by the relative constancy of crater number densities on the various surfaces (Shoemaker, Hackman, and Eggleton, 1962). The mare epoch must have occurred early in the moon's history on the following grounds. The moon is generally thought to be at least 4.5 billion years old (Kuiper, 1963; Urey, 1963). In some models calculated by MacDonald (1961) and others, the temperature at a depth of 200 km reaches a rather flat maximum (and at the moon's center, the melting point of iron) in 1 to 2 billion years. But these models assume (*a*) heat transport by conduction and radiation, (*b*) homogeneous distribution of radioactive material, and (*c*) a chondritic composition. Heat transport by convection, concentration of radioactive material near the surface, and the presence of short-lived radioisotopes would raise the subsurface temperature and shorten the time between the moon's formation and the mare epoch. (Mechanisms for producing short-lived isotopes have been discussed, e.g., by Anders and Stevens, 1960, and by Fowler, Greenstein, and Hoyle, 1962.) Therefore, it appears that the mare epoch occurred within the first 1.5 billion years of lunar history. Shoemaker, Hackman, and Eggleton (1962) propose that the crater density on the maria is consistent with a mare age of 4.5 billion years and with a constant flux of meteorites in this period. At this early period, the moon was much closer to the earth, as is known from the theory of tidal evolution, and Baldwin (1963, p. 203) has argued that the elongation of the earthward axis may represent the tidal bulge frozen into the moon's outer layers at the close of the mare epoch with the moon at 39 percent of its present distance. The correctness of the latter two ideas would imply a mare epoch as long ago as the first 0.2 billion years of lunar history.

Throughout the post-mare period, the moon must have appeared substantially as it is now, except

for the addition of some prominent recent ray craters. We observe that the mare surfaces clearly did not undergo major internal disruptions after they formed. The flux of incoming meteorites was much less than in pre-mare time as evidenced by the sparseness of craters on the maria and on the earth. Tectonic activity was negligible in its effect upon large-scale surface structure and the moon was essentially dead. On the earth, we can trace only the most recent fraction of this period because of the continued erosional and tectonic activity of the earth, which has erased its earliest pre-Cambrian structures. Because of this continued activity the presently observed large-scale, tectonic structure of the earth's active crust may be fundamentally different from the dead, impact-scarred lunar surface, and the proposed similarity of the mare basins to ocean basins (von Bülow, 1958, p. 36), or of faults in the Apennines to the San Andreas fault (Fielder, 1963, p. 87) is very questionable.

The history of the moon sketched on these pages is schematically outlined in Figure 2, which is largely self-explanatory. An attempt is made to correlate the three-phase terminology here with the five-phase stratigraphic nomenclature of Shoemaker (1962). Plate 36.26 schematically outlines the radial lineament systems of the lunar basins as discussed here.

Acknowledgments. Thanks are due to Dr. G. P. Kuiper, Miss Barbara M. Middlehurst, Mr. D. W. G. Arthur, Mr. E. A. Whitaker, and other colleagues at this Laboratory, and to Dr. Spencer R. Titley and Dr. Evans P. Mayo of the Department of Geology for many helpful discussions; and to Dr. Kuiper for critically reading the manuscript. I relied extensively on Mr. Whitaker's help in selection of photographs from the LPL collection, many of which were taken by Mr. Elliot Moore. Some of the rectified negatives were made by Mr. Harold Spradley. The work reported here was supported by the National Aeronautics and Space Administration through Grant NsG 161-61.

General remarks on plates. The following plates are oriented to show the radial structures, usually with the basin direction downward, and thus the orientation with respect to lunar coordinates is variable. Data at the end of each caption identifies those plates which have been rectified by globe projection, and gives original plate number, scale, and colongi-

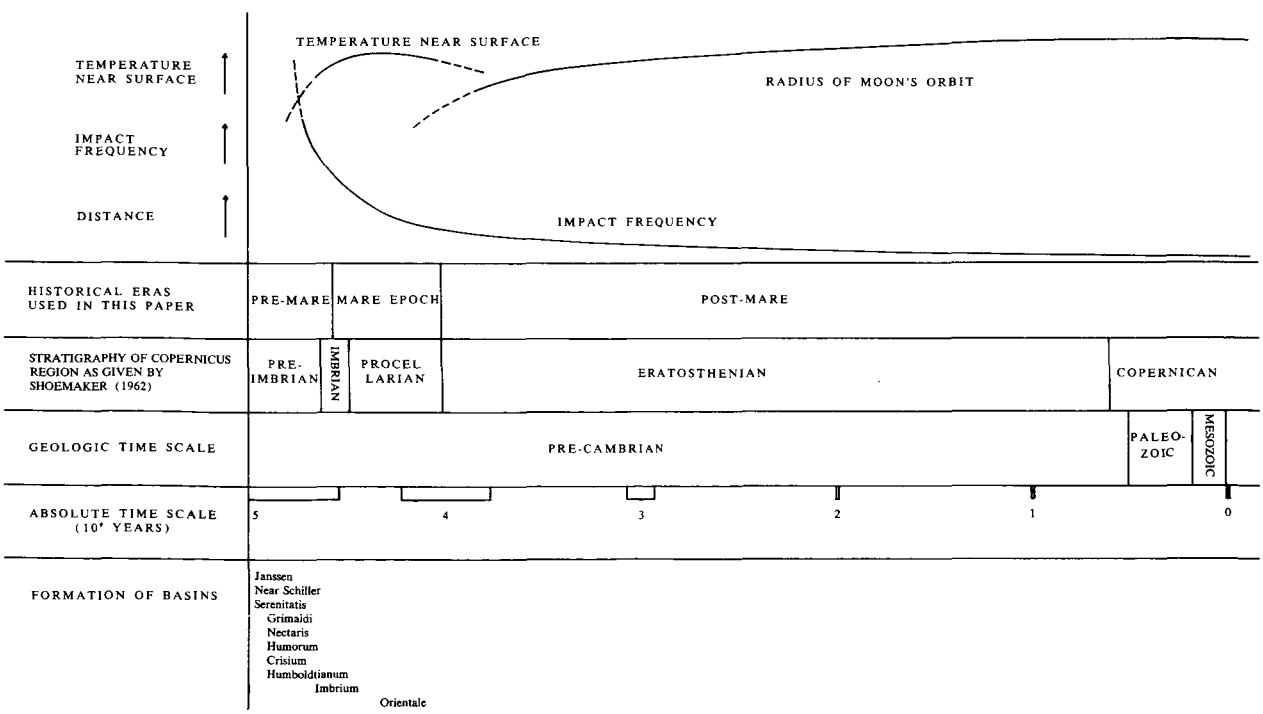


Fig. 2. Simplified schematic outline of lunar history. Various time scales used in geologic and lunar studies are compared. The probable histories of lunar structures, heating, distance, and impact frequency are shown in the upper part of the diagram. The chart illustrates the hypothesis that most of the lunar structures date from a considerably earlier evolutionary stage than is detectable on the earth.

tude of the sun. These plates conclude a long series of photographs specially chosen to illustrate lunar basin systems and published in *Communications of the Lunar and Planetary Laboratory,* Nos. 12, 24, and 36. A catalogue of these photographs is presented in the Appendix.

REFERENCES

Anders, E., and Stevens, C. M. 1960, *J. Geophys. Res., 65,* 3043.

Arthur, D. W. G. 1963, private communication.

Baldwin, R. B. 1963, *The Measure of the Moon* (Chicago: University of Chicago Press).

Blagg, Mary A. and Müller, K. 1935, *Named Lunar Formations* (London: Percy Lund, Humphries, and Co., Ltd.).

Bülow, K. von 1958, *Wiss. Zeitschr. der Univ. Rostock, Math.-Naturwiss. Reihe, 1,* 19.

Dunbar, Carl O. 1963, *Historical Geology* (New York, Wiley).

Fielder, G. 1961, *Structure of the Moon's Surface* (New York: Pergamon Press).

———. 1963a, *Nature, 198,* 1256.

———. 1963b, *Quart. J. Geol. Soc. London, 119,* 65.

Fowler, W. A., Greenstein, J. L., and Hoyle, F. (1962), *Geophys. J., 6,* 148.

Gilbert, G. K. 1893, *Bull. Phil. Soc. Washington, 12,* 241.

Hartmann, W. K. 1963, *Comm. L. P. L., 2,* 1.

———. 1964, *Comm. L. P. L., 2,* 197.

Hartmann, W. K. and Kuiper, G. P. 1962, *Comm. L. P. L., 1,* 51.

Kuiper, G. P. 1959, *Vistas in Astronautics,* eds. M. Alperin and H. F. Gregory (London: Pergamon Press), vol. *2.*

———. 1963, *Space Science,* ed. D. P. Le Galley (New York: Wiley), chap. 15.

MacDonald, G. J. F. 1961, *Science, 133,* 1045.

Rittman, A. 1962, *Volcanoes and Their Activity* (New York: Wiley).

Sitter, L. U. de 1956, *Structural Geology* (New York: McGraw-Hill Book Co., Inc.).

Shoemaker, E. M., Hackmann, R. J., and Eggleton, R. E. 1962, in *Advances in the Astronautical Sciences, 8* (New York: Plenum Press, Inc.).

Shoemaker, E. M. 1962, *Physics and Astronomy of the Moon,* ed. Z. Kopal (New York: Academic Press, Inc.), chap. 8.

Spurr, J. E. 1948, *Geology Applied to Selenology* (Lancaster, Pa.: Science Press), vol. *3.*

Strom, R. G. 1964, *Comm. L. P. L., 2,* 205.

USAF and NASA 1963, *Lunar Charts* (St. Louis: ACIC).

Urey, H. C. 1955, *Proc. Nat. Acad. Sci., 41,* 423.

———. 1961. *Smithsonian Report for 1960,* p. 251.

———. 1963. *Space Science,* ed. D. P. Le Galley (New York: Wiley), chap. 4.

Vening Meinesz, F. A. 1947, *Trans. A. G. U., 28,* 1.

Warner, B. 1961, *J.B.A.A. 71,* 388.

Whitaker, E. A., Kuiper, G. P., Hartmann, W. K., and Spradley, H. L. 1963 *Rectified Lunar Atlas* (Tucson: University of Arizona Press).

APPENDIX

Catalog of Lunar Photographs Published in LPL Communications Nos. 12, 24**, and 36****

PLATE NUMBER	DESCRIPTIVE TITLE	ORIGINAL	RECTIFIED	APPROXIMATE SCALE km/cm	BASIN INVOLVED
12.1	Mare Crisium, SS	Y 369	X	60	Crisium
12.2	Nectaris Ring System, SR	Y 65	X	56	Nectaris
12.3	Nectaris Ring System, SS	Y 1200	X	56	Nectaris
12.4	Nectaris Ring System, with overlay	Y 65	X	56	Nectaris
12.5	Altai Scarp, SS	W 97	X	56	Nectaris
12.6	Mare Nectaris, SS	Y 1334	X	25	Nectaris
12.7	Mare Nectaris & rilles to N, SR	L 175		25	Nectaris
12.8	Three rings in Nectaris system, SR	Y 65	X	25	Nectaris
12.9	Three rings in Nectaris system, SS	Y 1335	X	25	Nectaris
12.10	Theophilus region, SR	L 193		25	Nectaris
12.11	Theophilus region, SS	W 97		25	Nectaris
12.12	Humorum Ring System, SR	M 694	X	47	Humorum
12.13	Humorum Ring System, SS	M 191	X	47	Humorum
12.14	Humorum Ring System, with overlay	M 191	X	47	Humorum
12.15	W part of Humorum basin	M 694	X	30	Humorum
12.16	Mare Humorum, SR	M 630		30	Humorum
12.17	Rilles and Ridges E of Mare Humorum, SR	M 611		25	Humorum
12.18	Imbrium Ring System, SR	Y 160	X	85	Imbrium
12.19	Imbrium Ring System, SS	W 115	X	90	Imbrium
12.20	W part of Mare Imbrium, SS	W 252	X	43	Imbrium
12.21	E part of Mare Imbrium, SS	W 115	X	43	Imbrium
12.22	W part of Mare Imbrium, SR	Y 163		30	Imbrium
12.23	E part of Mare Imbrium, SR	Y 1267		30	Imbrium
12.24	Imbrium Ring System, with overlay	W 115	X	90	Imbrium
12.25	Imbrium radial lineaments, M. Vaporum	Y 1350	X	45	Imbrium
12.26	Apennines and Archimedes Island	Y 1269		28	Imbrium
12.27	Archimedes Island	W 121		18	Imbrium
12.28	Moon from above Imbrium basin	Y 577	X	22	Imbrium
12.29	Moon from above Orientale basin	Y 1614	X	200	Orientale
12.30	Orientale Ring System, high lighting	Y 1614	X	65	Orientale
12.31	Orientale Ring System, SR	M 74	X	65	Orientale
12.32	Orientale Ring System, SR	M 372	X	65	Orientale
12.33	Orientale Ring System, SR	M 372	X	41	Orientale
12.34	Orientale Ring System, SR	Y 108	X	65	Orientale
12.35	Orientale Ring System, SR	Y 108	X	48	Orientale
12.36*a*	E part of Orientale Ring System, SR	Y 1502	X	58	Orientale
12.36*b*	E part of Orientale Ring System, SR	Y 468	X	64	Orientale
12.37	Orientale Ring System, high lighting	M 121		30	Orientale
12.38*a*	Orientale Ring System, high lighting	M 831		27	Orientale
12.38*b*	Orientale Ring System, high lighting	Y 1589		27	Orientale
12.38*c*	Orientale Ring System, high lighting	Y 1578		27	Orientale
12.39*a*	Orientale Ring System, SR	Y 1614		27	Orientale
12.39*b*	Orientale Ring System, SR	Y 836		27	Orientale
12.39*c*	Orientale Ring System, SR	M 74		27	Orientale
12.40	Orientale Ring System, high lighting	Y 1592	X	63	Orientale
12.41	Orientale Ring System, SS	W 172	X	55	Orientale
12.42	Orientale Ring System, with overlay	M 74	X	60	Orientale
12.43	Orientale Ring System, synthesis	(Drawing)		35	Orientale
12.44	Moon from above SE limb basin	Y 1614	X	160	SE Limb Basin
12.45	SE limb basin, SR	Y 1614	X	80	SE Limb Basin
12.46*a*	SE limb basin, SR	Y 1614		30	SE Limb Basin
12.46*b*	SE limb basin, SR	Y 1654		30	SE Limb Basin
12.47*a*	SE limb basin, high lighting	M 831		30	SE Limb Basin
12.47*b*	SE limb basin, high lighting	M 121		30	SE Limb Basin
12.48	Humboldtianum Ring System, SS	Y 482	X	45	Humboldtianum
12.49	Humboldtianum Ring System, SR	Y 686	X	45	Humboldtianum
12.50	Humboldtianum Ring System, SR	Y 781	X	45	Humboldtianum
12.51	Humboldtianum Ring System, SS	M 30	X	45	Humboldtianum
12.52	Crisium Ring System, SR	Y 784	X	60	Crisium
12.53	Crisium Ring System, with overlay	Y 784	X	60	Crisium
12.54	N part of Crisium Ring System, SR	Y 784	X	40	Crisium

*Concentric Structures Surrounding Lunar Basins
**Radial Structures Surrounding Lunar Basins, I: The Imbrium System
***Radial Structures Surrounding Lunar Basins, II: Orientale and Other Systems; Conclusions

APPENDIX (Continued)

PLATE NUMBER	DESCRIPTIVE TITLE	ORIGINAL	RECTIFIED	APPROXIMATE SCALE km/cm	BASIN INVOLVED
12.55	N part of Crisium Ring System, SS	Y 369	X	40	Crisium
12.56	W part of Crisium system, SS	Y 1315	X	60	Crisium
12.57*a*	Maria Marginus and Smythii, high lighting	L 172, 204	X	100	Smythii
12.57*b*	Maria Marginus and Smythii, high lighting	Lunik III	(X)	100	Marginus
12.58	Maria Marginus and Smythii, SR	Y 686	X	60	Marginus
12.59	Maria Marginus and Smythii, SS	M 479	X	60	Marginus
12.60	Basin near Schiller, SR	Y 1122	X	34	Basin near Schiller
12.61	Basin near Schiller, SR	Y 1011	X	34	Basin near Schiller
12.62	Basin near Schiller, SR	M 694	X	38	Basin near Schiller
12.63	Basin near Schiller, SS	W 171	X	38	Basin near Schiller
12.64	Grimaldi, SR	Y 1502	X	40	Grimaldi
12.65	Grimaldi, SR	Y 108	X	40	Grimaldi
12.66	Grimaldi, SS	Y 1395	X	40	Grimaldi
12.67	Janssen, SS	Y 1335	X	30	Janssen
12.68	Janssen, SS	Y 369	X	38	Janssen
12.69	Janssen, SR	Y 193	X	32	Janssen
12.70	Moon from above S pole	Y 1614	X	150	S Polar (?)
12.71	Leibnitz Mountain arcs	Y 1604	X	65	S Polar (?)
12.72	Bailly and Pingré, SR	Y 1170	X	41	Bailly (?)
12.76	Mare Smythii, high lighting	Y 204	X	65	Smythii
12.77	Full moon with outlines of ring systems	L 224	X	230	All basins
24.1	Moon from above Imbrium basin center	Y 160	X	130	Imbrium
24.2	Looking S from above Mare Imbrium, SS	Y 1350	X	70	Imbrium
24.3	Apennines and Mare Vaporum, SS	Y 1350	X	45	Imbrium
24.4*a*	Straight Wall, SR	Y 1271		20	Imbrium
24.4*b*	Straight Wall, SS	W 119		20	Imbrium
24.5*a*	Cauchy Scarp, SR	L 175		20	Imbrium
24.5*b*	Cauchy Scarp, SS	W 80		20	Imbrium
24.6	Haemus Mountains, SR	Y 1262		15	Imbrium
24.7	Haemus Mountains, SS	W 111		15	Imbrium
24.8	Apennines and Mare Vaporum, SR	Y 150		30	Imbrium
24.9	Apennines and Mare Vaporum, high lighting	Y 1207		30	Imbrium
24.10	Apennines and Mare Vaporum, SS	W 111		30	Imbrium
24.11	Region of Julius Caesar, SR	Y 744		30	Imbrium
24.12	Region of Julius Caesar, SS	W 111		30	Imbrium
24.13	Region of Ptolemaeus, SR	Pic 34		30	Imbrium
24.14	Region of Ptolemaeus, high lighting	Y 466		30	Imbrium
24.15	Region of Ptolemaeus, SS	W 119		30	Imbrium
24.16	Region of Arzachel, SR	Y 1254		30	Imbrium
24.17	Region of Arzachel, SR	Pic 34		30	Imbrium
24.18	Region of Arzachel, high lighting	Y 466		30	Imbrium
24.19	Region of Arzachel, SS	W 119		30	Imbrium
24.20	Region of Arzachel, with overlay	W 119		30	Imbrium
24.21	Region of Ptolemaeus, with overlay	W 119		30	Imbrium
24.22	Region of Fra Mauro, SR	Y 1267		30	Imbrium
24.23	Region of Fra Mauro, SR	M 285		30	Imbrium
24.24	Region of Fra Mauro, high lighting	Y 466		30	Imbrium
24.25	Region of Fra Mauro, SS	Y 1247		30	Imbrium
24.26	Carpathian Mountains, SR	Y 163		30	Imbrium
24.27	Carpathian Mountains, SS	M 184		30	Imbrium
24.28	Region of Hansteen, SR	M 694	X	45	Imbrium
24.29	Region of Sirsalis Rille, SS	W 230	X	45	Imbrium
24.30	Region of Otto Struve, SR	M 373	X	50	Imbrium
24.31	Western reaches of Mare Imbrium, SR	M 700	X	65	Imbrium
24.32	Vicinity of Aristarchus plateau, SS	W 173	X	50	Imbrium
24.33	Aristarchus plateau, SR	M 700	X	30	Imbrium
24.34	Aristarchus plateau, high lighting	M 184	X	30	Imbrium
24.35	Aristarchus plateau, SS	W 231	X	30	Imbrium
24.36	Region of W. Bond, SR	Y 1350	X	45	Imbrium
24.37	Region of W. Bond, SS	Y 160	X	45	Imbrium
24.38	Region of J. Herschel, SR	M 10	X	40	Imbrium
24.39	Lineaments in Mare Tranquillitatis, SR	Y 72	X	45	Imbrium
24.40	The Imbrium Radial System, with overlay	Y 577	X	180	Imbrium
36.1	Orientale lineaments near Wargentin, SR	Y 108	X	40	Orientale
36.2	Radial lineaments SE of Orientale, SR	Y 1170	X	80	Orientale
36.3	Radial lineaments SE of Orientale, high lighting	Y 1592	X	80	Orientale
36.4	Valleys in and beyond Schickard, SR (120 in.)	Lick 33		10	Orientale
36.5	Lineaments NE of Orientale	M 372	X	50	Orientale

APPENDIX (Continued)

PLATE NUMBER	DESCRIPTIVE TITLE	ORIGINAL	RECTIFIED	APPROXIMATE SCALE km/cm	BASIN INVOLVED
36.6	The Orientale Radial System, with overlay	M 74	X	80	Orientale
36.7	Valleys SE of Nectaris, SS	Y 1310	X	60	Nectaris
36.8	Valleys SSE of Nectaris, SR	L 193	X	60	Nectaris
36.9	Valleys SSE of Nectaris, SS	Y 1200	X	60	Nectaris
36.10*a*	Extension of Snellius valley toward limb, SR	Y 686	X	80	Nectaris
36.10*b*	Extension of Snellius valley toward limb, SR	Y 727	X	80	Nectaris
36.11	Valleys ESE of Nectaris, SS	Y 369	X	80	Nectaris
36.12	The Nectaris Radial System, with overlay	Y 482	X	120	Nectaris
36.13	Lineaments SE of Humorum, SS	W 171	X	40	Humorum
36.14	Orthogonal pattern W of Humorum, SR	Y 468	X	40	Humorum
36.15	Orthogonal pattern W of Humorum, SS	W 230	X	40	Humorum
36.16	The Humorum Basin System	W 172	X	80	Humorum
36.17*a*	Lineaments NW of Crisium, SS	Y 1206	X	50	Crisium
36.17*b*	Lineaments NW of Crisium, SR	L 175	X	50	Crisium
36.18	Mare Crisium, SR	Y 784	X	45	Crisium
36.19	The Crisium Radial System, with overlay	Y 738	X	80	Crisium
36.20*a*	Region of Humboldtianum basin, SR	Y 686	X	80	Humboldtianum
36.20*b*	Region of Humboldtianum basin, SS	L 237	X	80	Humboldtianum
36.21	Region of Humboldtianum basin, SS	Y 482	X	80	Humboldtianum
36.22*a*	Aristillus, SR	Pic (1945)		30	Humboldtianum
36.22*b*	Aristillus, SS	W 121		30	Humboldtianum
36.22*c*	Bullialdus, SS	L 163		30	Humboldtianum
36.22*d*	Bullialdus, SR	W 171		30	Humboldtianum
36.23*a*	Copernicus, SR	M (1959)		30	Humboldtianum
36.23*b*	Eratosthenes, SR	Y 1267		30	Humboldtianum
36.23*c*	Copernicus, SR	Pic 37b		30	Humboldtianum
36.23*d*	Aristarchus, SR	M 624		30	Humboldtianum
36.24*a*	Trough near Aristarchus plateau, SS	W 231		50	Imbrium
36.24*b*	Trough in Haemus Mountains, SR	W 111		50	Imbrium
36.24*c*	Trough near W. Bond, SS	Y 1350	X	50	Imbrium
36.24*d*	Rheita valley, SR	L 193	X	50	Nectaris
36.24*e*	Valley near Herschel, SS	Y 1261		50	Imbrium
36.24*f*	Valley in Julius Caesar, SR	W 111		50	Imbrium
36.24*g*	Mallet Valley, SR	L 193	X	50	Nectaris
36.24*h*	Valley W of Ptolemaeus, SR	Y 1261		50	Imbrium
36.25*a*	Orthogonal lineaments near Archimedes, SS	W 115		50	Imbrium
36.25*b*	Orthogonal lineaments near Macrobius, SR	L 175	X	50	Crisium
36.25*c*	Orthogonal lineaments near Schickard, SR	W 230	X	50	Humorum
36.25*d*	Scarp radial to Humboldtianum, SS	Y 482	X	50	Humboldtianum
36.25*e*	Scarps radial to Nectaris, SR	L 193	X	50	Nectaris
36.25*f*	Scarps radial to Orientale, SR	Y 1170	X	50	Orientale
36.25*g*	Damaged crater Réaumur, SR	Y 1261		50	Imbrium
36.25*h*	Damaged crater Parry M, SR	Y 557		50	Imbrium
36.25*i*	Damaged crater in Palus Epedemaiarum, SS	W 171	X	50	Humorum
36.36	Radial and concentric basin systems	L 224		190	All basins

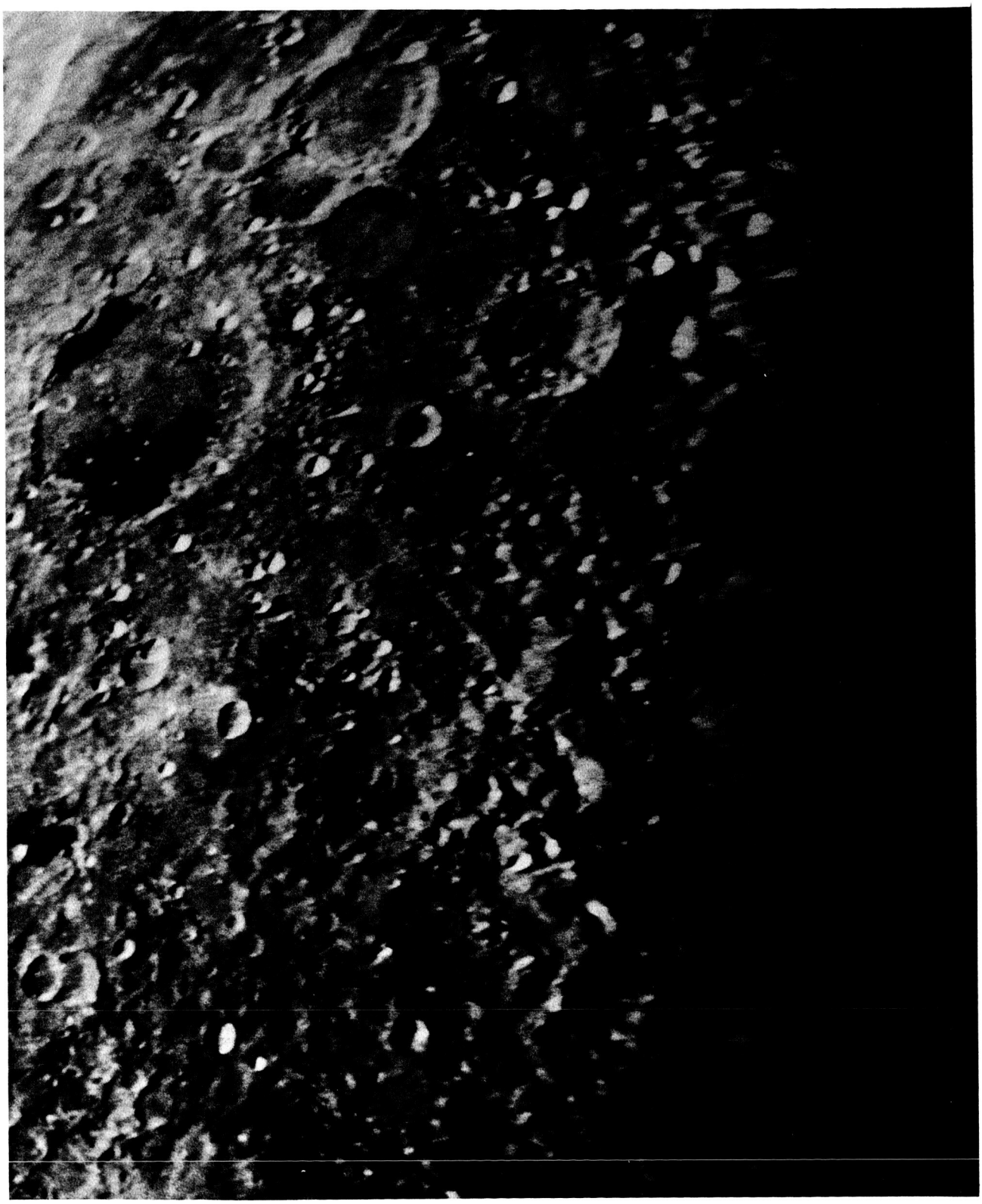


Plate 36.1. Radial system of Mare Orientale in the region of Wargentin, Schickard, and Inghirami, viewed from above Mare Orientale. South is up; cf. Plate 36.2. Rectified; Y108; scale ~ 4.0 km/mm (1:4,000,000); col. 78°8.

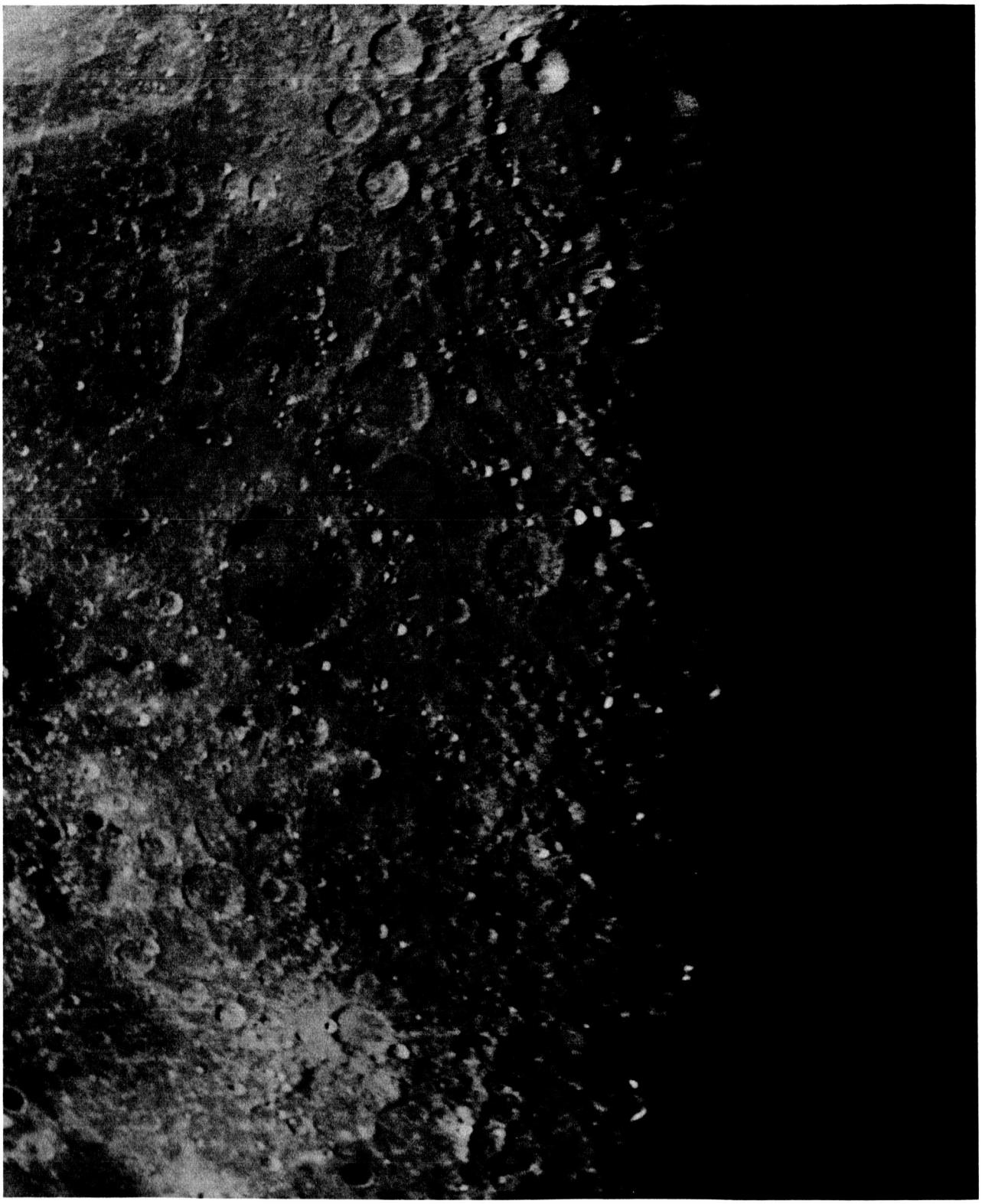


Plate 36.2. Radial system, extending SE from Mare Orientale. Many scarps and valleys are prominent. Compare with Plate 36.3 of same region in full sunlight. Rectified; Y1170; scale ~ 8.0 km/mm (1:8,000,000) col. 82°1.

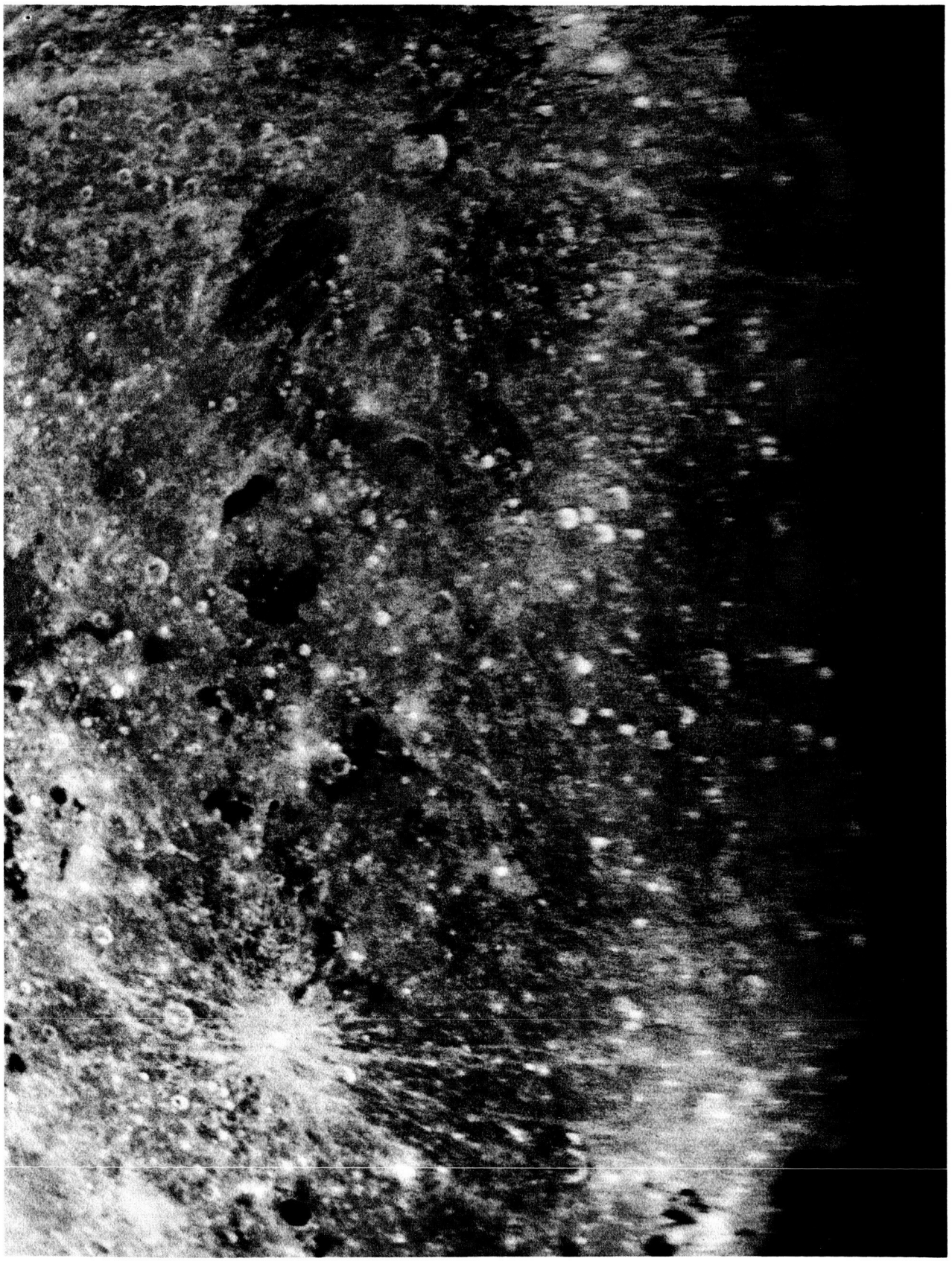


Plate 36.3. Same region at high lighting, showing lack of distinguishing photometric properties of radial structures. Rectified; Y1592; scale ~ 8.0 km/mm (1:8,000,000); col. 120°3.

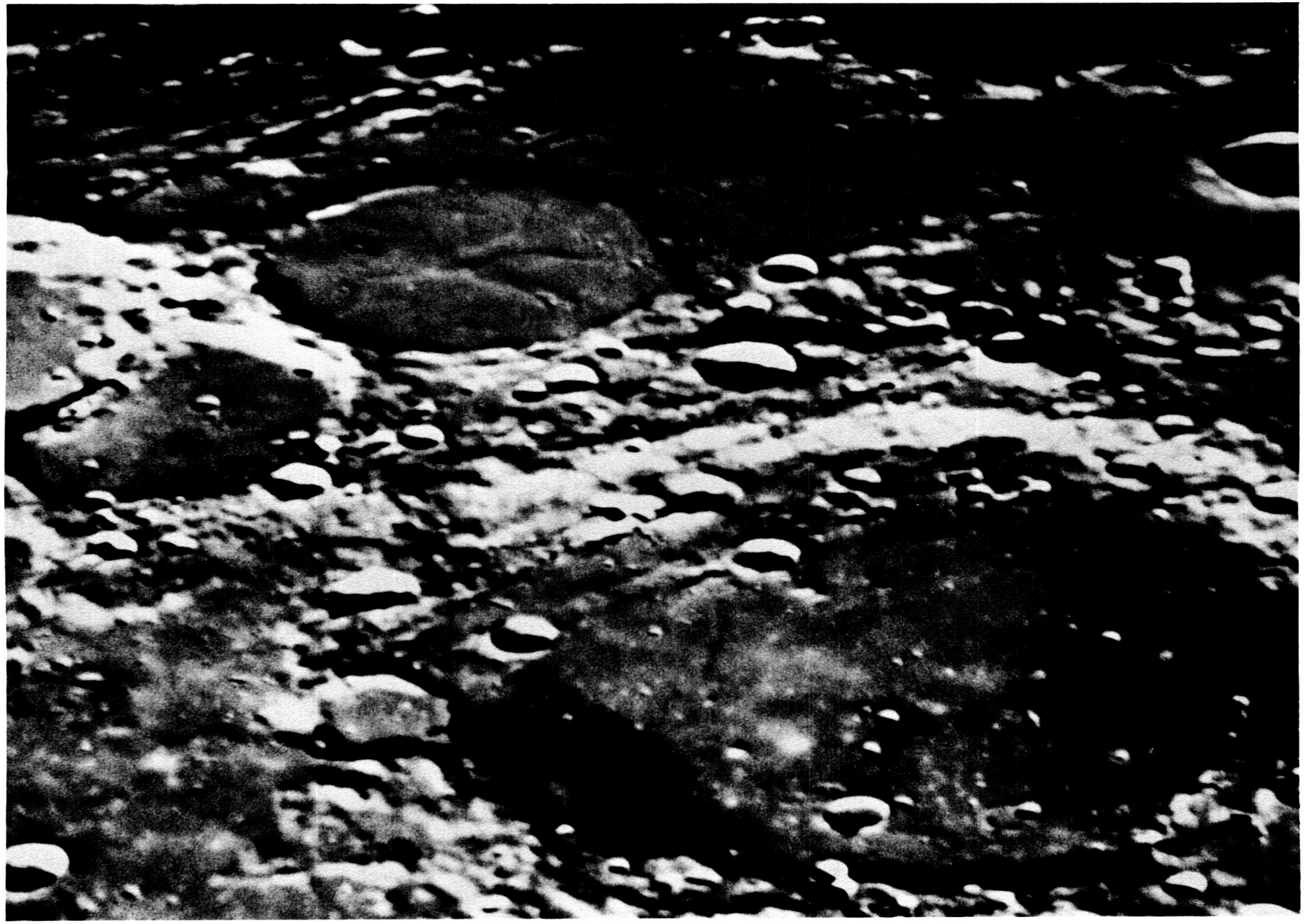


Plate 36.4. Valleys radial to Mare Orientale in and beyond Schickard. Valleys on the far floor of Schickard appear softened or buried. Compare those beyond Wargentin. Not rectified, Lick 120-inch, no. 33; scale ~ 1.0 km/mm (1:1,000,000); col. 67°8 (*Courtesy Lick Observatory*).



Plate 36.5. Region from E to N of Mare Orientale. Nearly orthogonal lineament pattern is prominent NE of basin. Rectified; M372; scale ~ 5.0 km/mm (1:5,000,000); col. 85°7.

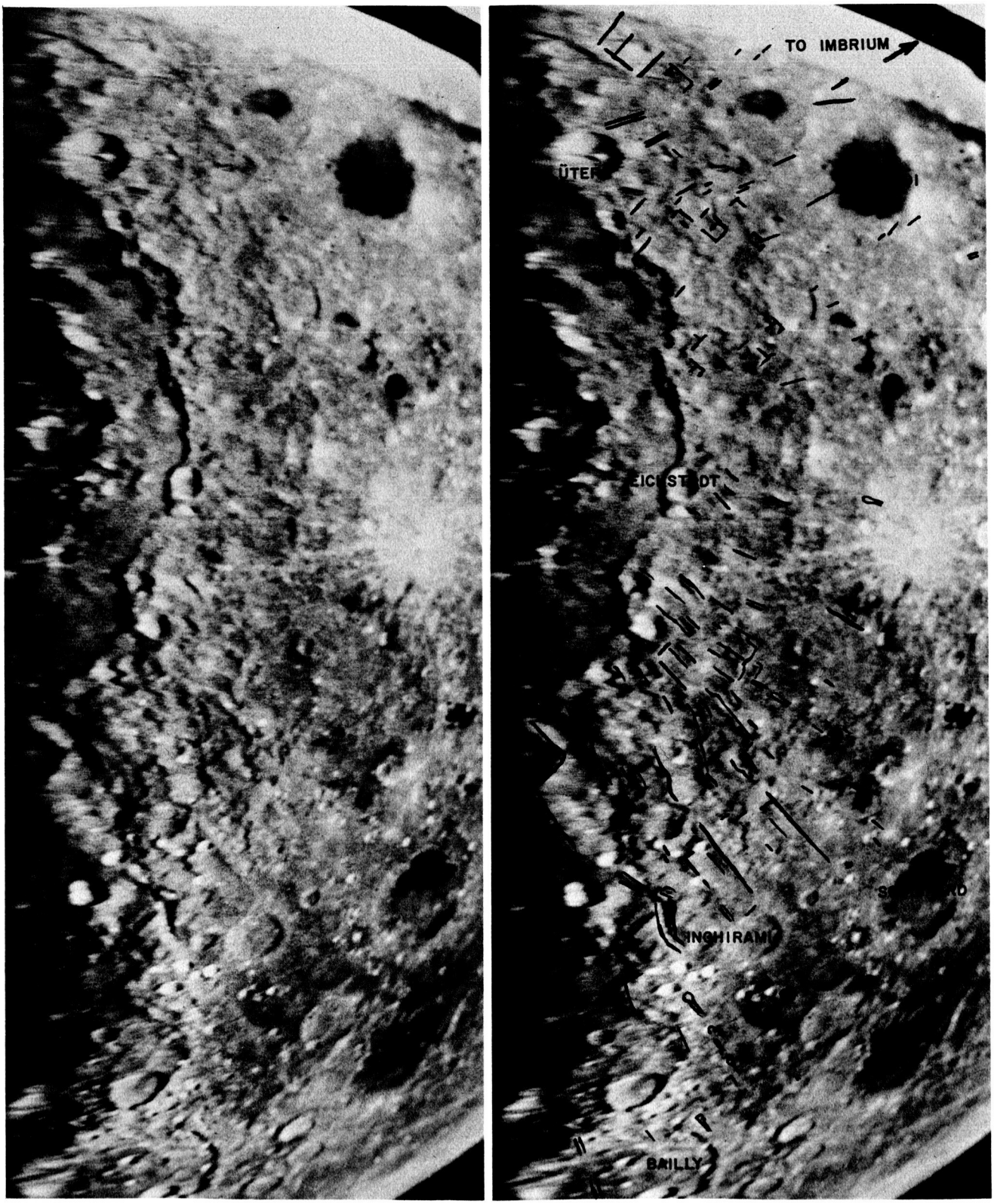


Plate 36.6. The Orientale basin system from an effective altitude of 4900 km above the surface. Overlay marks the most prominent members of the radial system. The concentric rings are clearly defined. Rectified; M74; scale ~ 8.0 km/mm (1:8,000,000); col. 88°9.

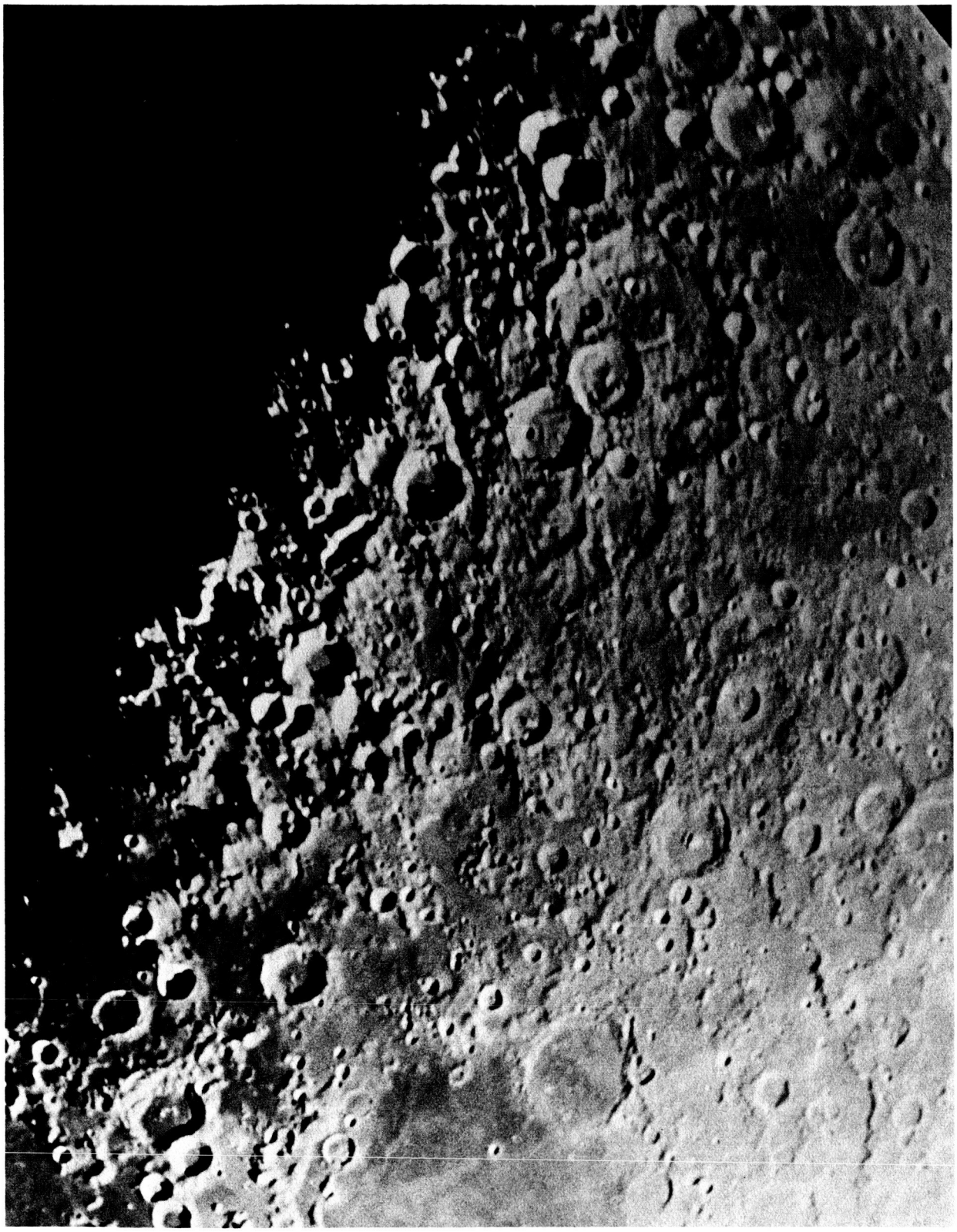


Plate 36.7. Low sun on the region SE of the Nectaris basin. Rheita Valley and W end of Snellius Valley are visible. For map and nomenclature of valleys, see Plate 36.12. Rectified; Y1310; scale ~ 6 km/mm (1:6,000,000); col. 127°1.

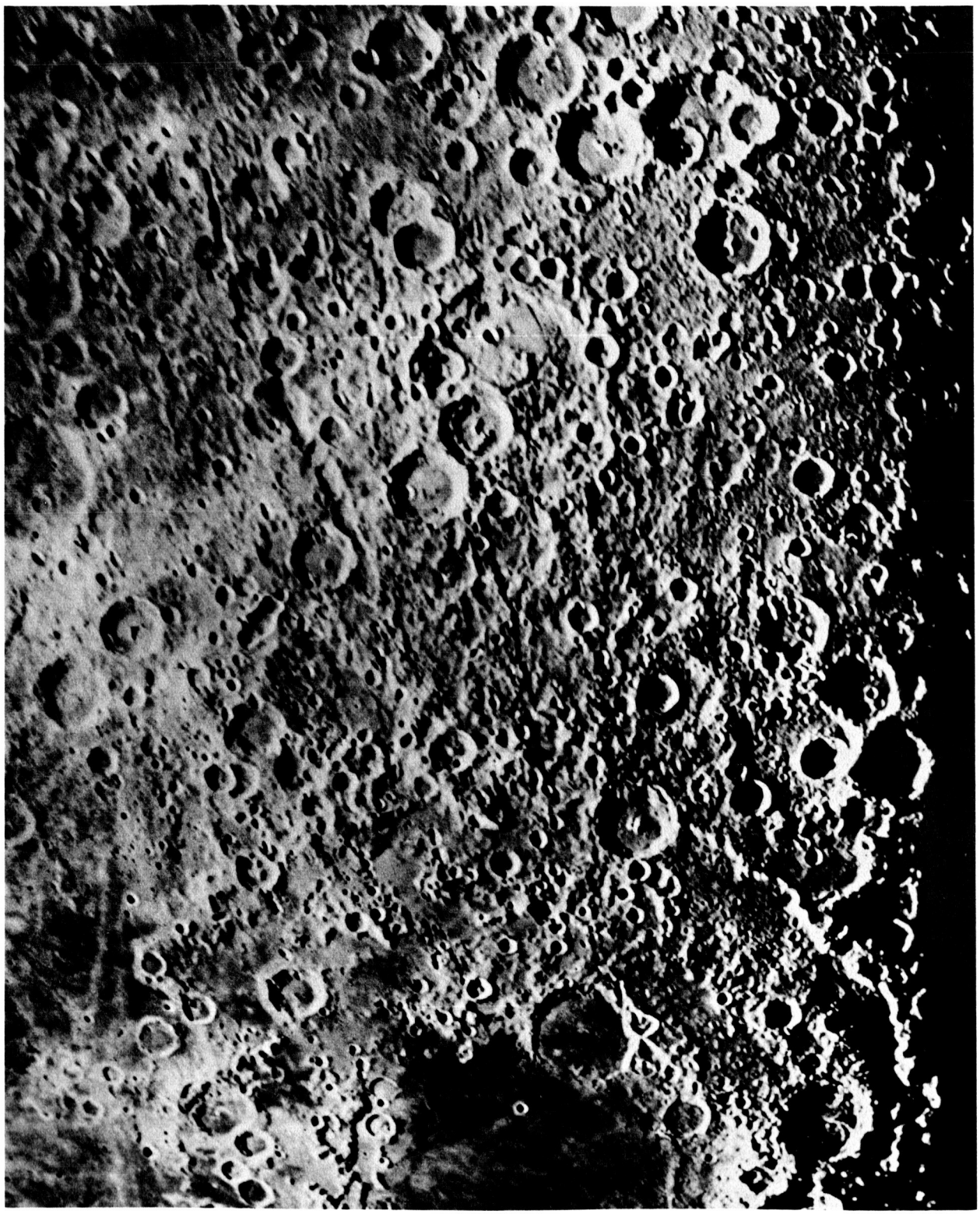


Plate 36.8. Valleys and other lineaments SSE of the Nectaris basin under sunrise lighting. Compare Plate 36.9 at same scale and orientation. Rectified; L193; scale ~ 6.0 km/mm (1:6,000,000); col. 338°9.

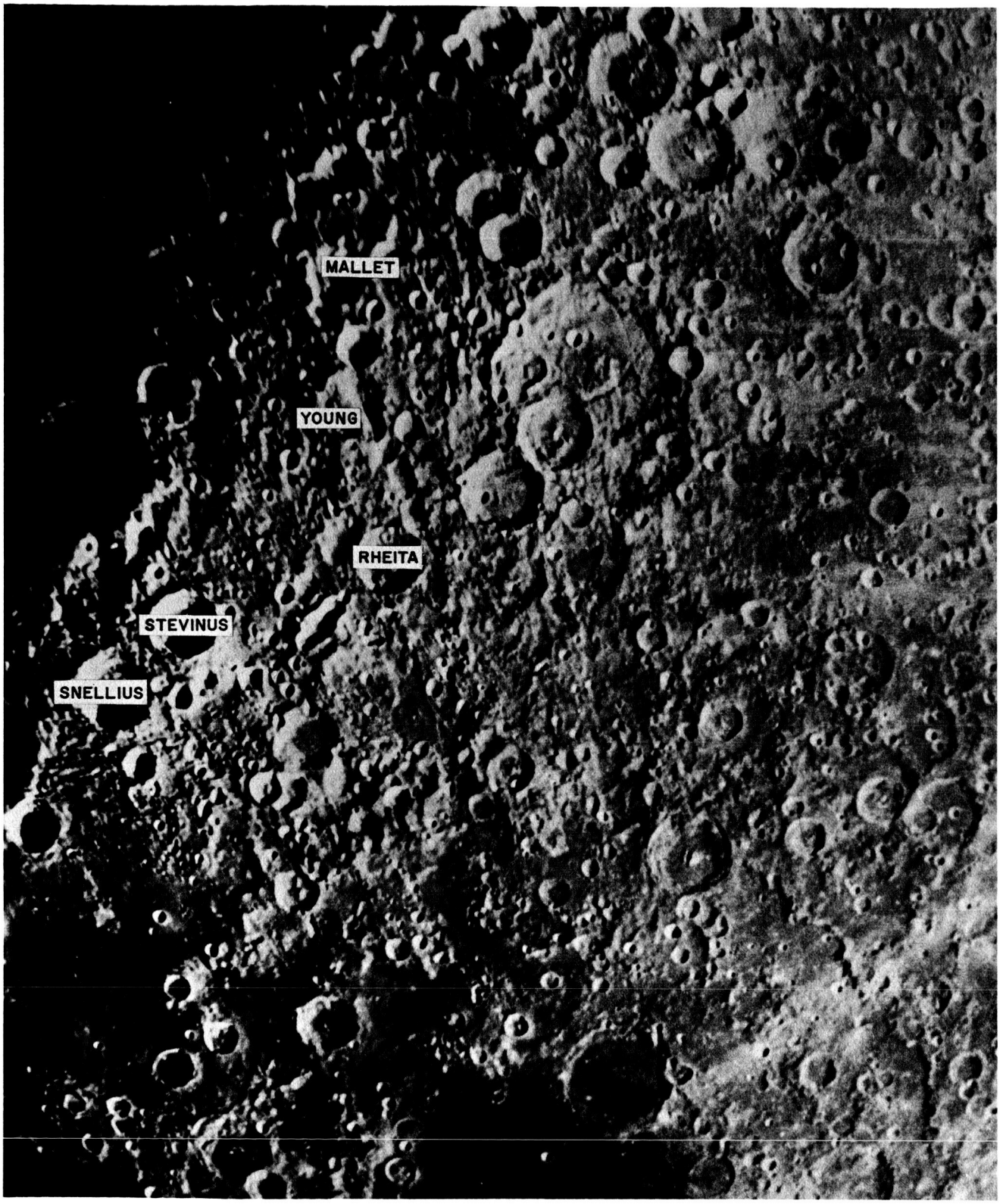


Plate 36.9. The same area under sunset lighting. Cf. Plate 36.8 at same scale and orientation. Rectified; Y1200; scale ~ 6.0 km/mm (1:6,000,000); col. 120°2.

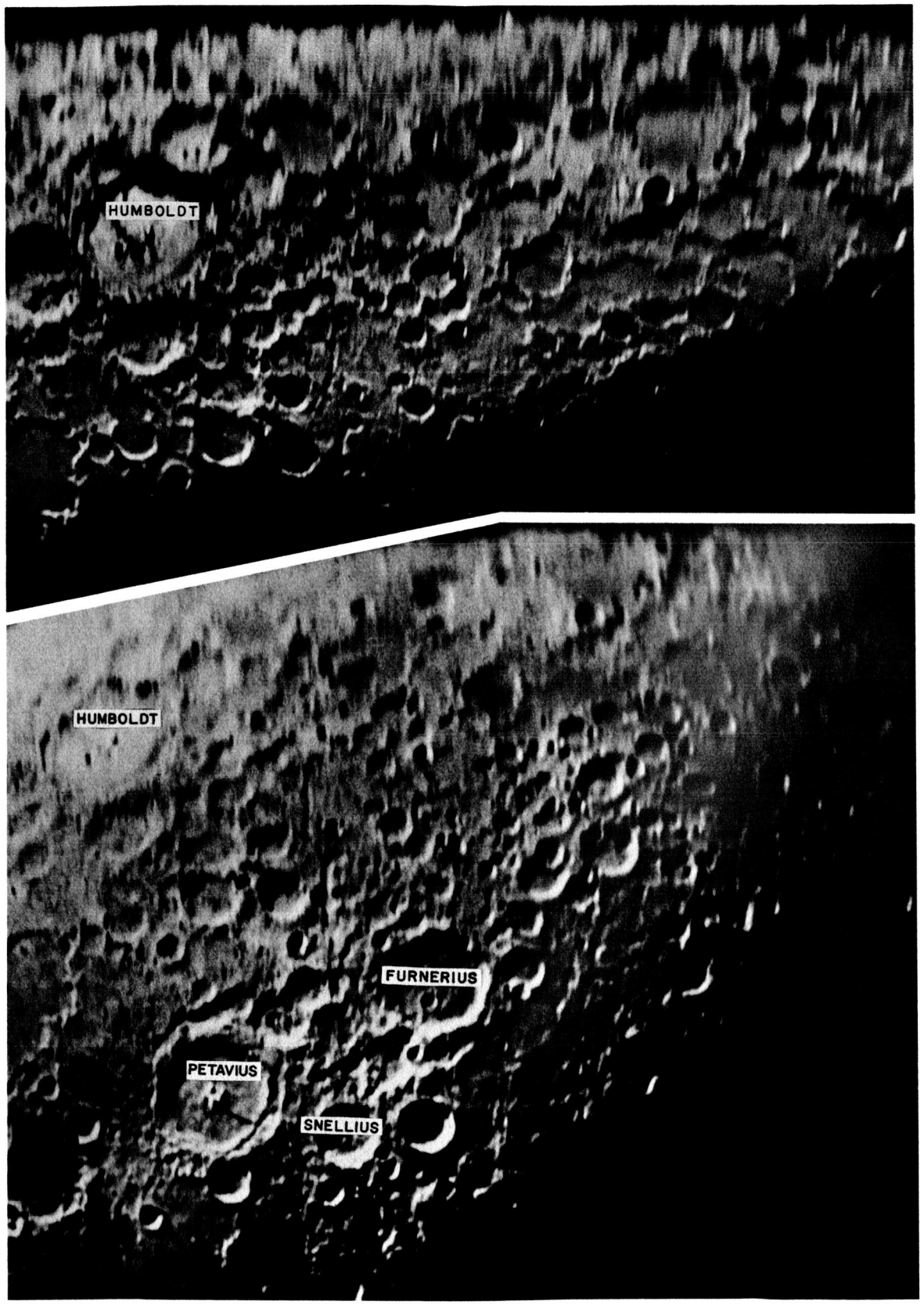


Plate 36.10. The limb ESE of the Nectaris basin, showing the eastward, *en échelon*, extension of the Snellius Valley. Total length of this valley is some 800 km. Cf. facing Plate 36.11. (*a*) Rectified; Y686; scale ~ 8 km/mm (1:8,000,000); col. 294°4. (*b*) Rectified; Y727; scale ~ 8 km/mm (1:8,000,000); col. 311°9.

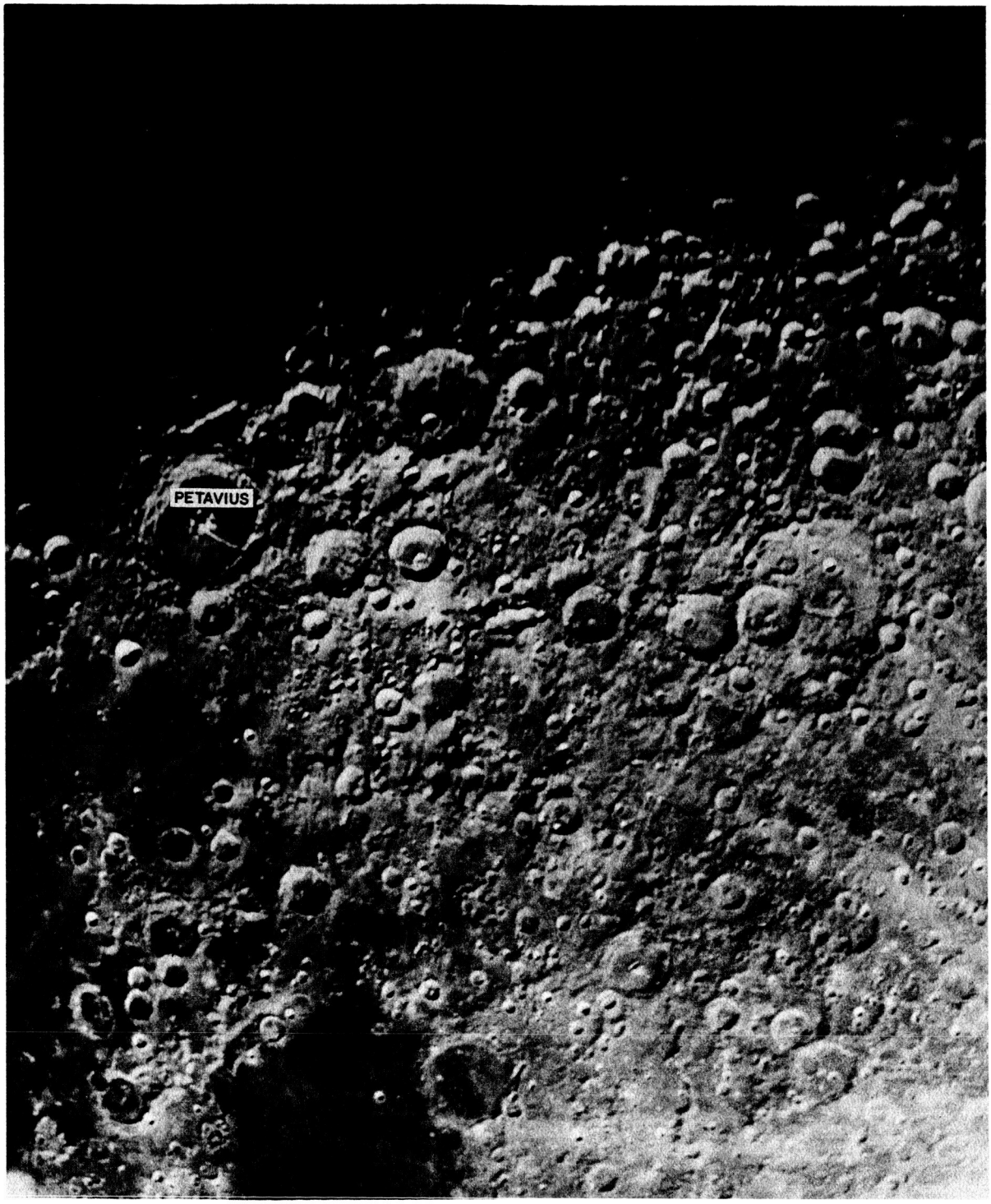


Plate 36.11. Region of major valleys ESE of the Nectaris basin. The W part of the Snellius Valley, running between Petavius and Furnerius, is well seen. Cf. Plate 36.10 for the eastward extension of this area. Rectified; Y369; scale ~ 8 km/mm (1:8,000,000); col. 113°1.

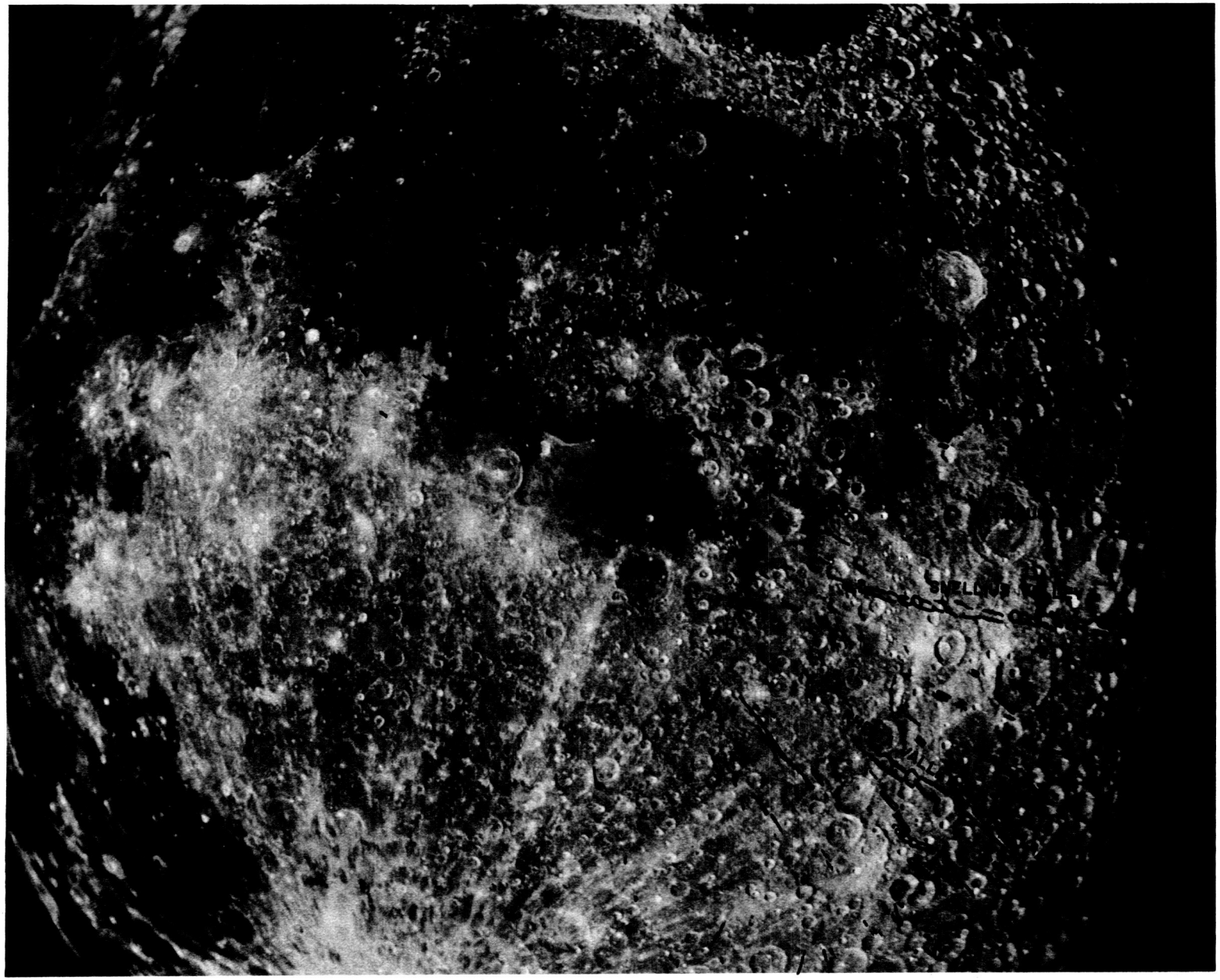


Plate 36.12. The Nectaris basin system. Overlay marks the most prominent lineaments, many converging toward a center in the Nectaris inner basin. In addition, it can be seen that the Imbrium radial pattern extends into this region. Rectified; Y482; scale ~ 12 km/mm (1:12,000,000); col. 100:8.

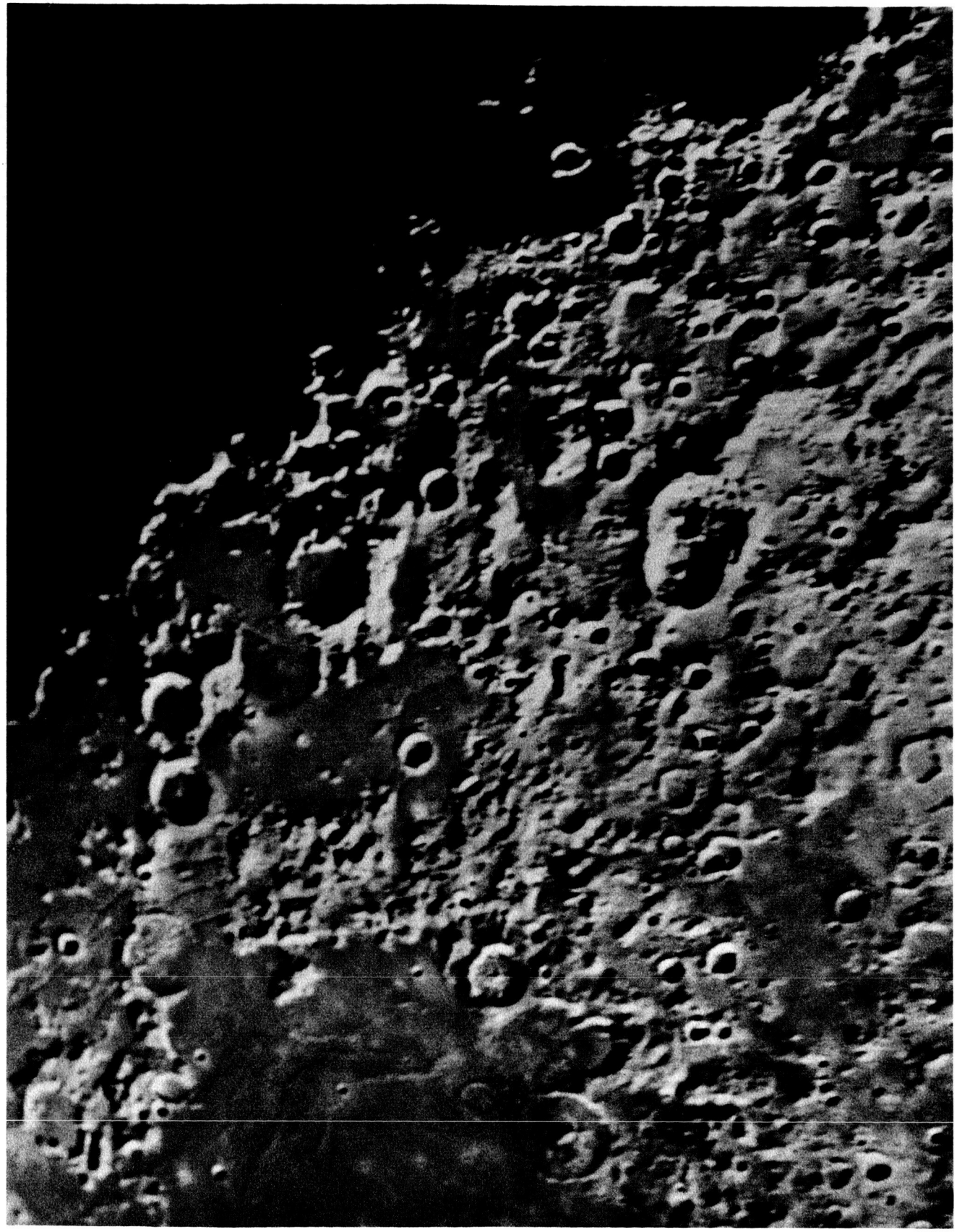


Plate 36.13. Region SE of the Humorum basin. A lineament pattern running vertically through the photograph may be recognized. Rectified; W171; scale ~ 4.0 km/mm (1:4,000,000); col. 202°6.



Plate 36.14. Orthogonal lineament pattern W of the Humorum basin, sunrise. Upper central part of photograph shows a region of damaged craters, ridges, and apparent rectilinear faults. Radial patterns also evident closer to the inner basin. Cf. facing Plate 36.15. Rectified; Y468; scale ~ 4.0 km/mm (1:4,000,000); col. 63°1.

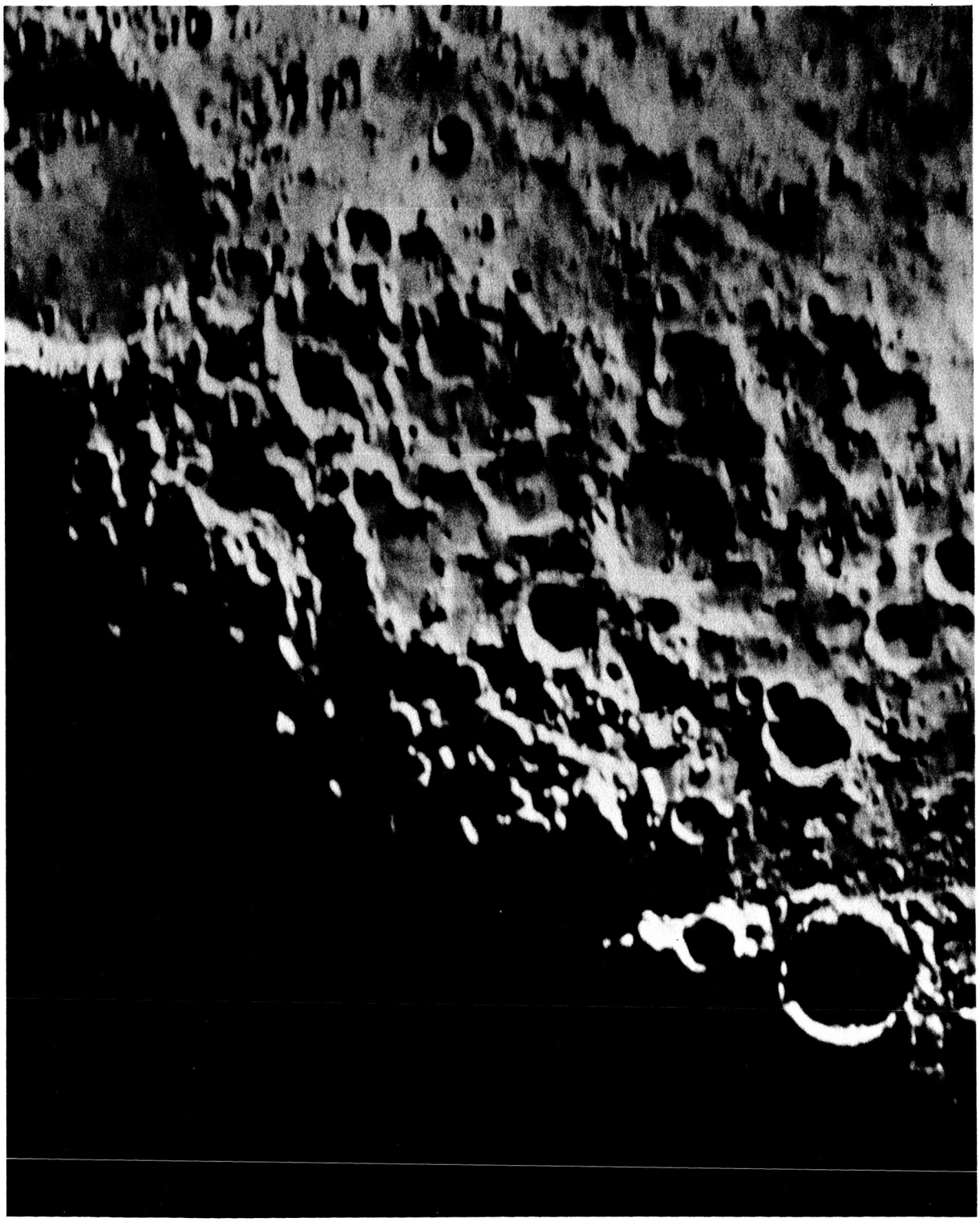


Plate 36.15. Same as Plate 36.14, sunset. This shows that the region has been partially flooded. Rectified; W230; scale ~ 4.0 km/mm (1:4,000,000); col. 229°1.

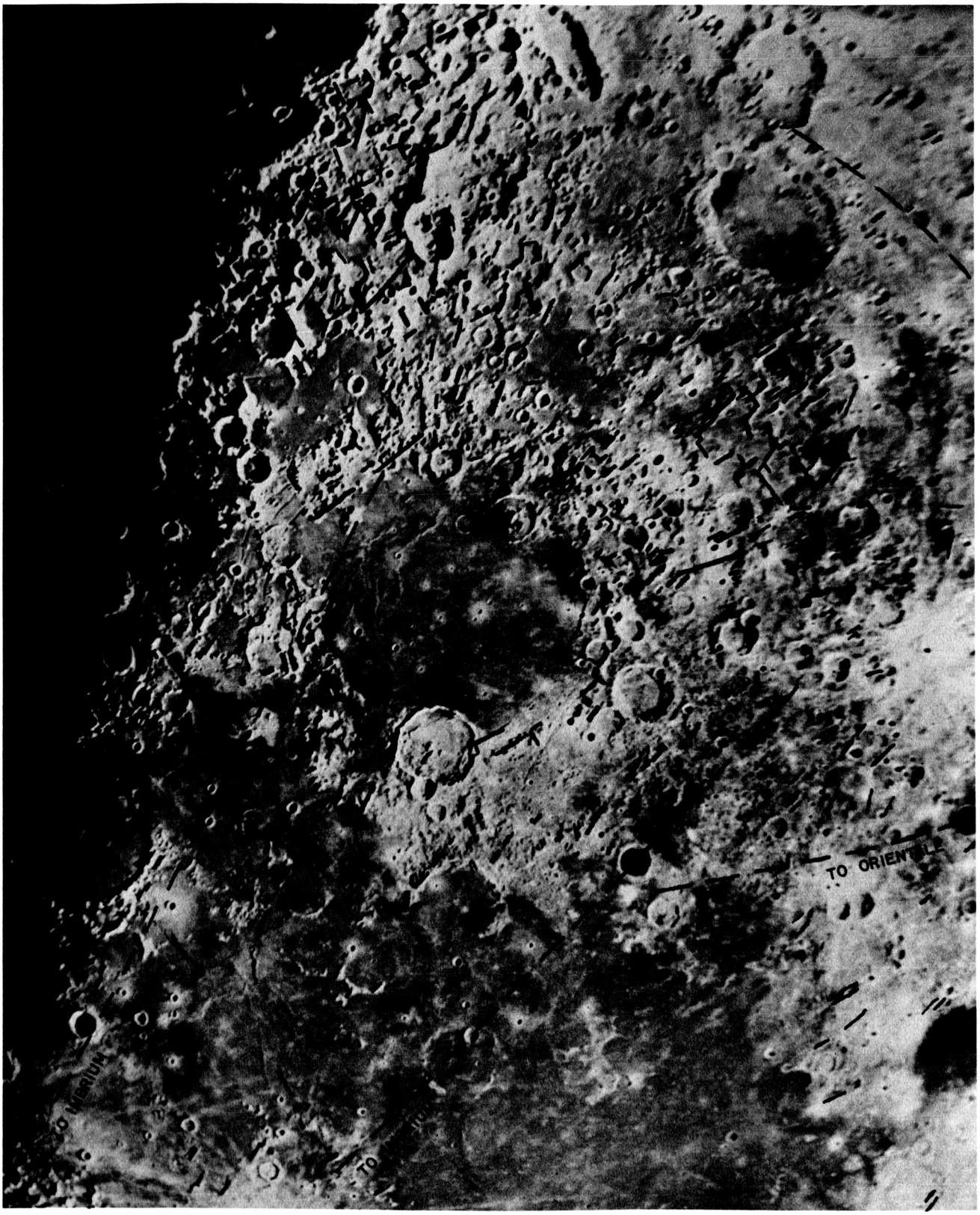


Plate 36.16. The Humorum basin system. The tendency for local parallelism can be seen. Dashed lines show directions to Imbrium center and Orientale center. Rectified; W172; scale ~ 8.0 km/mm (1:8,000,000); col. 202°6.

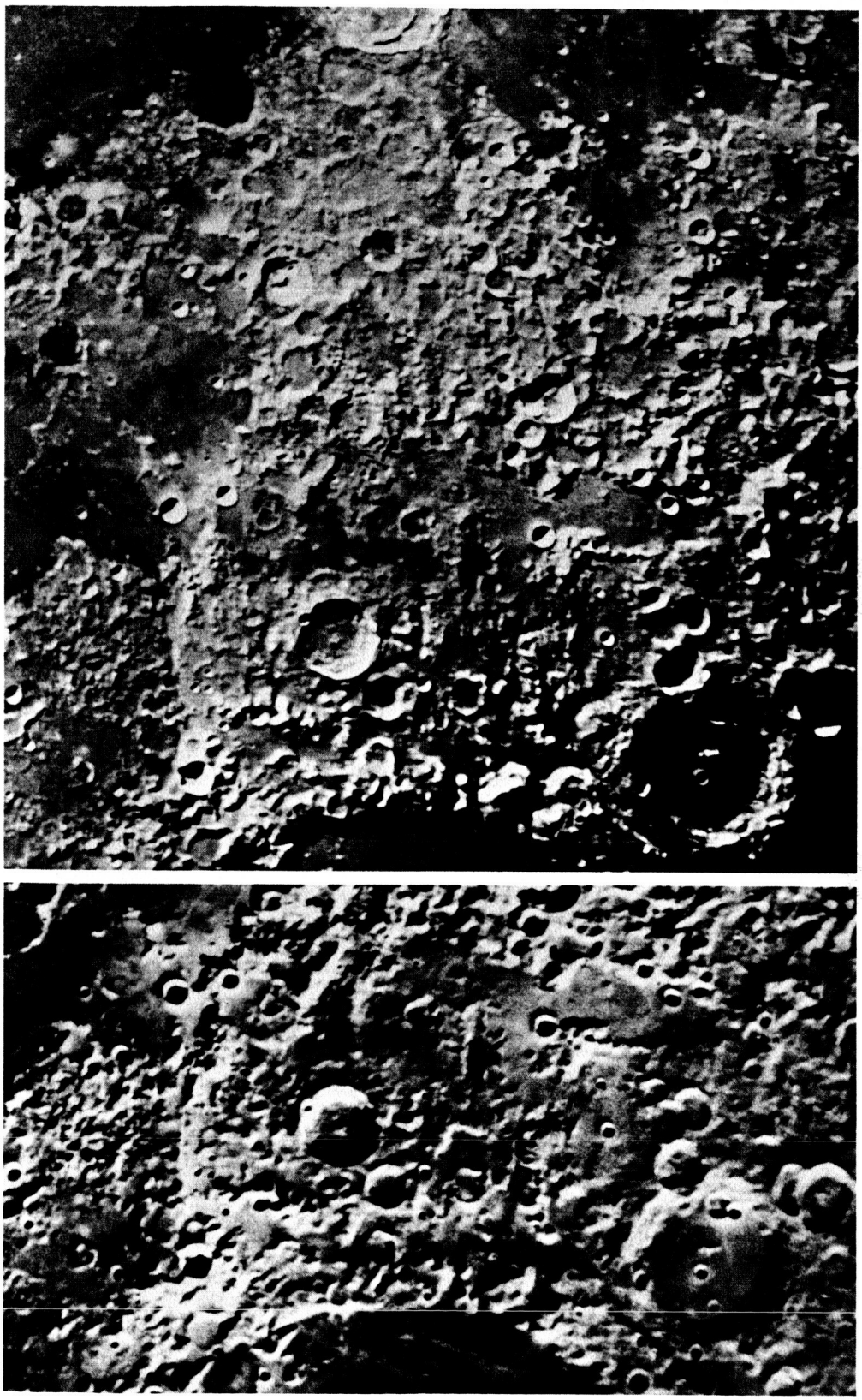


Plate 36.17. Lineaments NW of the Crisium inner basin, between the two major rings of the concentric system. Note the juxtaposition of the local flooding and the lineaments. (*a*) Rectified; Y1206; scale ~ 5.0 km/mm (1:5,000,000); col. 120°5; (*b*) rectified; L175; scale ~ 5.0 km/mm (1:5,000,000); col. 328°7.

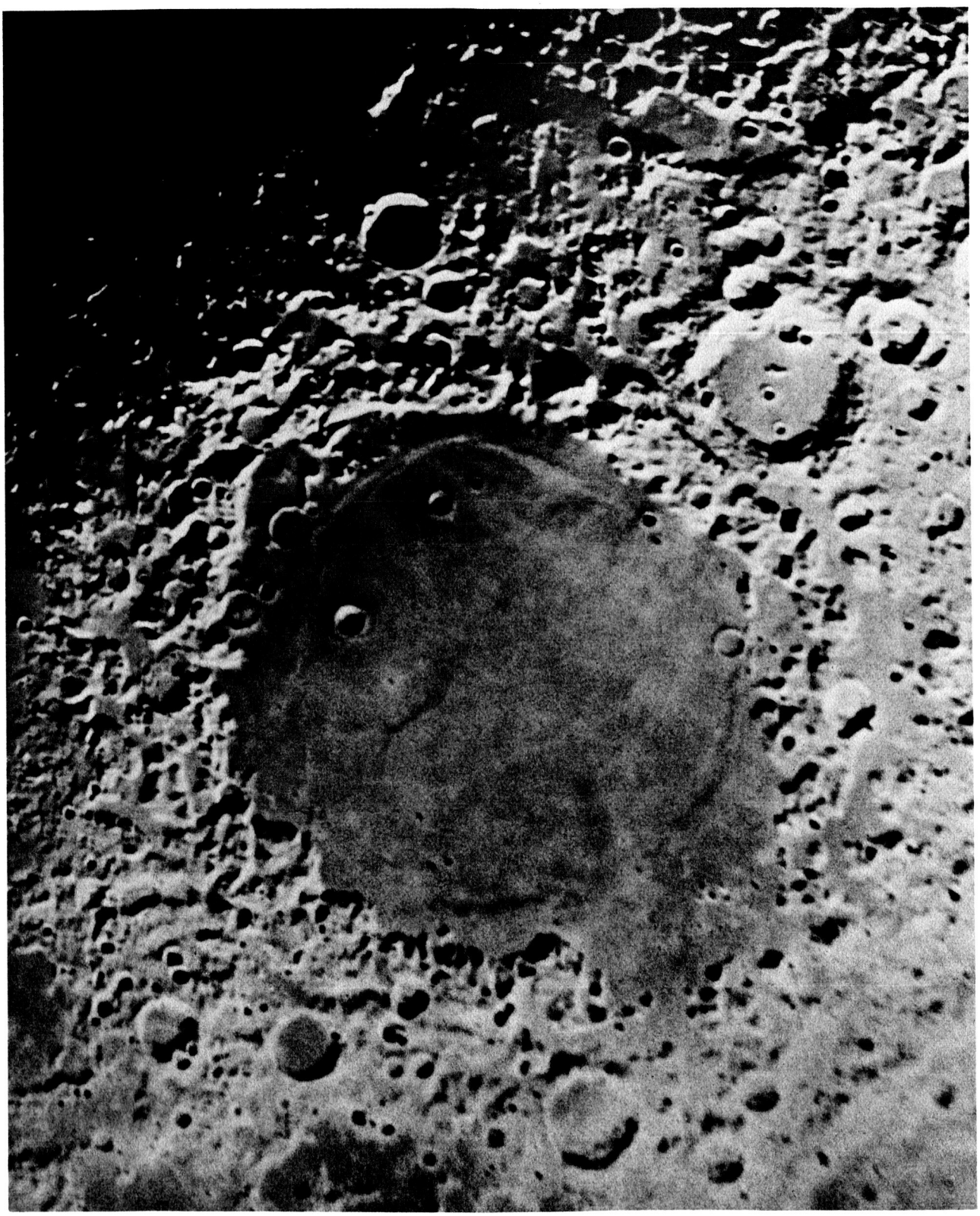


Plate 36.18. Mare Crisium at sunrise. Note step-pattern of lineaments in NW wall (lower left). Rectified; Y784; scale ~ 4.5 km/mm (1:4,500,000); col. 317°1.

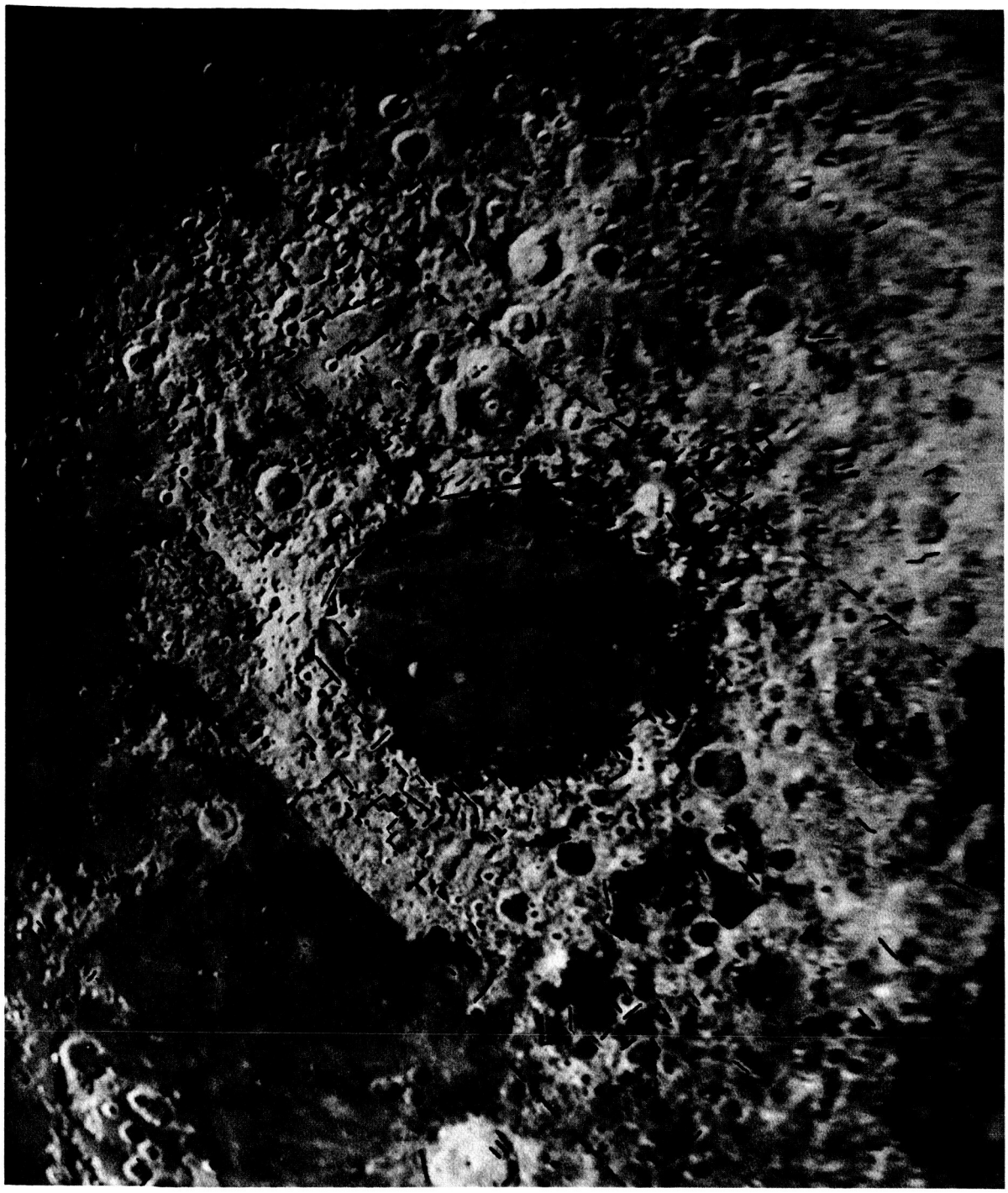
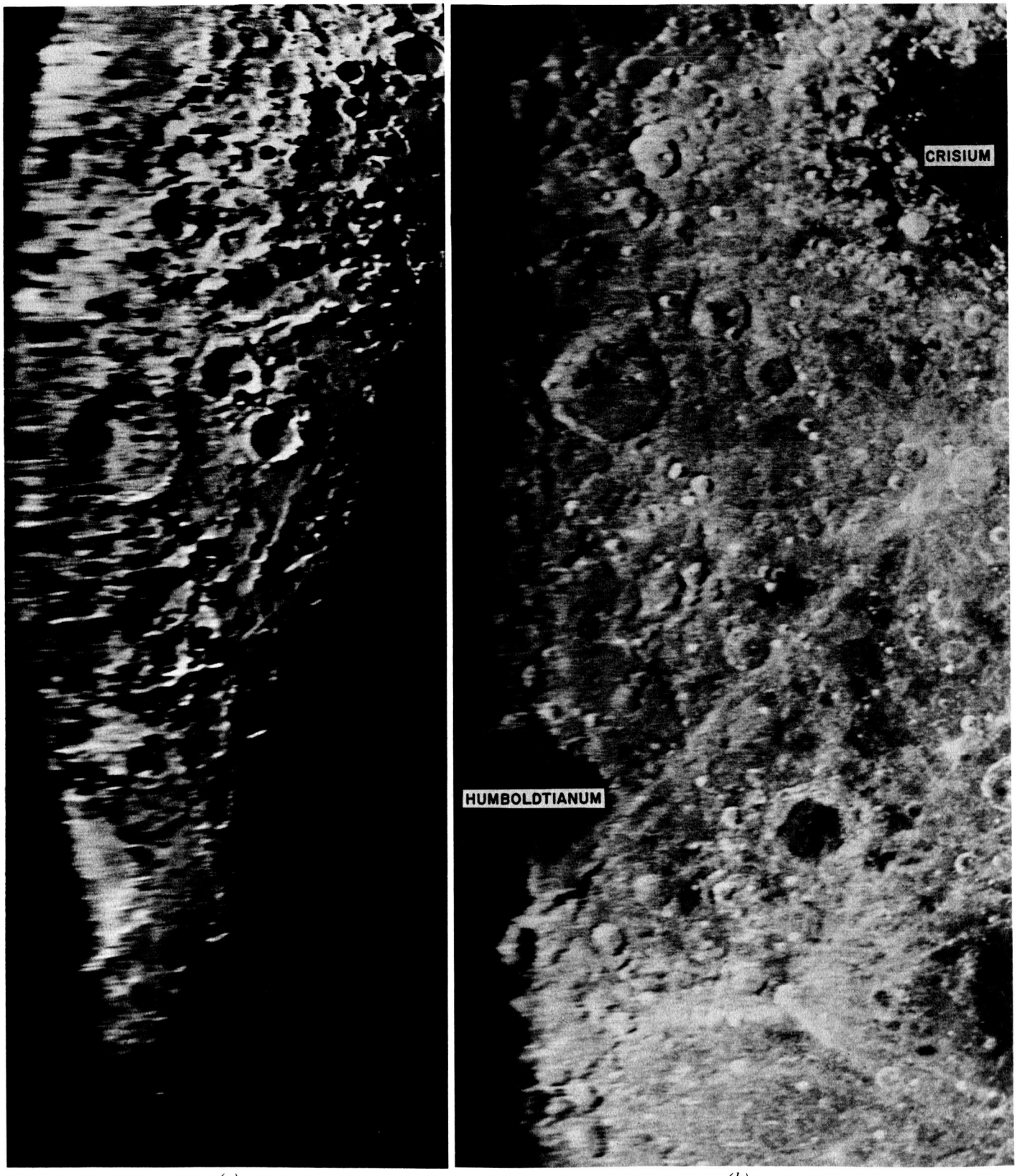


Plate 36.19. The Crisium basin system, showing prominent lineament patterns. The lack of complete symmetry with the Imbrium basin rules out the possibility that all these are outlying members of the Imbrium system. Rectified; Y738; scale ~ 8.0 km/mm (1:8,000,000); col. 337°5.



(*a*) (*b*)

Plate 36.20. Environs of the Humboldtianum basin. Plate (*a*) shows the "ghost scarps" between Humboldtianum and Crisium. Compare facing plate. (*a*) Sunrise; rectified; Y686; scale ~ 8.0 km/mm (1:8,000,000); col. 294°4; (*b*) sunset; rectified; L237; scale ~ 8.0 km/mm (1:8,000,000); col. 87°8.

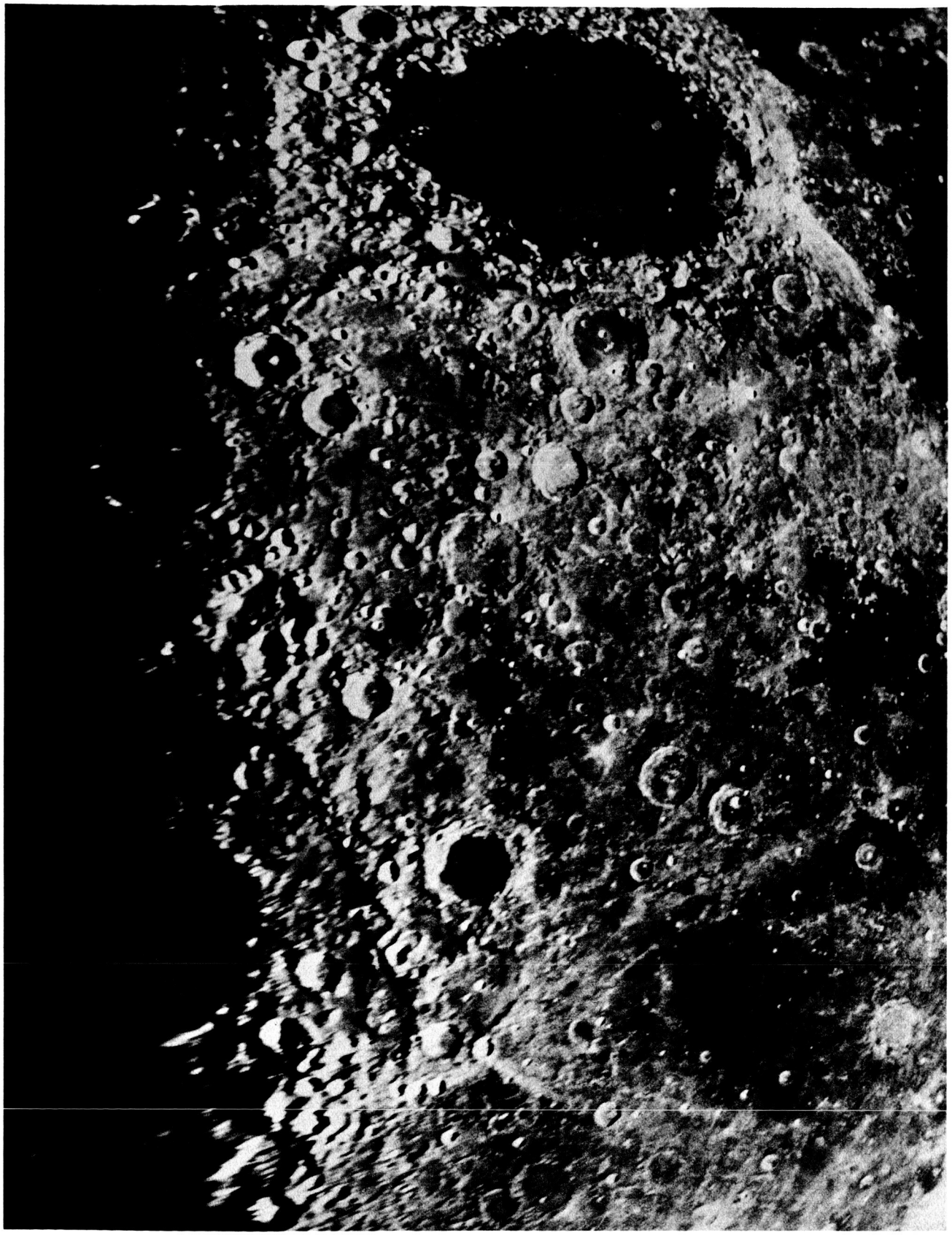
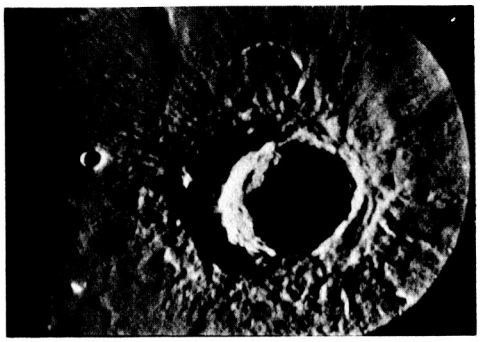
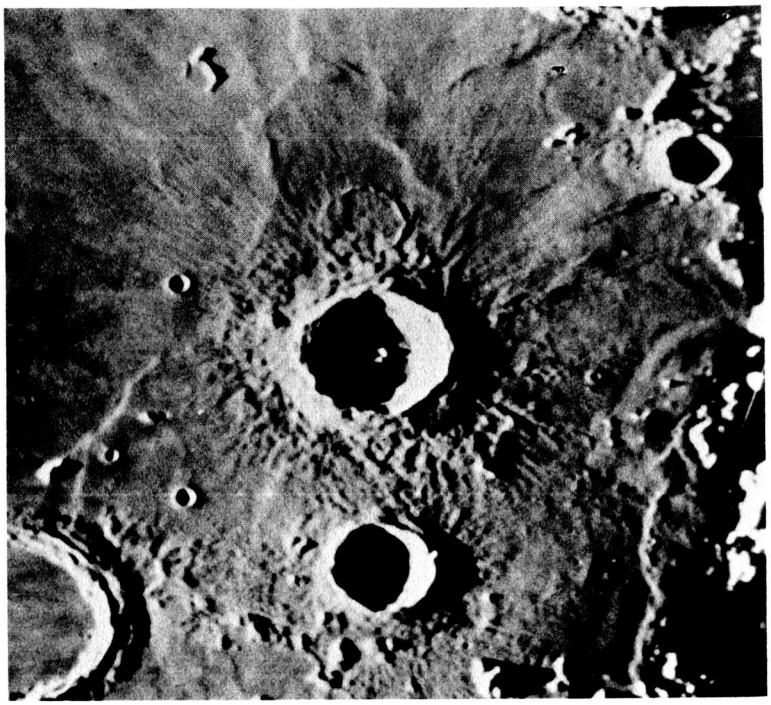


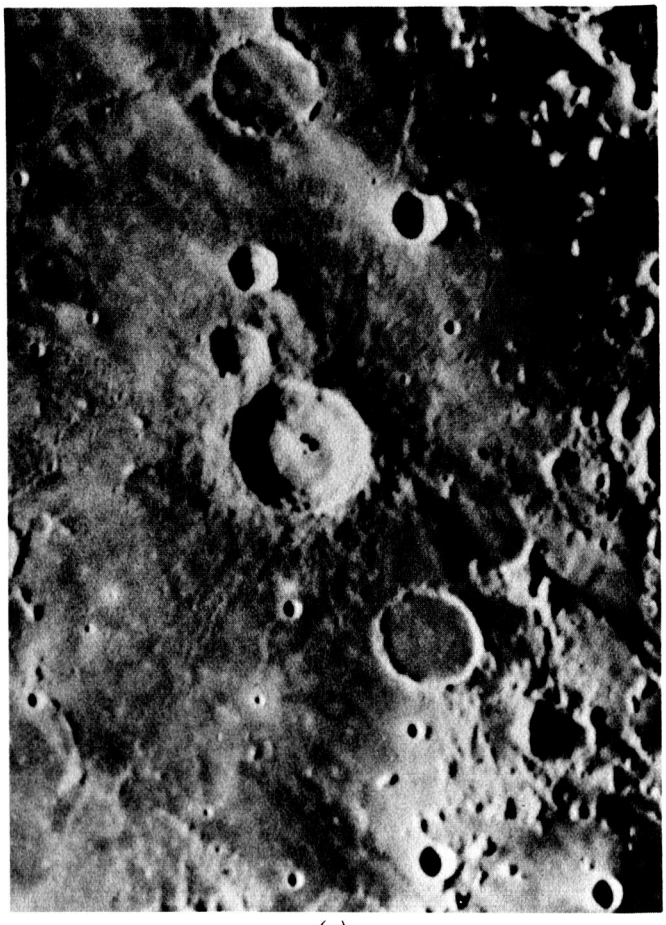
Plate 36.21. Environs of the Humboldtianum basin. The two "ghost scarps" between Crisium and Humboldtianum are well shown. Between the inner and outer rings of the Humboldtianum basin system is a radial scarp, apparently bordered on the lower side by patches of maria, as seen on facing Plate 36.20b. Rectified; Y482; scale ~ 8.0 km/mm (1:8,000,000); col. 100°8.



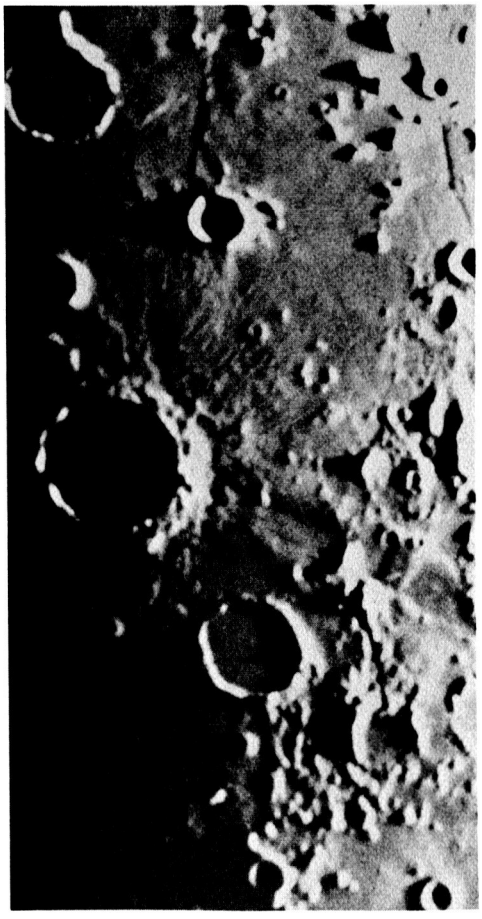
(a)



(b)

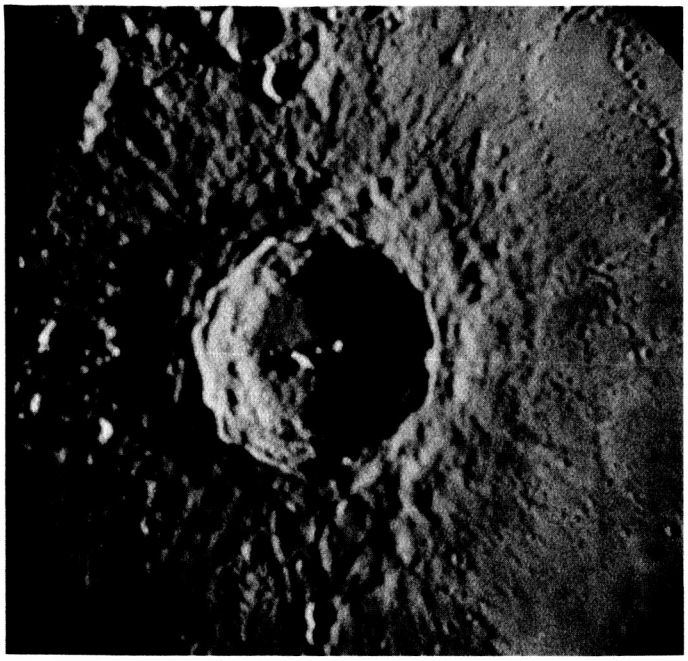


(c)

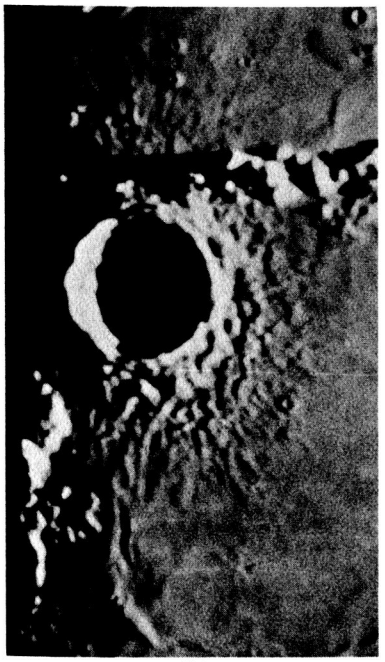


(d)

Plate 36.22. Four photographs of radial systems around craters. These lineaments are finer and of different character than those around basins. Scale ~ 3 km/mm. (*a*) Aristillus; Pic du Midi, Mar. 21, 1945; col. 6°2; (*b*) Aristillus; W121; col. 172°1; (*c*) Bullialdus; L163; col. 38°2; (*d*) Bullialdus; W171; col. 202°6.



(a)



(b)



(c)



(d)

Plate 36.23. Four photographs of radial systems around craters. Note rilles trailing out of small pits in (*d*). Scale ~ 3 km/mm (*a*) Copernicus; McDonald, Mar. 19, 1959; col. 24°0; (*b*) Eratosthenes; Y1267; col. 13°5; (*c*) Copernicus; Pic du Midi 37b; col 22°9; (*d*) Aristarchus; M624; col. 50°0.

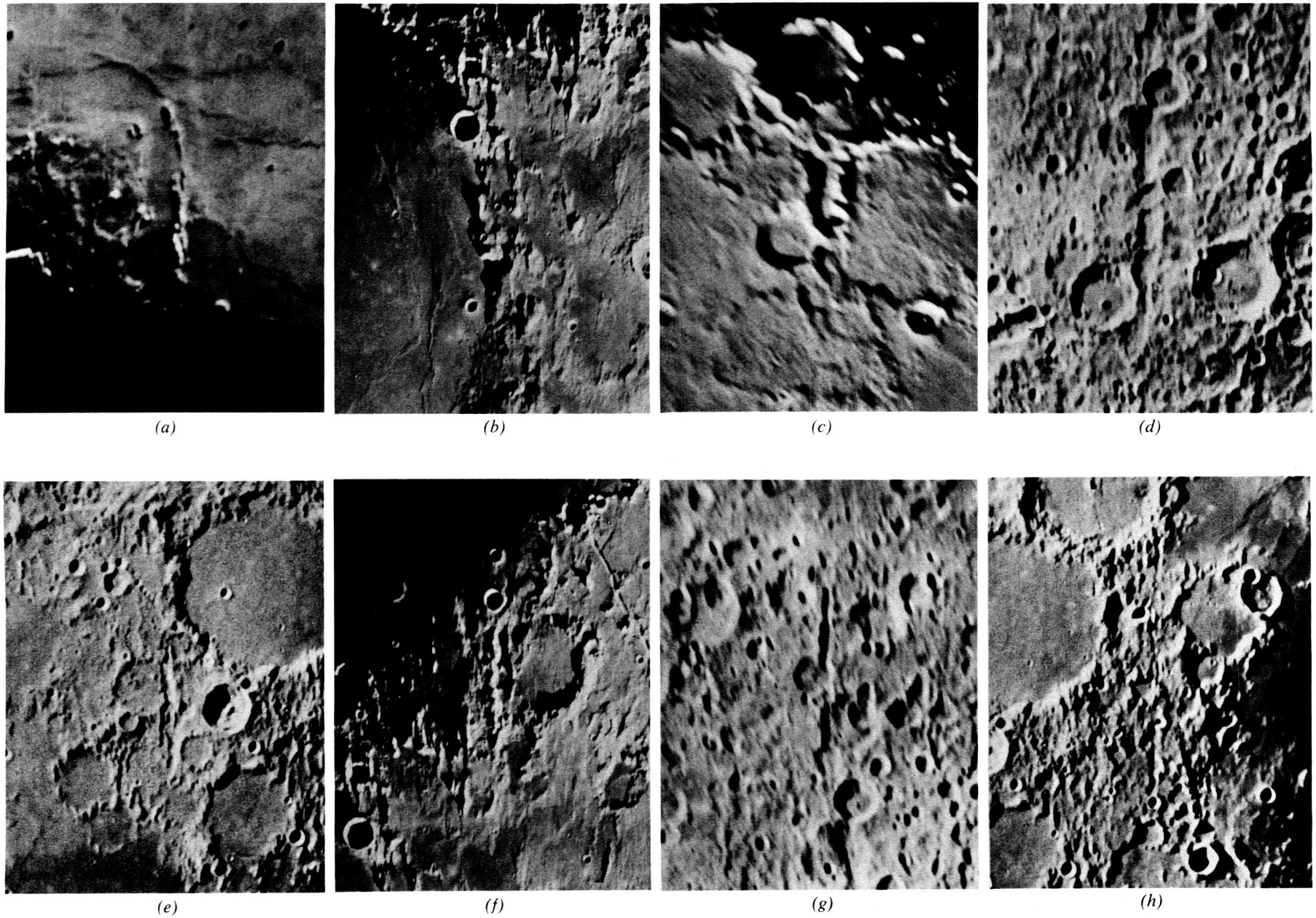


Plate 36.24. Valleys and troughs of radial systems. Direction toward basin is downward. Scale ~ 5 km/mm. (*a*) Trough on N edge of Aristarchus plateau; Imbrium system; ~ 34 × 170 km; W231; (*b*) trough in Haemus Mts.; Imbrium system; ~ 30 × 110 km; W111; (*c*) trough in wall of W. Bond; ~ 28 × 140 km; Y1350; (*d*) Rheita Valley; Nectaris system; ~ 25 × 330 km; L193; (*e*) valley E of Herschel; Imbrium system; ~ 11 × 94 km; Y1261; (*f*) valley in NE wall of Julius Caesar; Imbrium system; ~ 17 × 85 km; W111; (*g*) Mallet Valley; Nectaris system; ~ 12 × 190 km; (*h*) multiple valley W of Ptolemaeus; Imbrium system; ~ 6 × 230 km; Y1261.

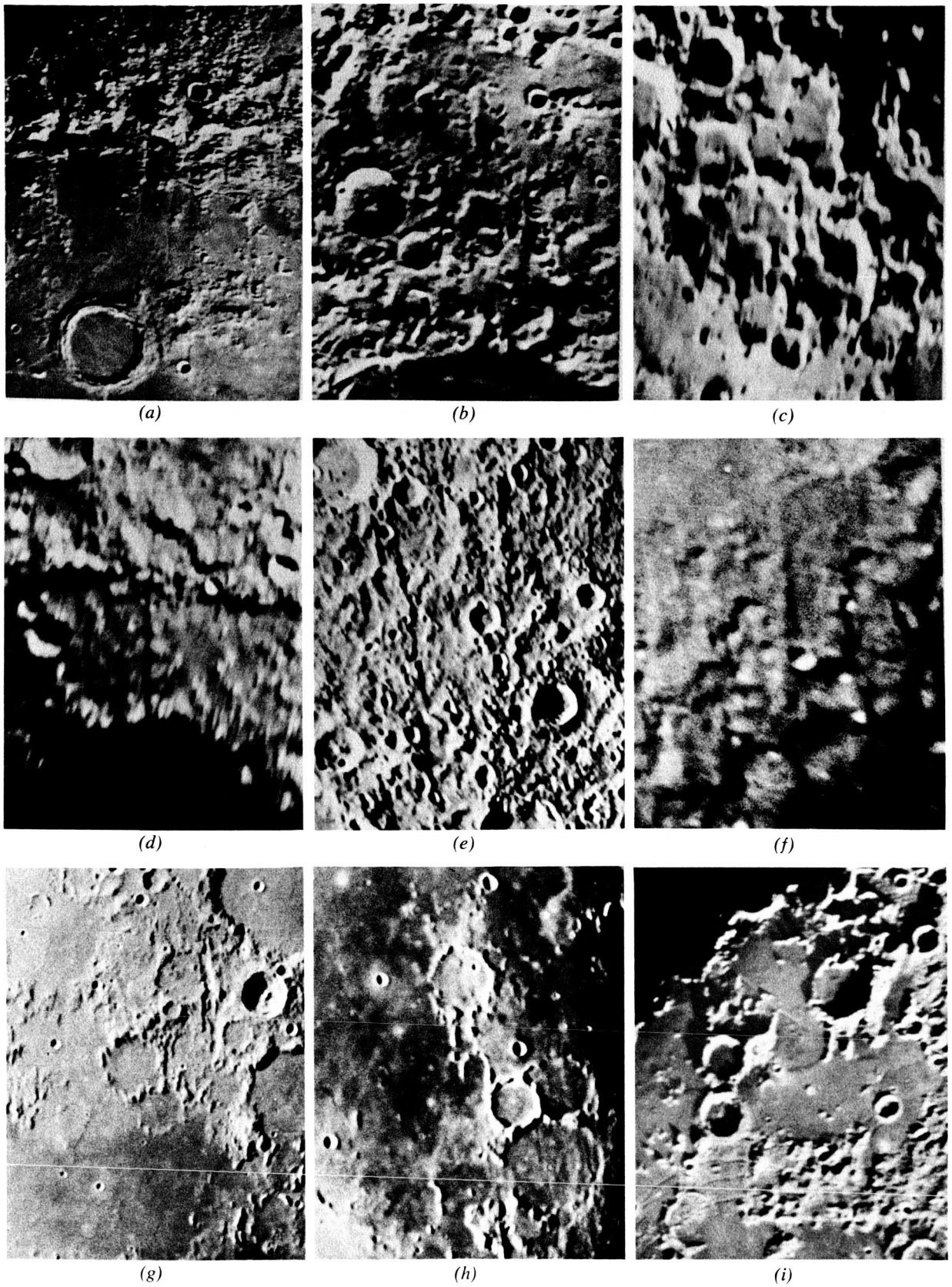


Plate 36.25. Orthogonal lineaments (*a*, *b*, and *c*), scarps (*d*, *e*, and *f*), deformed craters (*g*, *h*, and *i*) of radial systems. Direction toward basin is downward. Scale ~ 5 km/mm. (*a*) Partial flooding and lineaments near Archimedes; Imbrium system; W115; (*b*) partial flooding and lineaments near Macrobius; Crisium system; L175; (*c*) partial flooding and lineaments near Schickard; Humorum system; W230; (*d*) scarp radial to Humboldtianum; Y482; (*e*) scarps radial to Nectaris; L193; (*f*) scarps radial to Orientale; Y1170; (*g*) Réaumur and Oppolzer; Imbrium lineaments; Y1261; (*h*) Parry M; Imbrium lineaments; Y557; (*i*) Palus Epidemiarum; Humorum lineaments; W171.

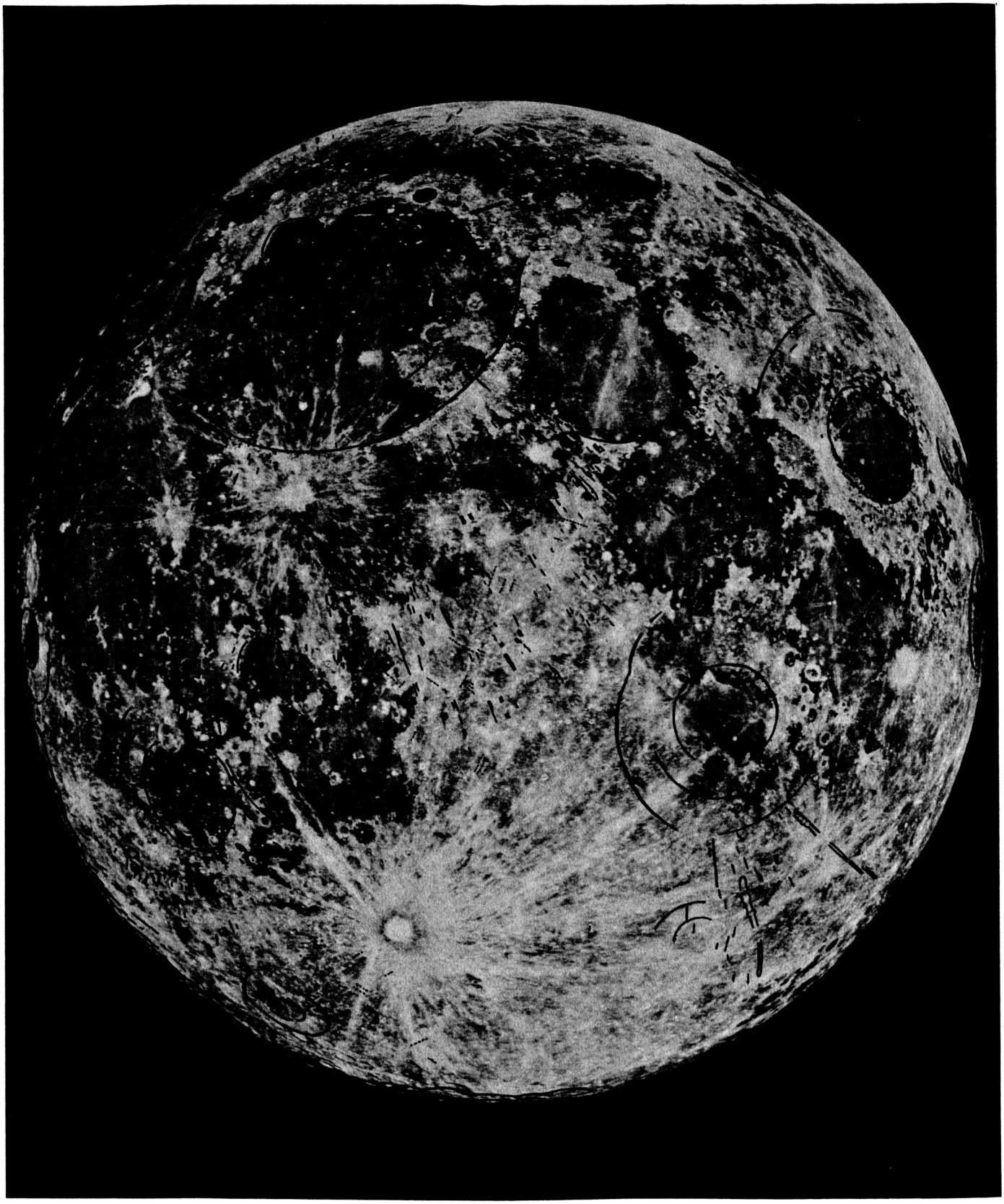


Plate 36.26. Full moon with overlay showing the basin systems discussed here. Each line marks a concentric arc or a relatively prominent lineament and each is drawn to proper scale and orientation. Dotted lines give examples of some prominent local grid patterns, not related to basin systems. Not rectified; L224; scale ~ 19 km/mm; col. 82°2.

NO. 37. COMPARISON OF THE INFRARED SPECTRUM OF MARS WITH THE SPECTRA OF SELECTED TERRESTRIAL ROCKS AND MINERALS

by ALAN B. BINDER* AND DALE P. CRUIKSHANK*

March 17, 1963

ABSTRACT

Infrared studies indicate that spectra of certain weathered igneous rocks match the infrared reflection spectrum of Mars.

1. Introduction

In recent years attempts have been made to match the albedo, color excess, and polarization of Mars with those characteristics of terrestrial rocks. Kuiper (1952) observed the reflection spectra of a number of rock samples from 0.8–1.8 μ and found that hematite, yellow volcanic ash, and sandstone were a poor match; but that a brownish, felsitic rhyolite matched the spectrum of the bright areas of Mars fairly well. Sharonov (1961) has found that in the visual part of the spectrum, the albedo and color excess of earthly, ochre-colored limonite ($FeO(OH) \cdot nH_2O$) closely approximate the Mars data. Dollfus (1961) also found visually that powdered limonite has polarization properties equivalent to Mars. Using Kuiper's same Mars spectra, Draper, *et al.* (1964) compared spectra of synthetic mixtures of goethite and hematite, but their laboratory data were obtained with a spectrometer and detector different from that used for making the Mars spectra and without a cross calibration of the instruments. Therefore, their data cannot be accurately compared with Kuiper's spectra.

During the past year the problem has been reinvestigated at the Lunar and Planetary Laboratory. Dr. Kuiper observed Mars on August 12, 1963 with the 82-inch telescope of the McDonald Observatory, using the low-dispersion mode of the infrared spectrometer described previously (Kuiper *et al.*, 1962). The laboratory and solar comparisons were obtained by the authors in Tucson with the same equipment and matching resolution. The detector was a 0.1 mm PbS cell used with a rapid scan rate (1.3 μ per minute), giving a resolution ($\lambda/\triangle\lambda$) of about 60 at 1.5 μ. This resolution is sufficient to resolve the CO_2 bands at 2.01 and 2.06 μ. The solar comparisons were made from an illuminated MgO block, which, however, may not have been neutral "white".

2. Discussion

The rock and mineral samples were observed using solar illumination in the laboratory in Tucson. A representative spectrum of weathered rhyolite is shown in Figure 1. The deep absorptions at 1.13, 1.39, and 1.87 μ are due to terrestrial water vapor. The four maxima between these absorptions constitute the points measured. For such measures to be consistent the water vapor content of the atmosphere must be reasonably constant. The data were reduced by setting the amplitude of the 1.25 μ maximum equal to 1.00 and then measuring the amplitudes of the 1.05, 1.55, and 2.1 μ maxima on this arbitrary scale. The intensity ratios of Mars and of samples of sun + MgO were taken at each of the four wavelengths and their values plotted in Figures 2, 3, and 4. The spectra are limited on the short-wavelength end by the sensitivity of the PbS cell and on the long-wavelength end by the H_2O absorptions at 2.7 μ and the reduced solar intensity.

The four wavelengths used cover an interval of 1.05 μ, one octave. This portion is not affected by

*Jointly of Department of Geology and Lunar and Planetary Laboratory, University of Arizona.

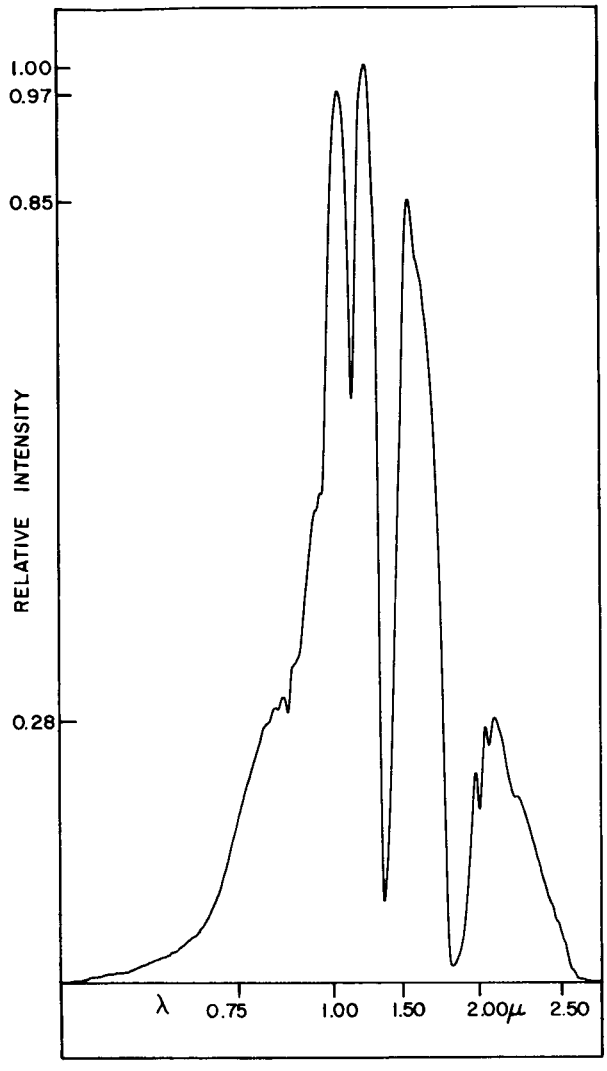


Fig. 1. Representative tracing of the reflection spectrum of rhyolite with limonite stain.

the strong scattering in the atmosphere of Mars in blue light, though the 1.55 and 2.1 μ maxima will be somewhat affected by terrestrial and Martian CO_2. To circumvent the terrestrial CO_2 correction, one may observe the comparison samples with the sun at approximately the same zenith distance as for the Mars observations, as was done. Corrections for the Martian CO_2 were not made, but these should cause an uncertainty in the 2.1 μ maximum of no more than 1–2 percent.

Because of various tentative identifications for the Martian surface made before, samples of fresh and weathered igneous rocks were selected for these comparisons. In an arid desert environment, the iron-bearing minerals (biotite, hornblende, augite, etc.) in igneous rocks may have limonite as a weathering product. Red sandstone, red mudstones, red soils, and pure hematite (Fe_2O_4) and limonite were also examined.

Out of 50 samples, only five had reflection curves that matched the Mars curve within the estimated errors of the Mars data at each of the four points. The estimated errors of the Mars data are indicated by verticle lines in Figures 2, 3, and 4. The data are inherently less accurate at the longest wavelength, but it is there that deviations of the various samples from the Mars data are the smallest. The most important point distinguishing the curves is the 1.05 μ point, at which the estimated error of the Mars data is small and the samples show the greatest deviations.

Figure 2 shows that pure hematite and pure limonite do not match the 1.05 μ point if 1.25 μ is used as reference, whereas, the 1.55 and 2.1 μ points are reasonably well represented. Figure 3 shows the results of three representative rock samples which do not completely match the Mars data. Red sandstone is a poorest match; pink granite is less discordant; and the rhyolite sample used is discordant at 1.05 μ but agrees well at 1.55 and 2.1 μ. It was noted that the various samples of a given rock type, as expected, showed some spread in their curves. The samples in Figure 4 are rocks with weathered surfaces. The weathering has produced a thin surface coating of limonite, varying in thickness. It is seen that these weathered surfaces (of the igneous rocks rhyolite, granite, andesite, and basalt) well represent the Mars reflectivities in this region. The red *sedimentary* rock and soils examined, whose coloring agent is hematite, have reflective characteristics similar to hematite. Although this result suggests that reddish sedimentary rocks do not make up large portions of the Martian deserts, more detailed comparisons with Mars are needed. Other much less common coloring agents of sedimentary rocks are goethite, $HFeO_2$, and lepidocrocite, FeO(OH); goethite is the major constitutent of limonite. However, these two minerals color a rock yellow.

3. *Concluding Remarks*

The limonite coating on igneous rocks described above may be either a powdery coating or a surface stain, both of which are formed and preserved in arid desert environments. A powdery surface would be suggested by the polarization measurements. All samples having the heavy limonite stain or limonite powder surface matched the Mars spectra, but no

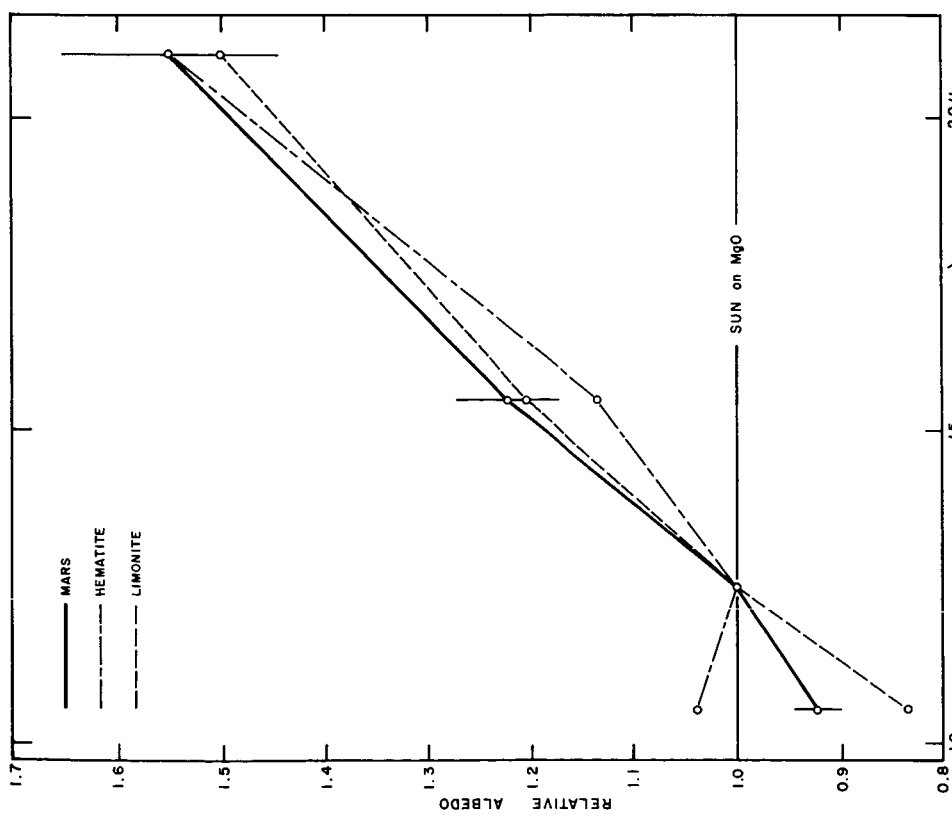


Fig. 2. Relative albedos of pure hematite and pure limonite compared to Mars. The divergence at the 1.05 μ point is the most significant characteristic of these samples.

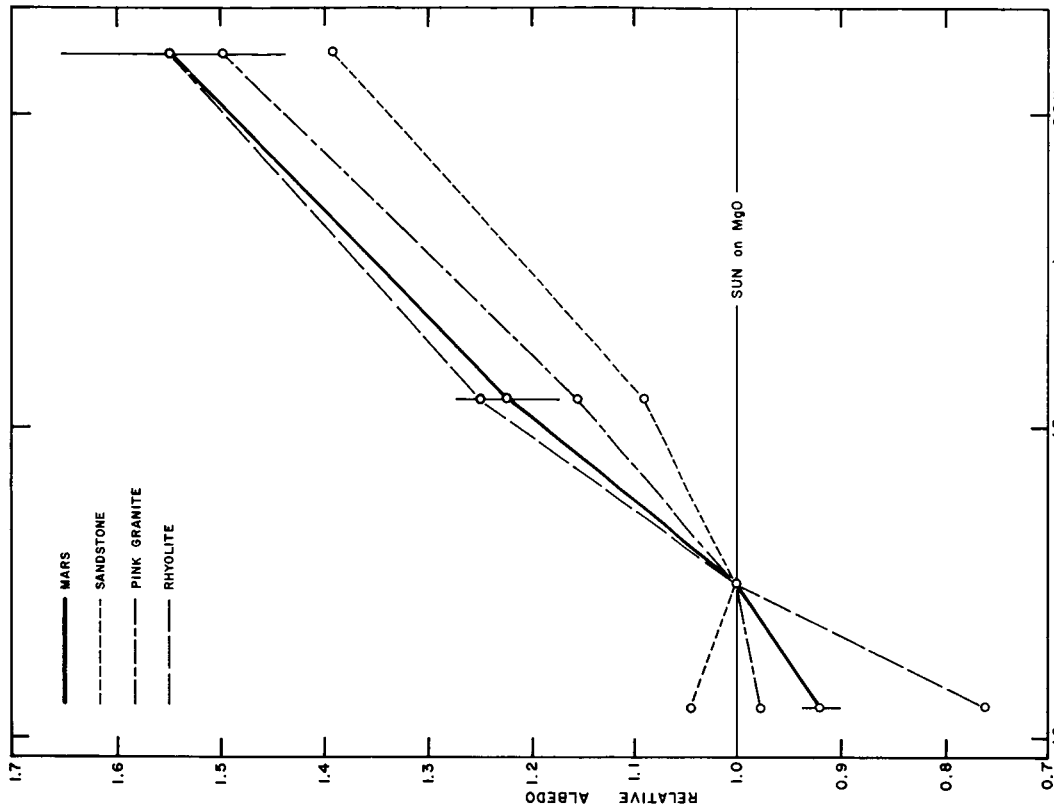


Fig. 3. Diverse albedos of various fresh reddish rock samples compared to Mars.

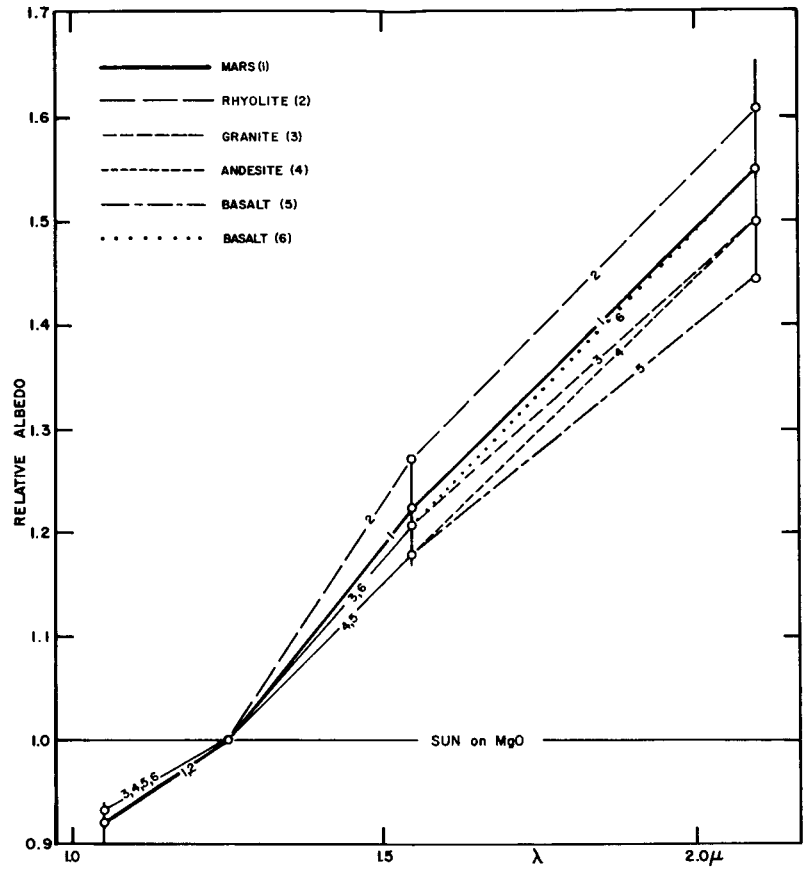


Fig. 4. Albedos of five types of rock stained with limonite measured relative to the 1.25 μ peak are compared with the spectrum of Mars (solid line) relative to sunlight on a reflecting surface of MgO. Vertical lines indicate the accuracy of the respective points on the Mars spectrum. The five samples in this figure are those found to approximate the Mars spectra most closely.

other samples agreed. Field observations indicate that in terrestrial deserts the stained surface is more common than the powdery surface; if a Martian analogy can be drawn with terrestrial deserts, it may be assumed that the Mars surface is composed partly of stained outcrops, rock fragments, and finer material.

Acknowledgments. We are grateful to Prof. S. R. Titley of the Department of Geology for discussions and for providing some of the rock samples; and to Prof. G. P. Kuiper for making available the Mars spectra and laboratory facilities, and for a discussion of the results. The program on IR planetary spectroscopy is supported by Grant NsG 161-61.

REFERENCES

Dollfus, A. 1961, *Planets and Satellites,* eds. G. P. Kuiper and B. M. Middlehurst (Chicago: University of Chicago Press), p. 379.

Draper, A. L., Adamcik, J. A., Gibson, E. K. 1964, *Icarus, 3,* 63.

Kuiper, G. P. 1962, *The Atmospheres of the Earth and Planets,* ed. G. P. Kuiper (Chicago: University of Chicago Press), p. 258.

Kuiper, G. P., Goranson, R., Binder, A., Johnson, H. L. 1962, *Comm. LPL, 1,* 119.

Sharonov, V. V. 1961, *Soviet Astronomy–A. J., 5,* 199.

Postscript. I am indebted to Mr. Binder for pointing out to me that the spectrophotometric comparison made in 1952 was with slightly weathered rhyolite, not a fresh rhyolite surface. The new observations reported above and my 1952 observation are therefore consistent, although this is not proof, as is apparent from the above paper, that the Martian rock is rhyolite. The identification made above encompasses a broad class of igneous rocks.

G.P.K.

NO. 38. ON THE DISTRIBUTION OF LUNAR CRATER DIAMETERS

by WILLIAM K. HARTMANN

May 1, 1964

ABSTRACT

In the first two lunar quadrants, the diameters *(D)* of both "young" and "old" craters follow the frequency distribution, d (log F)/d (log D) $\simeq -2.1$. For the "youngest" craters, this function remains valid down to $D = 8$ km. It is probable that throughout the period of crater formation this relationship was valid for newly-formed craters; certainly this is the case at the larger diameters. There is a deficiency of small craters which increases toward the "oldest" classes; there appears to be a process that has eroded very old small craters. The assumption that lunar craters were formed by impacts of bodies having the presently-observed asteroidal or meteoritic mass distribution closely predicts the observed lunar crater diameter distribution.

1. Observed Diameter Distribution

The compilation of lunar crater diameters (D) for craters of $D > 3.5$ km. by Arthur and his associates (1963, 1964) provides basic data for many studies of lunar history. This work is more complete, especially at small diameters, than the work by Young (1953). In the present analysis of Arthur's data on quadrants I and II (northern hemisphere) the distributions of different "age" classes of craters are compared and the implications for crater and mare formation are discussed.

The first task is a determination of the frequency distribution of D among the youngest craters. It is important to select a sample of fresh craters, because the battered craters have been deformed or partly obliterated.

The category of "youngest" craters, as used in this paper, includes all class 1 craters plus the post-mare craters of the other four classes, as defined by Arthur *et al.* (1963, p. 76). The Arthur classes (1 = freshest, 5 = most battered) are based on appearance alone, and are not entirely equivalent to those used by Baldwin (1963, p. 189). In the "young" category of the present paper, effects such as overlapping and flooding are minimal, so that essentially the complete initial population is preserved.

The following steps were taken in the reduction of the data:

(a) Craters in the limb regions were excluded because of the difficulty of seeing the small craters there. A comparison of distribution for the whole first quadrant with the central regions used here confirmed that when all craters out to the limb were included, a relative deficiency in small craters was introduced. The regions included here are shown in Figure 1.

(b) The remaining craters were sorted into increments of log D.

(c) The distribution was normalized by dividing the number of craters in each increment by the number with diameters larger than 35 km, on the assumption that in all classes, the initial population larger than 35 km would be essentially intact, so that all populations could be directly compared through use of this normalizing factor. Thus the incremental frequency parameter F is defined as:

$$F = \frac{\text{craters in log } D \text{ increment}}{\text{craters of } D > 35 \text{ km}} \qquad (1)$$

(d) Log F was plotted against log D.

The result for the youngest craters is shown in Figure 2. The observational effect of missing the smallest craters is clearly the main reason for the

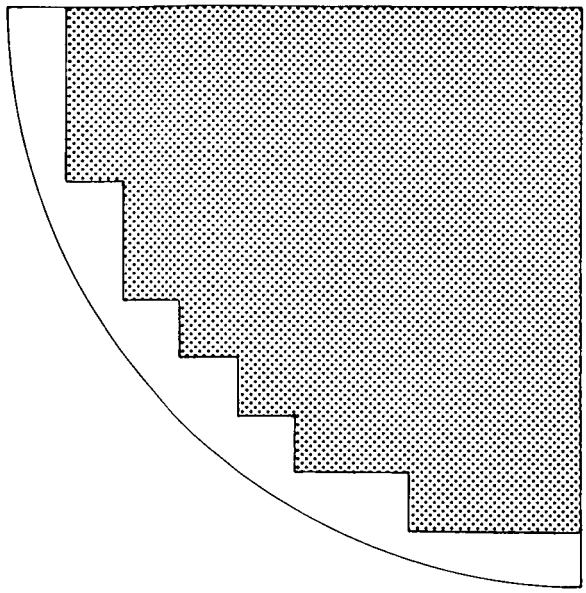


Fig. 1. Area of lunar quadrant studied in this paper. Only the shaded area (quadrants I and II) was included to reduce the effects of foreshortening.

turn-down found at diameters $D < 4$ km. (When all craters out to the limb were included, the turn-down occurred at about 9 km, confirming the need for omitting the limb regions.) We conclude that *the youngest craters, mostly post-mare, were formed with a diameter distribution obeying*

$$\frac{\mathrm{d}(\log F)}{\mathrm{d}(\log D)} = -S, \qquad (2)$$

with S constant, about 2.1.

We next compare the "oldest" craters with the "youngest." The category of "oldest" craters is defined to include all craters of Arthur classes 3, 4, and 5 which were catalogued as "continental." Craters on the continental borders were rejected if they were classified as postmare. Craters in the mare regions were not included because flooding might have affected the observed distribution. The same four steps [(*a*) to (*d*) above] were followed in treating the oldest craters.

A plot of the diameter distribution of the "old" craters is included in Figure 2. The curve is similar to that of the "young" craters in the following respects: *(a)* There is a linear portion at large diameters [eq. (2) is obeyed]; *(b)* the slopes of the linear portions are similar; *(c)* there is a turn-down at small diameters; and *(d)* the near coincidence of the F values for $D > 16$ km indicates that normalization to $D > 35$ km was safe and that all original craters of $D > 35$ km are detected even in the oldest populations.

2. *Interpretation of Distribution Curves*

The most prominent difference between young and old craters is the relative absence of small, old craters. Below 16 km, markedly fewer occur than expected if the initial distributions were the same and all craters were preserved. This issue is further considered below.

We next compare the slopes of the linear portions of Figure 2. Taking into account the limited accuracy of the statistics, one may conclude from Figures 2–4 that a value $S \simeq 2.1$ fits crater families of all ages.

If *(a)* the deficiency of small diameters is not a characteristic of the original population of older craters, and *(b)* crater families of all ages show linear branches of nearly the same slope, then *there is no evidence for a major secular change in the diameter distribution of newly-formed craters during lunar history*. This statement contradicts the commonly held opinion that large craters formed first and small ones last, which has been incorrectly inferred from the fact that small craters frequently overlap large craters while the reverse is rarely seen. The data used in Figure 2 show two relevant facts: *(a)* The number of small craters being formed at any time greatly exceeds the number of large ones; and *(b)* most presently-observed small craters are "young" and most large craters are "old."

These two facts explain the overlap problem. The high formation rate of small craters produces frequent overlap of small on large craters. The formation of large craters leads inevitably to the destruction of underlying objects. Moderate-sized underlying craters may partly survive, as is the case in Phocylides, Maurolycus, Aristoteles, and Janssen.

We now undertake a more detailed study of the depletion of small old craters, plotting each of the five classes separately by the same procedures as used in Figure 2. The results are shown in Figure 3. Two important conclusions follow: *(a)* All classes together define a linear branch which fits the relation

$$\frac{\mathrm{d}(\log F)}{\mathrm{d}(\log D)} = -2.1. \qquad (3)$$

(b) The depletion of small craters is greater among the more battered (presumably older) classes of craters.

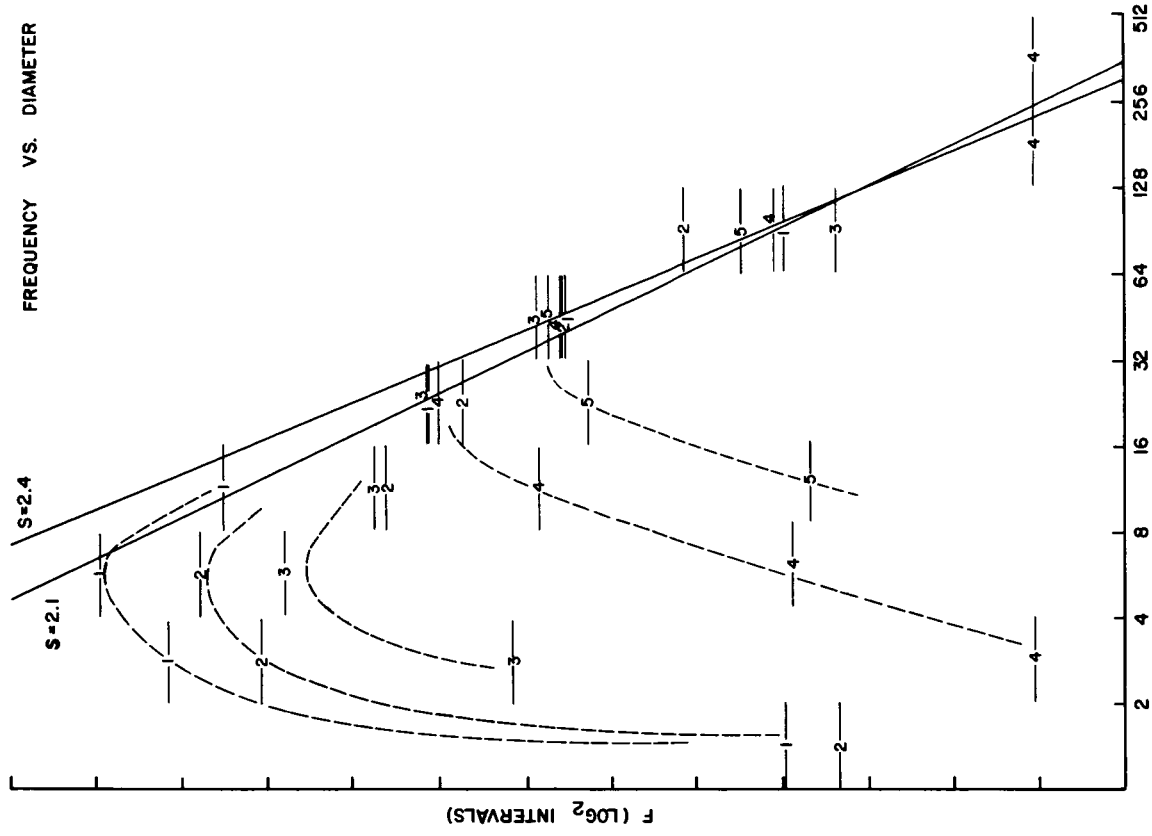


Fig. 3. Comparison of diameter distributions of five classes (1 = fresh; 5 = most damaged). All classes show the same slope at large diameters. F as defined in Eq. (1). Total number of craters in each class: 1, 1058; 2, 716; 3, 357; 4, 241; 5, 70.

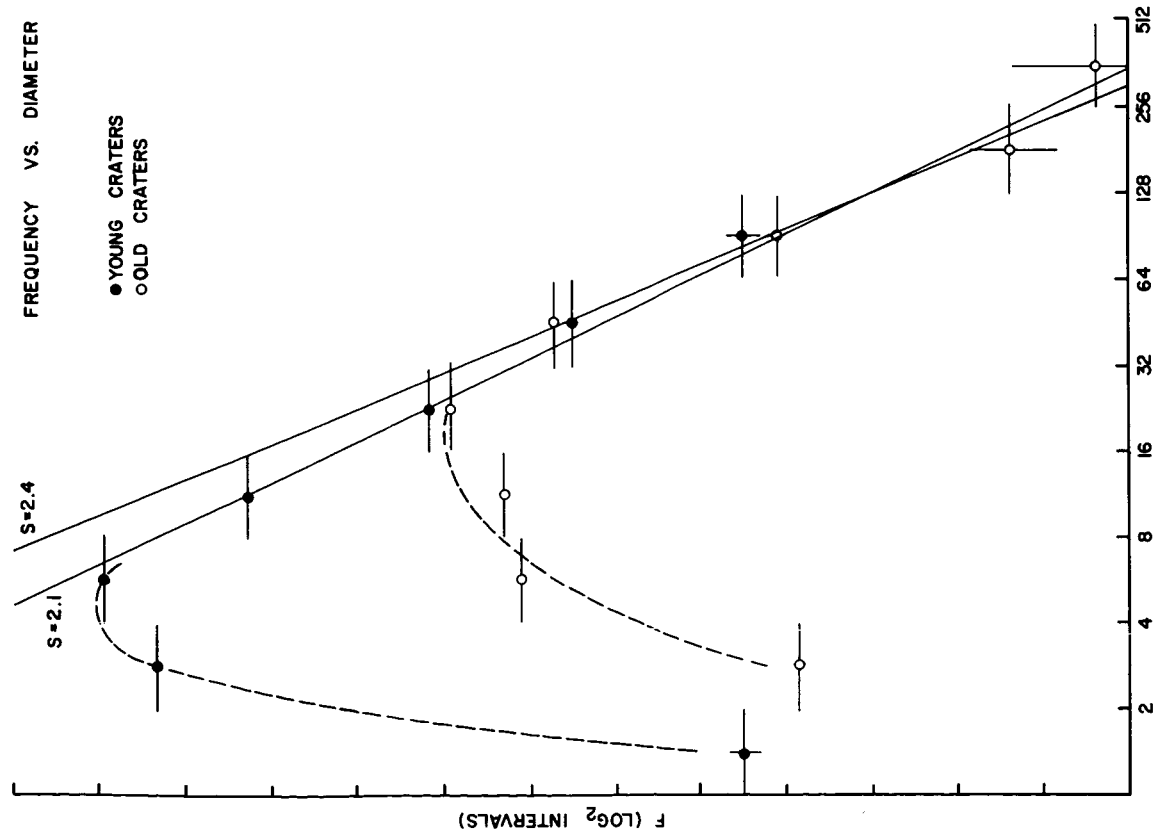


Fig. 2. Comparison of diameter distributions of "young" and "old" craters (for definitions see text, Sec. 1). Vertical bars show uncertainty in F corresponding to $\pm 1/\sqrt{n}$. F as defined in Eq. (1). Total number of "young" craters, 1448; of "old" craters, 520.

We have already suggested the interpretation: *At all epochs, craters were formed with the distribution given approximately by Equation (3) (a straight line in Figure 3,* and *the depletion of small, old craters measures the partial or complete obliteration of these objects.*

This interpretation is favored over the alternative that the five different curves of Figure 3 show a secular change in the distributions of craters formed during the five different periods, and is supported by at least three arguments: *(a)* Observations indicate that a log-log plot of the distribution of both meteorite and asteroid masses gives a linear curve (Brown, 1960). Assuming an impact origin for craters, a linear crater distribution of slope -2.4 may be derived (see below), in good agreement with the observations. It is unlikely that the linearity of the curves for meteorites, asteroids, and young craters is a property only of the present period of the solar system. *(b)* All curves show linearity in the portions where we expect the crater data to be most complete. *(c)* The most natural interpretation of the Arthur erosion classes 1–5 is a progression in age, with the erosion caused by crater-forming impacts. A single hypothesis then accounts for both the formation of the craters and their gradual destruction.

There are, however, some questions of procedure that still need review:

(a) Classification errors. Could the deficiency of small craters be an observational effect whereby small craters were classified too "young"? There was indeed a tendency to do this, but it cannot account for the depletion in the more damaged classes. If the classification only were in error, the total number of craters would be unaffected, and there would be no net loss of craters. Under this assumption the distribution function F for all craters should be of a form similar to the distribution for some undisturbed sample selected by a criterion independent of class. Figure 4 compares all craters with post-mare craters. It shows that the two F functions differ, with a marked deficiency in small craters in the comprehensive sample. Therefore, unless we are mistaken in rejecting a secular change in the diameter distribution, a large number of craters have disappeared since the earliest craters were formed.

The magnitude of the deficiency of small craters is shown by the following two examples: (1) Craters of $D > 35$ km have been well preserved. In Figure 2, there are 18 "young" craters and 77 "old" ones with $D > 35$ km. Thus, *the "old" group was initially more numerous by a factor of about four.* Yet the present total numbers (all D values) are reversed: "young" 1448, and "old" 520, apparently because of the destruction of old, small craters. (2) In our (undepleted) sample of "young" craters (Fig. 2), the ratio of the number of $D > 35$ km craters to the total number is 1:80. In the studied area there are 132 craters with $D > 35$ km. Therefore, in this area there should be of the order of 10,000 craters, whereas only 2442 were actually counted. Thus, some 8000 craters must have been lost in the portion of the moon here considered.

The five classes cannot be strictly age classes, because the oldest small craters have already been lost, while the oldest large craters still remain. At any given diameter, each Arthur damage class has its own average age, but in classes 2 through 5 these average ages are not necessarily the same for different diameters. Nevertheless, the comparison in Figure 2 of "old" with "young" groups is meaningful.

(b) Flooding. One might suggest that our data have been biased by inclusion of flooded areas. Actually, a comparison of all craters of classes 3 and 4 with the continental craters of classes 3 and 4 shows little difference. We conclude that distributions of $F(D)$ in this paper are little affected by the flooding itself.

(c) Tectonic adjustments. An increasingly large body of evidence, such as studies of the lineament "grid" systems, supports the view that the entire lunar surface has undergone tectonic activity, probably accompanying the flooding that produced the maria. These adjustments will indeed have contributed to the difficulties of tracing the oldest craters. Fielder (1963) attaches major importance to this effect.

(d) Isostatic adjustments. Baldwin (1963, p. 193) attributes much of the modification of old craters to isostatic adjustments. He shows that the depths of the floors have been reduced faster than rim heights, pointing out that this phenomenon is in accord with isostatic adjustment.

(e) Overlapping. Smaller craters are preferentially destroyed by overlapping of successive generations of craters. This may be seen from the following simplified model:

Define D_0 = crater diameter in an existing distribution of craters,

D_1 = crater diameter in a new generation of overlapping craters,

A = area of the moon,

n = the average number of craters of diameter D_0 per unit interval ΔD_0 destroyed by a single overlapping crater of diameter D_1,

N = the number of craters of diameter D_0 per unit interval ΔD_1 destroyed by all overlapping craters of diameter D_1,

$\mathcal{N}$ = the number of craters of diameter D_0 destroyed by all overlapping craters.

Suppose that a crater of diameter D_1 overlaps a crater of diameter D_0 (i.e., the D_1 impact follows the D_0 impact.) Assume, as a first approximation, that if $D_1 > D_0$ the latter crater is obliterated, while if $D_1 < D_0$ both craters remain visible.

The *fraction* of the D_0 craters destroyed by a single D_1 impact, if $D_1 > D_0$, is the area of the D_1 crater divided by the area of the moon, assuming a random uniform distribution of the D_0 craters. Therefore, the *average number* n of D_0 craters (per unit interval ΔD_0) destroyed per D_1 impact is, by Equation 2,

$$n = \frac{\pi {D_1}^2}{4A} \text{ Const. } {D_0}^{-S-1} \qquad \text{if } D_1 > D_0 ,$$

and

$$n = 0 \qquad \text{if } D_1 < D_0 . \quad (4)$$

Therefore, the number N of D_0 craters destroyed by all new craters of diameter D_1 (per unit interval ΔD_1) is

$$N = \frac{\pi {D_1}^2}{4A} \text{ Const. } {D_0}^{-S-1} \text{ Const. } {D_1}^{-S-1} \qquad \text{if } D_1 > D_0 ,$$

and

$$N = 0 \qquad \text{if } D_1 < D_0 , \quad (5)$$

and therefore, the total number of D_0 craters destroyed by *all* larger, overlapping D_1 craters is

$$\mathcal{N} = \frac{\pi \text{ Const.}}{4A {D_0}^{S+1}} \int_{D_0}^{D_{\text{Max}}} {D_1}^{1-S} \, dD_1$$

$$= \frac{\pi \text{ Const.}}{4A\,(2-S)} \frac{{D_{\text{Max}}}^{2-S} - {D_0}^{2-S}}{{D_0}^{S+1}} \qquad (\text{excluding } S = 2) \quad (6)$$

Therefore, the fraction of craters D_0 destroyed (per unit interval ΔD_0) is

$$\frac{\mathcal{N}}{F} = \frac{\pi \text{ Const.}}{4A\,(2-S)} \left({D_{\text{Max}}}^{2-S} - {D_0}^{2-S} \right) \quad (7)$$

In the case of $S = 2.1$, as found in Figures 2 and 3, we have

$$\mathcal{N} = \text{Const.} \left[\left(\frac{D_{\text{Max}}}{D_0} \right)^{0.1} - 1 \right] {D_0}^{1/3.1} , \quad (8)$$

and

$$\frac{\mathcal{N}}{F} = \text{Const.} \left[\left(\frac{D_{\text{Max}}}{D_0} \right)^{0.1} - 1 \right] \quad (9)$$

The fraction of destroyed craters thus increases toward small diameters, and the equations predict that each successive generation of impacts increases the departure from F at small diameters. Dr. Kuiper has pointed out an additional cause for this effect. In reality a given D_1 impact destroys an area greater than $\frac{\pi {D_1}^2}{4}$. For large D_0's this area of effective destruction approaches $\frac{\pi {D_1}^2}{4}$, but for small D_0's it is appreciably greater. Therefore in Equation (4) the exponent of D_0 might better be considered $-S-1-\epsilon$. This exponent carries through to Equation (6) so that the denominator in (6) becomes ${D_0}^{S+1+\epsilon}$ and in (7), ${D_0}^{\epsilon}$. The model is of the first order in Δt (time), and makes various assumptions as listed, but it does predict qualitatively the observed effect. The second generation craters follow the diameter distribution of equation (2) by assumption, so that only the losses need be considered in a first-order theory.

Further study will be needed, especially in the heavily-cratered quadrant IV (where Δt is obviously not small), to determine whether the area covered by craters and the degree of apparent overlap are compatible with the hypothesized crater losses, e.g., some 90 percent for 10-km craters.

(f) Erosion by external agents. Several authors have discussed mechanisms by which material is constantly eroded and redistributed on the lunar surface. Meteorite impacts may result in either accretion or mass loss by the moon, depending on impacting mass and the surface structure. Such processes, if of sufficient magnitude, would account for the softened appearance of the larger class 4 and 5 craters and could obliterate smaller craters with lower total relief. Quantitative estimates of the present rate of erosion make it too small to have the necessary effect (Fielder, 1963), but erosion, especially by meteoritic material, may have been significantly greater in early lunar history. If it is assumed that a 20 km crater can be lost by erosion the disturbed layer must be 1–2 km in depth.

In summary, it appears likely that craters are obliterated in time by several processes, with the smallest craters being most affected. More light will be shed on this problem by data from the other quadrants, especially IV, where unflooded continents predominate. Meanwhile, it is held that the distribution of craters forming at any epoch is characterized by equation (3).

Young (1940) published diagrams similar to Figure 2, using measures of some 1300 craters. He noted a discontinuity or maximum curvature of slope at about 20 km, when all craters were included, and at about 12 km for post-mare craters alone. The latter corresponds to the bend near 10 km in the "young" crater curve of Figure 2. In Figure 4, the plot for all craters confirms a departure from linear near 20 km. Young (1940, p. 316) suggested the possibility that his discontinuity in slope related to differences between "walled-plain and ringed-plain types of craters," and Fielder (1961, p. 219), who confirmed the discontinuity, also implied a possible anomaly in the original population of craters. According to the present paper, the discontinuity is the result of including samples deficient in observable small craters and does not represent the original distribution. This conclusion is supported by the facts that (*a*) the "young" curve shows very little curvature, (*b*) each class shows a different departure from linearity (Fig. 3), and (*c*) Young's discontinuity is best seen when all craters are mixed before plotting.

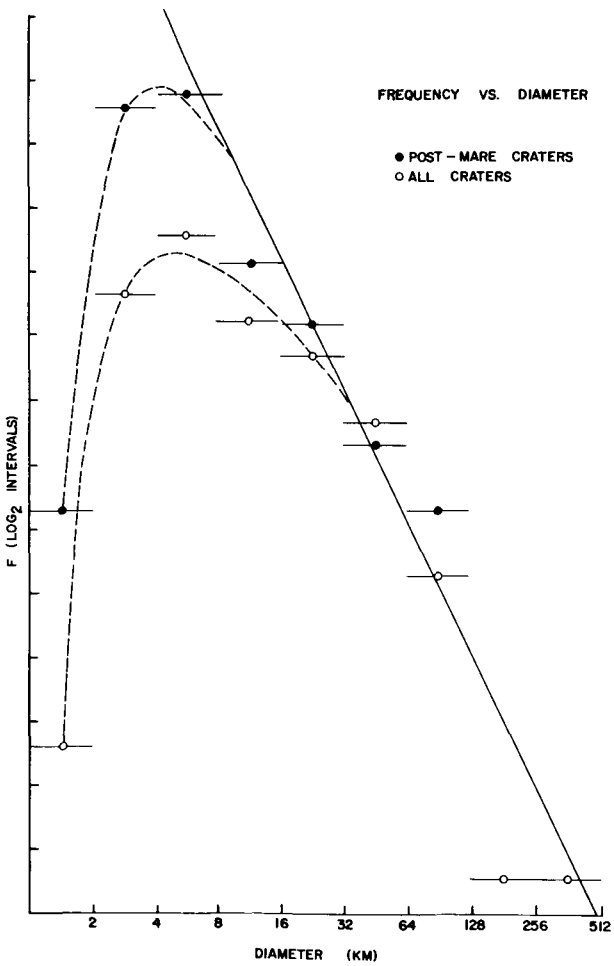


Fig. 4. Comparison of diameter distributions of all craters (2442) with post-mare craters alone (390), demonstrating that the deficiencies in small craters are not classification errors (see text, Sec. 2). F as defined in Eq. (1). Slope of the line $S = 2.1$.

The last point to be discussed involves the slope of the log F–log D curve. In the undisturbed parts this slope is approximately -2.1. Young's (1940, p. 315) value was -2.5. Assuming that the lunar craters are formed by impacts, one can theoretically predict this slope. The following discussion is based on that given by Shoemaker, Hackman, and Eggleton (1962). We let

E = energy available to form crater,
M = mass of impacting body,
V = velocity of impacting body,
D = diameter of crater,
$f(M)$ = distribution function of impacting bodies in log M increments,
$F(D)$ = distribution function of lunar craters in log D increments.

Brown (1960) has pointed out that the mass distributions of meteorites and asteroids are of the same form, namely,

$$\frac{\mathrm{d}\,[\log f(M)]}{\mathrm{d}\,[\log M]} = -.77\,. \qquad (10)$$

According to Shoemaker, Hackman, and Eggleton, the crater diameter D is proportional to a power of E less than 1/3, on the basis of theoretical considerations, and they give 1/3.4 as a value derived from studies of terrestrial explosion craters. Baldwin (1963, chap. 8) gives an extensive discussion of this problem, and his extrapolation to large diameters based on semiquantitative arguments on the nature of cratering gives

$$D = \text{Const.}\, E^{1/3.06}. \qquad (11)$$

If the full kinetic energy is applied to crater formation,

$$E = \frac{1}{2} MV^2\,. \qquad (12)$$

Substituting (11) into (12), and the result into (10), and assuming that variations in impact velocity have negligible effect on F, we have

$$\mathrm{d}[\log F(D)] = -.77(3.06)\,\mathrm{d}[\log D] \quad (13)$$

or

$$\log F = -2.4 \log D + \text{Const.} \quad (14)$$

The observed equation is

$$\log F = -2.1 \log D + \text{Const.} \quad (15)$$

In spite of the uncertainties in Brown's data, the cratering theory, and the crater statistics, the observed curve is thus predicted closely.

Jaschek (1960) made an analysis very similar to this and found the same results for asteroidal data, though he concluded that the meteoritic data did not agree. However, he used the older crater counts of Young, Baldwin's 1949 cratering theory, and, as Shoemaker, Hackman, and Eggleton point out, the unlikely exponent of 1/2.5 in equation (11). Shoemaker, Hackman, and Eggleton predicted a slope of -2.7 but their crater counts did not confirm this, and they suggested that the mass distribution of the crater-forming objects was significantly different from that presently observed among small solar system objects. The improved data used in this paper reduce the need for this assumption.

3. *Conclusions*

In terms of the impact hypothesis, the implications of the presently available data are:

(a) The diameter distribution of the impacting bodies did not appreciably change during the interval of crater formation.

(b) The typical overlap of small on large craters is not due to a change in the distribution of diameters of the impacting bodies.

(c) The period of mare formation must have been relatively short, since the mare surfaces have relatively similar post-mare crater densities. Mare formation must have occurred after most craters had formed, when the rate of crater formation was too low to produce numerous post-mare craters.

(d) Among the oldest generation of craters, small craters are not detected in their original numbers.

(e) The bodies that formed the craters by impact came from a population whose diameter distribution was essentially the same as that presently observed among the asteroids and meteorites.

Acknowledgments. I am indebted to Mr. D. W. G. Arthur for making the measures of crater diameters from his catalogs available in advance of publication; to Dr. G. P. Kuiper for general advice; and to other associates at this Laboratory and the Steward Observatory for helpful discussions. This study was supported under Grant NsG 161-61 of the National Aeronautics and Space Administration.

Note added in proof. This paper was completed before the first successful Ranger flight to the moon. In the first analysis of the Ranger VII photographs the cratering curve for post-mare craters was extended over three more orders of magnitude down to diameters of two meters. The incremental diameter distribution is apparently linear over the entire range. There are some irregularities in a small range around 125 meters, but these are probably due to clusterings of secondary craters. A second interpretation is that large numbers of secondary craters modify the shapes of the primary crater curve for diameters less than 500 meters. The best fit to the curve, either down to 2 meters or up to 500 meters, depending on the interpretation, is $S = 2.4$, in exact agreement with the calculations in this paper.

REFERENCES

Arthur, D. W. G., Agnieray, A. P., Horvath, R. A., Wood, C. A., and Chapman, C. R. 1963, *Comm. L.P.L., 2,* 71.

———. 1964, *Comm. L.P.L., 3,* 1.

Baldwin, R. B., 1963, *The Measure of the Moon* (Chicago: University of Chicago Press).

Brown, H. 1960, *J. Geophys. Res., 65,* 1679.

Fielder, G. 1961, *Structure of the Moon's Surface* (New York: Pergamon Press).

———. 1963, *Planet. Space Sci., 11,* 1335.

Jaschek, C. O. R. 1960, *The Observatory, 80,* 119.

Shoemaker, E. M., Hackman, R. J., and Eggleton, R. E. 1962, *Advances in the Astronautical Sciences,* (New York: Plenum Press), vol. 8.

Young, J. 1940, *J. B. A. A., 50,* 309.

———. 1953, *A Catalogue of Lunar Craters,* (Privately printed by D. W. G. Arthur).

N65-24186

NO. 39. ANALYSIS OF LUNAR LINEAMENTS, I: TECTONIC MAPS OF THE MOON

by ROBERT G. STROM

July 1, 1964

ABSTRACT

Lineaments within 60° of the moon's center of face have been mapped in detail. Four global lineament systems and radial systems associated with four circular maria are delineated. The majority of polygonal crater rims, linear portions of central peaks, crater chains, and certain linear mare ridges are related to the lineament systems. Spatial relationships of the lineament systems and other data indicate that the global systems resulted from compressive stresses in the moon's crust which were oriented in a north-south direction. Possible causes of these stresses are (1) the gradual subsidence of the "tidal bulge," (2) expansion and contraction of the moon, (3) lunar body tides, (4) convection currents within the moon as postulated by Runcorn, and (5) a shift of the moon's axis of rotation.

Author

1. Introduction

Approximately 10,000 linear structures have been mapped within 60° of the moon's center of face. For each of 41 fields of the Photographic Lunar Atlas (1960), covering the 60° area, the most suitable sheets were selected as a base for mapping the lineaments. Each base photograph was supplemented by 5–10 photographs exhibiting various angles of illumination in order to aid in the identification of linear structures. The lineaments were checked and verified with almost 100 percent agreement, by W. K. Hartmann and E. A. Whitaker. This procedure eliminated personal bias regarding overall patterns, because the lineaments were first mapped from photographs of small areas prior to being replotted on a larger base map. Hence, there was no way of knowing whether or not a particular lineament trend would carry over into another area. In fact, a general pattern was not discernible until all the lineaments had been plotted on the large base map.

The mapped region encompassed by the 60° longitude and 64° latitude lines, was divided into four quadrants, each containing 85 areas of 33,464 sq km each. Lineaments within the areas were numbered and tabulated according to morphology (valley, ridge, rille, etc.) and degree of prominence (very strong, strong, moderately strong, and weak). The end coordinates of each lineament were recorded and their length, true selenographic azimuth, and apparent azimuth, as seen in orthographic projection, have been computed on the IBM 7072 computer of the University of Arizona Numerical Analysis Laboratory. A statistical analysis of lunar lineaments and a comparison between lunar and terrestrial lineament patterns will be presented in a later *Communication*.

Lineaments mapped from the base photographs were replotted on the *USAF Lunar Reference Mosaic LEM-1*. It was possible to replot only about 80 percent of the lineaments since the quality of the Reference Mosaic was not adequate for identification of very small or relatively weak structures. Eight maps showing the lineament trends have been constructed and are listed below in Table 1. Maps 1A and 1B are to a scale of 1:3,800,000. All other maps have a scale of 1:5,700,000.

2. Lunar Lineaments

The *Dictionary of Geologic Terms* (1957) defines lineaments as: "(1) Significant lines of landscapes which reveal the hidden architecture of the rock basement. They are character lines of the earth's physiognomy. (2) An essentially rectilinear

TABLE 1

MAP	TITLE
1A-1B.....	Tectonic Map of the Moon
2.....	Radial Lineament Systems of the Moon
3.....	NW-SE Lunar Lineament System (Astronautical Directions)*
4.....	NE-SW Lunar Lineament System (Astronautical Directions)
5.....	N-S Lunar Lineament System (Astronautical Directions)
6.....	NNE-SSW Lunar Lineament System (Astronautical Directions)
7.....	Composite Map of the NW-SE, NE-SW and N-S Lunar Lineament Systems (Astronautical Directions)
8.....	Lunar Lineaments Unrelated to Major Systems

*Selenographic directions follow the convention adopted by the I. A. U. at Berkeley in 1961. North is at the top, while east is to the right and west is to the left.

topographic feature resulting from a fault. (3) A topographic line that is structurally controlled." These descriptions are applied to terrestrial lineaments, but may also be used to define linear structures on the moon. One further restriction is applied to lunar lineaments in this paper: since the features must be relatively linear in structure, arcuate features such as the Liebig fault, the Hippalus rilles, and concentric scarps are not classified as lineaments, although some of these features are shown on Maps 1A and 1B. This also applies to very sinuous mare ridges.

Lunar lineaments have been classified into eight morphological types: *(a)* ridges on terrae, *(b)* valleys, *(c)* polygonal crater rims, *(d)* definite linear faults, *(e)* crater chains, *(f)* linear rilles, *(g)* linear ridges in the maria, and *(h)* linear portions of central peaks.

(a) As their names imply, ridges on terrae are positive features occurring primarily in the uplands, while valleys are negative structures. Terrae ridges consist of upland material and do not usually exhibit any well-defined crustal displacement.

(b) Valleys are primarily associated with radial systems, although they are not necessarily restricted to these systems. A majority of valleys are related to the Imbrium radial system. They are probably graben with considerable vertical displacement, or fissures due to horizontal cracking of the crust. A number of features which are depicted as valleys may actually be series of coalescing craters. These features have engrailed walls but the photographic resolution is not sufficient for true crater-form outlines to be distinguished.

(c) Linear crater rims are classified as lineaments. They consist of the crest of the rim only, and do not include interior terracing, exterior linear structures on crater slopes, or the dissected crater rims which occur primarily in the Sinus Medii–Mare Vaporum region.

(d) Only those features which show definite displacement of the surface are classified as faults. These are mostly young, well-defined structures, e.g., the Straight Wall, and are probably normal faults. Many of the ridges may be faults also, but in most cases there is little or no indication of the type of movement which may have occurred.

(e) A series of craters is considered to be a crater chain if it consists of three or more evenly spaced craters lying along a straight line. Usually the craters forming the chain are similar in degree of sharpness and often have similar diameters, or a progressive decrease in diameter. Crater chains are depicted as rows of circles on the maps. However, neither the number of circles nor their diameters necessarily represent the true number or diameter of craters in any individual chain.

(f) Rilles can be classified into four types according to their geometry: (1) linear, (2) arcuate, (3) irregular, and (4) sinuous. Linear rilles, e.g., Ariadaeus rille, are straight and occur anywhere in marial areas, while arcuate rilles, e.g., the Hippalus rilles, are gently curved features which occur along the margins of maria or in the lava-filled interiors of craters. Irregular rilles, such as the Triesnecker and Littrow systems, are groups of branching, bifurcated rilles which are probably due to complex local forces. The sinuous rilles, e.g., the Marius, Hadley, and Conon rilles, are winding features having the appearance of meandering river beds. This type of rille generally starts at a small crater and may have an entirely different (nontectonic) origin than the other types of rilles. Schröter's Valley is a conspicuous example of this type of feature. In accordance with our definition of the term, only the linear type of rille is classified as a lineament.

(g) Mare ridges are classified as lineaments if they are straight. They usually occur in groups and often *en échelon,* as do the short mare ridges southwest of the Straight Wall. In some instances long mare ridges are broken up into linear segments, as in the Serpentine Ridge.

(h) Linear portions of central peaks in craters have the same morphology as terrae ridges and valleys. However, they may comprise either the entire central peak or small portions of the peak.

3. *Tectonic Maps*

(a) Tectonic Map of the Moon. (Map 1A, 1B) This map is in two halves which may be assembled by cutting along the medianal olive line on Map 1A and matching it to the north and south fiducial marks of Map 1B. All lineaments are shown on this map, together with the most prominent mare ridges and rilles.

(b) Radial Lineament Systems of the Moon. Map 2 shows radial lineament systems associated with (1) Mare Imbrium (black), (2) Mare Nectaris (red), (3) Mare Humorum (blue), and (4) Mare Crisium (green). The system surrounding Mare Crisium is incomplete because the eastern portion is outside the area of investigation. Similarly, the radial systems associated with Mare Orientale and Mare Humboldtianum are not shown (See *Comm.* No. 36).

Map 2 was drawn by constructing great circles radial to the circular maria and plotting the lineaments approximately parallel to these lines. Actually, the radial systems do not converge to a point source, but radiate from a circle-of-confusion coincident with the diameter of the inner basins.

An examination of the map reveals that there are east-west gaps in all radial patterns. Hartmann (1963, 1964), who has studied the radial systems in detail from rectified photographs, also reports gaps in the radial patterns east of Mare Orientale and Mare Crisium.

It might appear that the east-west gaps are due to observational error resulting from the difficulty of recognizing lineaments which parallel the sun's rays and therefore cast little or no shadow. However, this zone would be restricted to angles of about 5–10° to the north and south of latitude lines. With the exception of the western gap of Mare Nectaris and the east and west gaps of Mare Imbrium, all gaps are of the order of 80–90°. The east and west gaps of Mare Imbrium are about 30 and 50° respectively, while the western gap of Mare Nectaris is 45°. In addition, radial lineaments are relatively strong features and would be expected to show even under adverse lighting conditions. Also, if the gaps were due to poor visibility of lineaments parallel to the sun's rays, one would expect a gradual decrease in the apparent number of lineaments as an east–west orientation was approached. However, the transition from the radial pattern to the gaps is very abrupt, as is illustrated on Map 2. Therefore, it seems definite that the east-west gaps are structural breaks in the radial systems.

Another unique feature illustrated on Map 2 is that Mare Nectaris has two radial systems. The major system, represented by unbroken red lines, is centered on the inner basin, while a minor system (dashed red lines) is focused on the southern edge of the inner basin. The lineaments of both systems are of equal intensity, but the system centered near Fracastorius occurs only south of the mare. At first sight it might appear that the minor system is associated with Fracastorius rather than Mare Nectaris. However, it seems highly improbable that such a relatively small structure could cause such a strong radial system when craters the size of Janssen, Clavius, or Ptolemaeus are devoid of radial structures. Therefore, it seems certain that the secondary system is associated with Mare Nectaris and is contemporary with its formation. This minor system is also asymmetrically placed in regard to the concentric scarp system surrounding Mare Nectaris (See Hartmann and Kuiper, 1962). It seems probable that two sets of stresses were superposed in such a way as to produce two contemporaneous radial structures.

Mention should be made of the two prominent zones of radial lineaments to the southwest of Mare Nectaris and to the southeast of Mare Humorum. These zones are very pronounced because they coincide with the directions of the global NW-SE and NE-SW lineament systems. It is therefore impossible to determine which lineaments should be classed with the radial systems and which should be placed with the global systems. It is probable that the lineaments in these zones belong to both the radial and global systems.

From a detailed study of the radial systems, Hartmann (1963, 1964) has concluded that the structures radial to circular maria are caused by tectonic activity rather than being grooves produced by secondary ejecta. The writer agrees with this interpretation for the reasons given by Hartmann. Furthermore, it seems impossible to explain the existence either of two radial systems associated with one mare, or of the east-west gaps in radial patterns by the hypothesis of secondary ejecta. Also, the fact that the morphology of many radial lineaments is identical to that of the global systems, which are definitely the result of tectonic activity, appears incompatible with the secondary ejecta hypothesis. The radial lineament systems are probably tension fractures and graben which have resulted from tensile stresses concentrically oriented around the mare basins, and probably caused by the

gentle doming of a vast area surrounding the basins.

(c) Global Nonradial Lineament Systems. Maps 3–6 depict four global nonradial lineament systems. The directions given in the titles of Maps 3, 4, and 6 refer to the orthographic tangential plane and are approximate to selenocentric directions.

Azimuth-frequency diagrams of the lineaments have been constructed for various parts of the lunar surface, and were used as one basis for delineating the four nonradial lineament systems. Figures 1 and 2 are diagrams of the frequency of *apparent* azimuths in orthographic projection of lineaments which occur in portions of the moon's northern and southern hemispheres. The diagrams represent areas relatively free from radial lineaments and show the four principal directions of the global systems. Figure 1 also displays a strong peak formed by the Imbrium radial system. Figure 2 does not show the Imbrium radial system because (1) the Imbrium lineaments form a relatively uniform fan-shaped pattern in this area, (2) many of the Imbrium lineaments coincide with the directions of the nonradial systems, and (3) the density of the Imbrium lineaments in this area is much less than the density of the nonradial lineaments. The azimuth-frequency diagrams should be studied in conjunction with Maps 1A and 1B in order to visualize the spatial relations of the lineaments.

Fielder (1963) has investigated lunar lineaments and also delineated four global lineament systems. His "A," "B," and "C" systems of lineaments correspond to the author's NW-SE, NE-SW and N-S lineament systems. He also found limited evidence for an E-W lineament system (system "D") which I was unable to detect. I have been able to detect a weak NNE lineament system which Fielder (personal communication) has recognized in subsequent investigations. The correspondence in directions and spatial relations between our lineament systems is remarkable considering that the investigations were completely independent.

(d) NW-SE and NE-SW Lunar Lineament Systems. Maps 3 and 4 are a compilation of lineaments belonging to the NW-SE and NE-SW systems. These systems are approximately orthogonal and nearly coincide with the trend of small circles. Therefore, the lineaments are approximately parallel when viewed in orthographic projection. Actually, the systems are more nearly barrel-shaped as stated by Fielder (1963) and correspond to his systems "A" and "B." The poles of these systems are situated about 45–55° to the east and west of the moon's axis of rotation. Figures 3 and 4 are globe projections of the NW-SE and NE-SW systems as seen from directly over their southwestern and southeastern poles, respectively. They clearly show the small-circle trend of the lineaments, although the barrel shape of the systems has produced a very slight flattening of the small circles. Both systems have a paucity of lineaments in the limb regions of their equatorial planes.

Linear mare ridges in Mare Frigoris, Mare Nubium, and Oceanus Procellarum, as well as the Abulfeda crater chain and the major axes of Schiller and Rheita E, coincide with the directions of these systems.

(e) N-S Lunar Lineament System. The N-S system nearly lies on great circles approximately parallel to the meridians. Actually the north-south lineaments slightly deviate from the meridians so that they converge on the area encompassed by the 75° latitude. The poles of this system are the same as the moon's axis of rotation. Fielder (1963) has mapped this system which he denotes as system "C." However, he finds that the lineaments lie on small circles. If he has placed some of the radial lineaments south of Mare Humorum and Mare Nectaris in this system, this would make them appear to lie on small circles. Also, Fielder (personal communication), has mapped the N-S system only within 40° of the center of face. When the mapped lineaments are extended to 60° from the center of face it is obvious that those associated with the N-S system are approximately parallel to meridians (See Fig. 5). There are small groups of parallel lineaments in the Taurus Mountains region and southeast of Mare Humorum which deviate from the meridianal directions and would coincide with Fielder's north-south small-circle system (See Map 8). However, the dominant trend in these regions is nearly along the meridians, and therefore the author does not feel that the small groups of lineaments which deviate from this trend are sufficiently numerous to justify their inclusion into a separate system.

(f) NNE-SSW Lunar Lineament System. The NNE-SSW system is less well developed than the other major systems. The lineaments of this system lie on small circles whose planes are at angles of about 15–20° to the moon's axis of rotation. It is difficult to determine the aerial distribution of this system because great-circle N-S lineaments coincide with the direction of NNE-SSW small-circle lineaments in the southeast limb region. There is probably an intermingling of the two systems in this area.

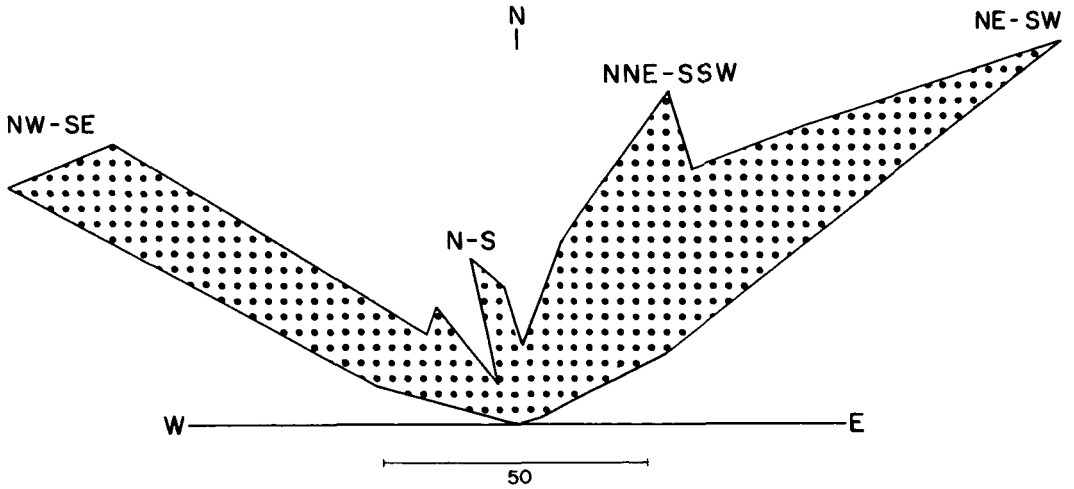
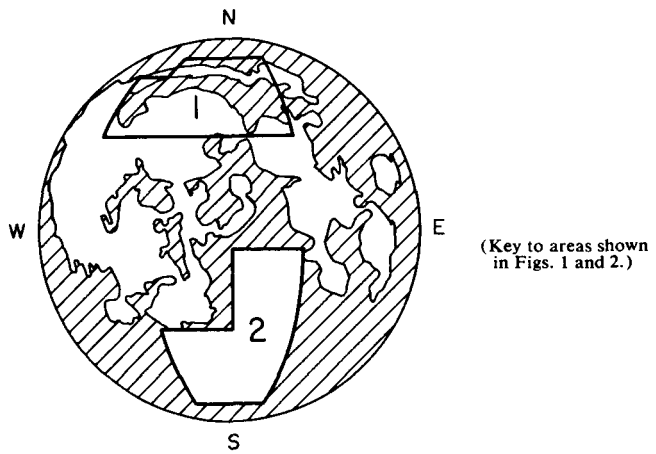


Fig. 1. Azimuth-frequency diagram of lineaments in a portion of the moon's northern hemisphere. The diagram represents the apparent azimuths as viewed in orthographic projection.



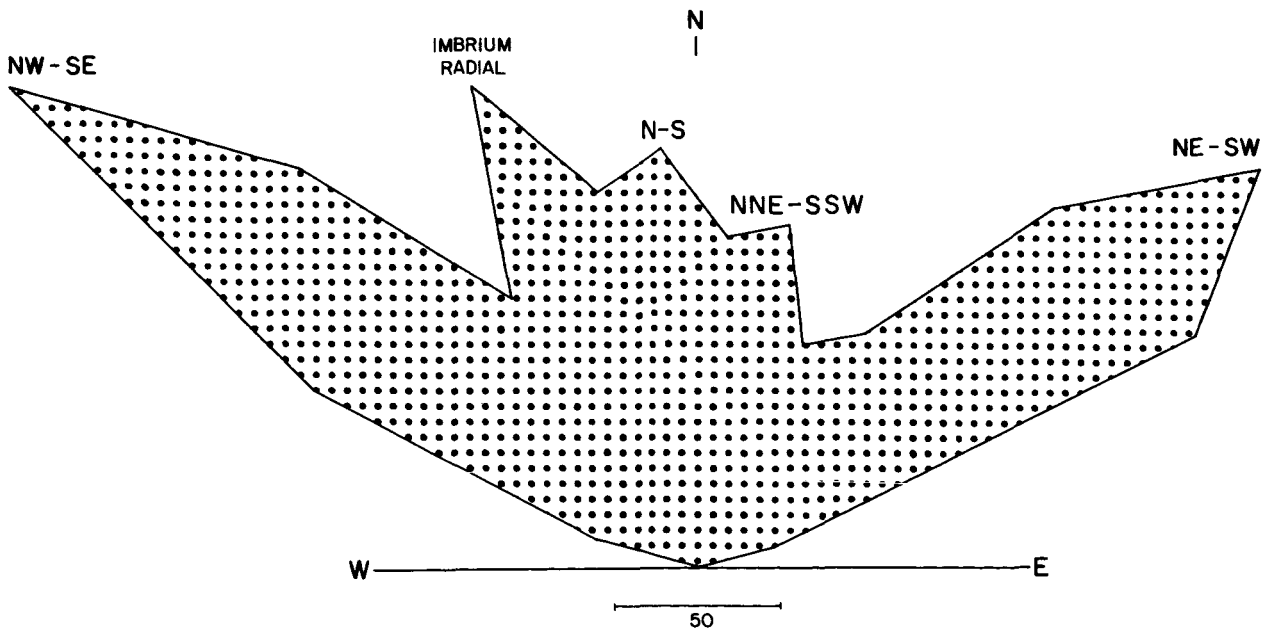


Fig. 2. Azimuth-frequency diagram of lineaments in a portion of the moon's southern hemisphere. The diagram represents the apparent azimuths as viewed in the orthographic projection.

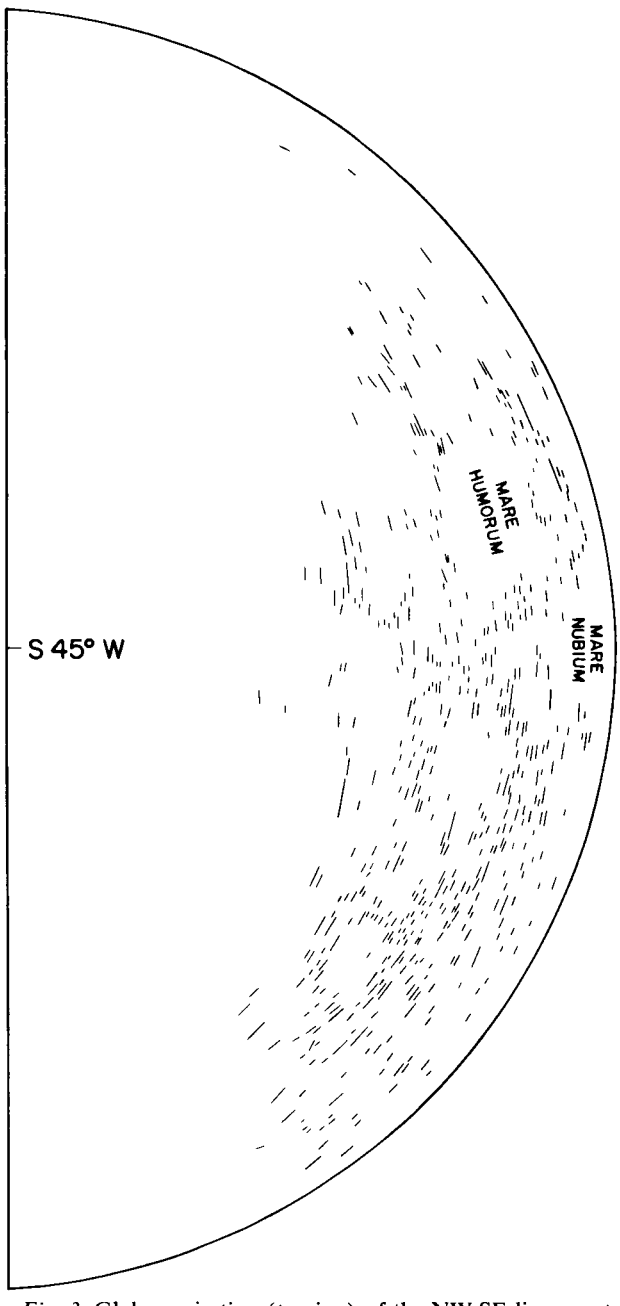


Fig. 3. Globe projection (tracing) of the NW-SE lineament system as seen from directly over its southwestern pole.

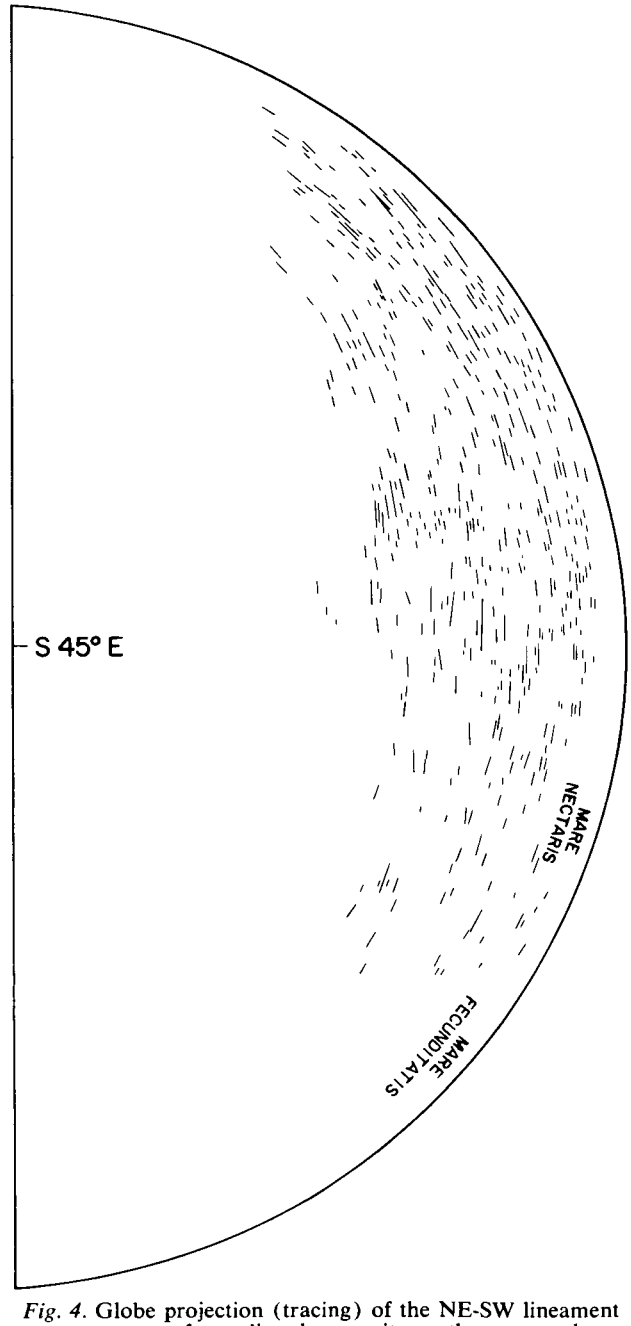


Fig. 4. Globe projection (tracing) of the NE-SW lineament system as seen from directly over its southeastern pole.

This observational difficulty accounts for the lack of NNE-SSW lineaments shown in the southeastern limb region of Map 6.

(g) Composite Map of the NW-SE, NE-SW, and N-S Lunar Lineament Systems. Map 7 is a composite of the three major nonradial lineament systems, and illustrates their spatial relationships. In the orthographic plane, the axes of symmetry of the NW-SE and NE-SW systems are lines situated approximately 45–55° to the east and west of the moon's axis of rotation. The angles of intersection of these systems vary from 90–120° as seen in orthographic projection.

(h) Lunar Lineaments Unrelated to Major Systems. Map 8 is a compilation of all lineaments which do not belong to the major global or radial systems. A comparison of this map with Maps 1A and 1B demonstrates that no more than five percent of the

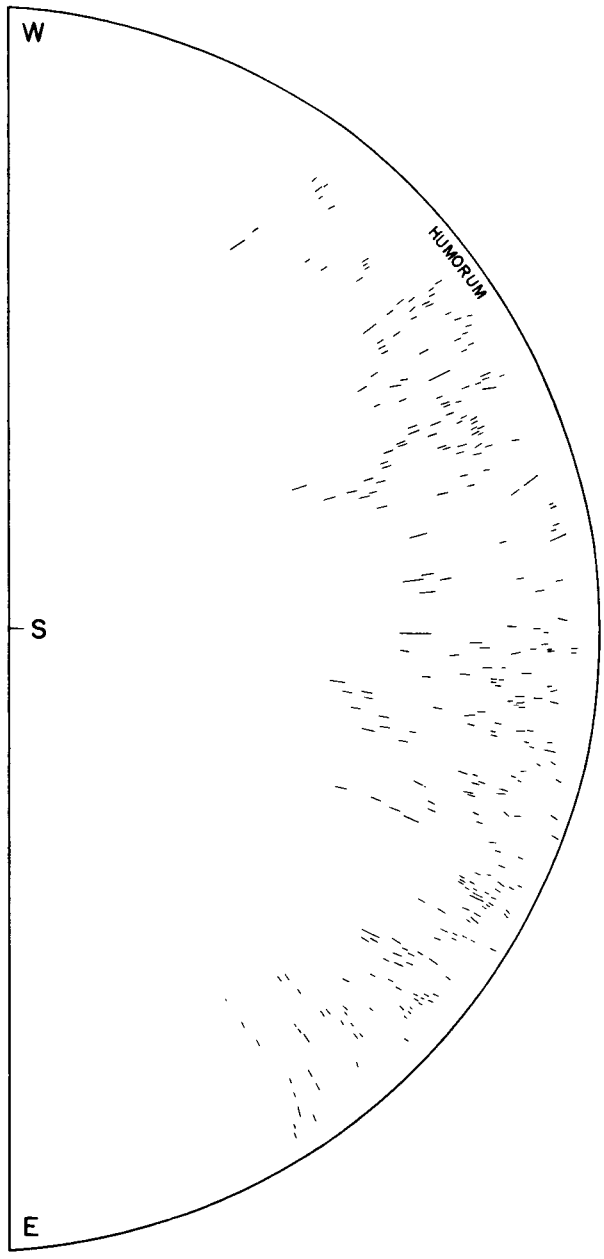


Fig. 5. Globe projection (tracing) of the N-S lineament system as seen from directly over its southern pole.

lineaments are unrelated to the radial or nonradial systems. Nevertheless, many of these occur as groups of parallel lineaments which present fairly extensive trends, such as the NNW-SSE trending lineaments in the vicinity of Mare Nubium. The lineaments depicted on Map 8 are probably fractures which have resulted from local stresses induced by the primary stresses which formed the major lineament systems.

4. Morphological Relationships

A preliminary count of the number of different types of lineaments which occur in the various lineament systems is shown in Table 2. The count is not complete since about 20 percent of the lineaments could not be replotted on the larger base map. However, the sample is large enough to insure that the statistical relationships will hold when the remaining lineaments have been classified.

Of a total of 362 polygonal crater rims, 94 percent coincide with the directions of the radial and nonradial systems. Eight-three percent of the total are coincident with the directions of the four nonradial systems. Only six percent are unrelated to either the radial or global systems. It seems evident from these figures that polygonal crater rims are related to the lineament systems, particularly to the nonradial systems. The polygonal outline of craters is undoubtedly due to the fracture patterns which governed their shape along pre-existing zones of weakness associated with major lineament trends. Many terrestrial calderas, explosion craters, and impact craters exhibit similar polygonal rims. It has been demonstrated that these polygonal rims are the result of pre-existing joint or fracture patterns. Fullmer and Roberts (1963) have studied explosion craters and found "that the parent joint fabric of the rock medium is an important controlling factor, influencing crater shape and the character of the larger ejected fragments." Darling (1948) has observed similar conditions during cratering tests in basalt. He states, "The hardness of the material and the varying joint conditions of basalt contribute greatly to the fluctuations. It can be seen that original horizontal and vertical jointing affected the shape and size of the craters." Meteor Crater, Arizona, is a terrestrial impact crater which also exhibits a polygonal shape. The crater is roughly rectangular in outline, and its shape has been controlled by regional jointing (Shoemaker, 1959).

A total of 43 crater chains has been mapped. Eighty-seven percent of these features coincide with the directions of the radial and nonradial lineament systems. Sixty-nine percent are associated with the four nonradial systems only, and 13 percent are unrelated to any system. These figures suggest that the majority of crater chains are volcanic craters which have arisen along fractures associated with the major lineament systems.

A similar case exists for the linear portions of central peaks. The azimuths of 92 percent of these features, out of a total of 58, correspond to the direc-

tions of the radial and nonradial systems. Seventy percent coincide with the four directions of the nonradial systems, while only eight percent are unrelated to either the radial or nonradial systems. Here, again, is a strong relationship between the central peaks which exhibit linear structures and the major lineament systems. It would appear that the majority of central peaks exhibiting linear structures have risen along fractures associated with the major lineament systems, or, at least, their configuration has been influenced by the regional fracture patterns.

Nectaris, (4) Crisium, (5) Humorum, (6) Humboldtianum.

(b) Mare Nectaris possesses two radial systems. The major system is focused on the inner basin. A minor system is south of the mare only and is centered on the southern edge of the inner basin.

(c) All radial systems have an east-west structural gap in their radial pattern. With the exception of the Imbrium system and the western portion of the Nectaris system, the magnitudes of the gaps are generally 80–90°.

TABLE 2.
MORPHOLOGICAL RELATIONSHIPS

Lineament Systems	Number of Polygonal Crater Rims		Number of Linear Central Peaks		Number of Crater Chains	
	Undifferentiated*	Radial Only	Undifferentiated*	Radial Only	Undifferentiated*	Radial Only
Radial						
Imbrium	37	31	9	8	8	7
Nectaris	23	5	9	4	3	1
Humorum	17	0	4	1	1	0
Crisium	13	5	0	0	0	0
Totals	90	41 (11%)	22	13 (22%)	12	8 (18%)
Nonradial						
NW-SE	108		12		8	
NE-SW	127		7		8	
N-S	53		20		5	
NNE-SSW	13		2		9	
Totals	301 (83%)		41 (70%)		30 (69%)	
Unrelated	20 (6%)		4 (8%)		5 (13%)	
Totals	362		58		43	

*Lineaments coincident with both radial and nonradial systems.

As previously mentioned, the azimuths of certain groups of linear mare ridges conform to the directions of the major lineament systems (see Pls. 1*a*, 1*b*, 2*a*, and 2*b*). The similarity in spatial relationships of the terrae lineaments and the linear mare ridges is too striking to be fortuitous. These linear ridges in the maria have probably resulted from the same stresses which gave rise to the terrae lineaments, indicating that the stresses which produced the lineament patterns were still active — but considerably reduced in magnitude — after the mare flooding had occurred. This should not be interpreted as meaning that *all* mare ridges have resulted from these same forces; they definitely have not. Most of the mare ridges are very sinuous and form a concentric pattern which follows the outline of the mare basin. These concentric mare ridges probably resulted from local forces within the basins.

5. *Summary and Conclusions*

(a) Radial lineament systems are associated with six circular basins; listed in decreasing order of intensity they are: (1) Imbrium, (2) Orientale, (3)

(d) There are four global nonradial systems: (1) NW-SE, (2) NE-SW, (3) N-S, (4) NNE-SSW.

(e) The global systems cross the moon's surface in well-defined directions for thousands of kilometers.

(f) The N-S system nearly lies on great circles and roughly parallels the meridians.

(g) The lineaments of the NE-SW and NW-SE systems nearly coincide with the trend of small circles and therefore are approximately parallel when viewed in orthographic projection.

(h) In the orthographic plane, the axes of symmetry of the NW-SE and NE-SW system are lines situated approximately 45–55° to the east and west of the moon's axis of rotation.

(i) The angles of intersection of the NE-SW and NW-SE systems vary from 90–120°, as seen in orthographic projection.

(j) Both the NE-SW and NW-SE systems contain few lineaments in the limb regions of their equatorial plane.

(k) The majority of polygonal crater rims, linear portions of central peaks, crater chains, and certain

linear mare ridges are preferentially oriented in the same directions as the radial and nonradial lineament systems.

The lineaments of the global nonradial systems cross the moon's surface in well-defined directions for thousands of kilometers, indicating that the forces which produced them were relatively uniform in magnitude and direction (as Anderson, 1951, found for the earth), and affected the entire crust of the moon. This essentially eliminates large meteorite impacts as a source of the stresses which caused the nonradial systems, although minor deviations in the directions of the systems may have resulted from such stresses. It seems conclusive that lunar lineaments are fractures or zones of weakness which were internally produced by tectonic activity.

The genesis of the nonradial lineament systems can be readily explained by compressive stresses in the moon's crust which have acted in a north-south direction (see Fig. 6). It is well known from geological studies that a principal compressive stress acting in the horizontal plane will produce planes of maximum shearing stress which lie at angles of about 45° on either side of the axis of maximum compression (Billings, 1954; de Sitter, 1956). The planes of actual shear do not necessarily coincide with the planes of maximum shearing stress but may be located at angles of 30–55° from the axis of maximum compression. Physical properties of the material and the orientation of the principal stresses are factors which contribute to the deviation in direction between the actual shear and the theoretical maximum stress. Tension fractures will develop at right angles to the least principal stress axis which is perpendicular to the axis of maximum compression (see Fig. 7). Under these considerations the NW-SE and NE-SW lineament systems are probably shear fractures which have formed at angles of 45–55° from north-south axes of maximum compression, and the N-S lineament system consists of tension fractures parallel to these axes.

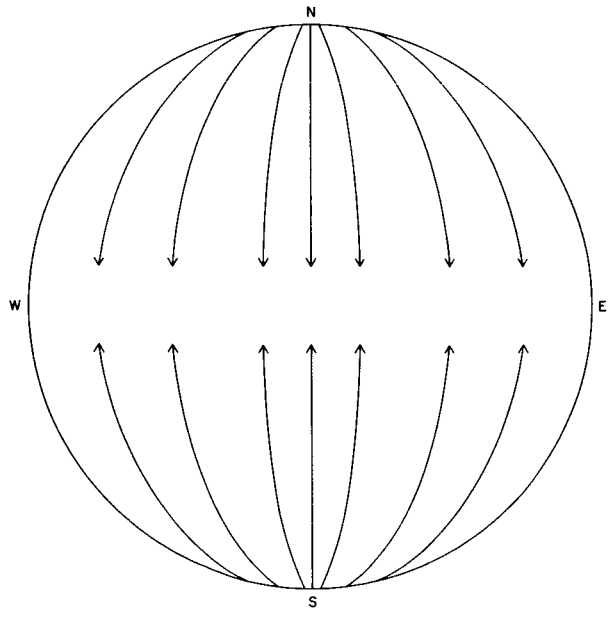


Fig. 6. Probable orientation of crustal stresses which produced the nonradial lineament systems.

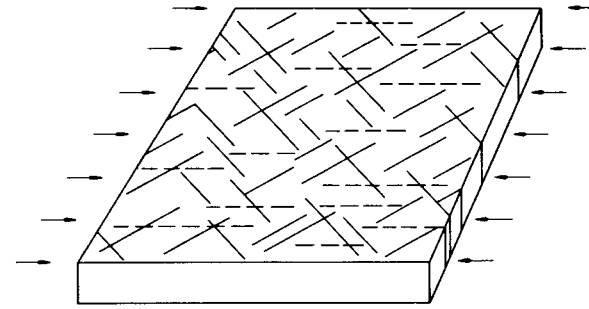


Fig 7. Shear (unbroken lines) and tension (broken lines) fractures produced by horizontal compression.

If this theory is correct then the bisectors of the angles made by the NW-SE and NE-SW systems will be oriented along the directions of the axes of maximum compression and should parallel the directions of the N-S system. Figure 8 is a diagram of the three major nonradial systems as seen from directly above the moon's south pole. The diagram was constructed by projecting the composite lineament map (Map 7) onto a globe and photographing it from directly over the south pole. The lineament directions of each system were smoothed and the bisectors of the angles made by the orthogonal systems (NW-SE and NE-SW) were constructed. The bisectors are represented by arrows in Figure 8 and point to the angles they bisect. They may also be regarded as the axes of maximum compression. It is apparent that the bisectors radiate from the south polar region and nearly parallel the north-south lineament directions. These orientations of the maximum stress axes account for the small-circle trend of the NW-SE and NE-SW lineament systems.

The NNE-SSW lineament system probably consists of second-order shear fractures which have

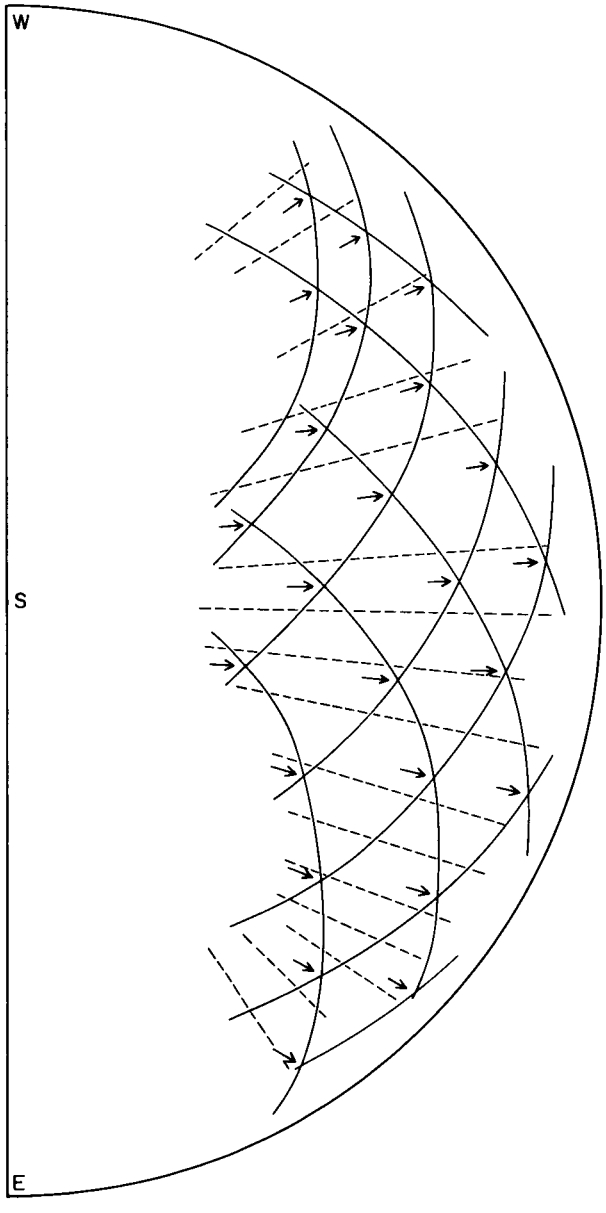


Fig. 8. South polar projection of the lineament systems, showing the smoothed directions of the NW-SE, NE-SW and N-S (dashed lines) systems. The arrows are bisectors of angles formed by the NW-SE and NE-SW systems. They may also be regarded as axes of maximum compression.

resulted from local reorientation of compressive stresses due to inertial, frictional, or body forces involved during movement on the primary shear planes. Second-order features of this nature often accompany primary shear fractures on earth and usually form at angles of 15–30° from the primary shear direction (Moody and Hill, 1956). The NNE-SSW system intersects the NE-SW system at angles of about 30°. One would expect a complementary second-order shear system associated with the NW-SE system. Previous mention was made of a weak NNW-SSE group of lineaments shown on Map 8 in the vicinity of Mare Nubium. This set of lineaments may represent a very weak second-order shear system associated with the primary NW-SE system.

According to theory one might expect a major lineament system consisting of compression fractures or thrust faults which are oriented at right-angles to the axis of maximum compressive stress, or in an east-west direction. However, no east-west lineament system could be found. There are several widely dispersed lineaments oriented in an east-west direction but these are too infrequent and widely disseminated to warrant their inclusion into a lineament system. Three possible explanations may account for the apparent lack of an east-west system. As previously mentioned, east-west oriented lineaments would be difficult to recognize because they parallel the sun's rays and therefore cast little or no shadow. Secondly, these lineaments would presumably consist of compression fractures or thrust faults, and whenever there is a fault scarp marking the edge of a thrust sheet, it is likely to be less imposing and more sinuous and irregular in plan than one associated with a wrench or normal fault. Therefore, this type of feature would be much more difficult to recognize than shear or tension fractures. A third possibility is that compression fractures did not form. It is known from laboratory experiments that compression fractures are usually the last type of fault to form, because the compressive strength of rocks is greater than either their tensile or shearing strengths. Hence, it is possible that all or most of the stresses were dissipated during the formation of the tension and primary and second-order shear fractures. Any remaining stresses may have been insufficient to form thrust faults.

The east-west structural gaps in radial systems are additional evidence strongly suggesting a global north-south compression. As previously stated, the radial systems have probably resulted from tensile stresses concentrically oriented around the mare basins. East and west of the basins this tensile stress would have acted in a north-south direction. However, a north-south oriented compression would counteract the north-south tension and produce a zone of no stress to the east and west of the basins. Therefore, no radial lineaments would form in these regions. The Imbrium system probably has smaller east-west gaps (30–50°) because the forces which formed the system were obviously far greater than

the forces that formed the other radial systems and were able to overcome the north-south compression to a greater degree.

There have been many statements in the literature about the apparent absence of strike-slip movement on the moon. Most of these statements cite the absence of horizontal displacement of crater rims as evidence against wrench faulting. However, Fielder (1963, 1964) has found evidence for strike-slip faulting based on small displacements of crater rims and elliptical craters in the Mare Vaporum region. He cites evidence of horizontal movement along the Capella Fault, Deslandres-Regiomontanus fault, the Alpine Valley, and the Abulfeda crater chain. The amount of offset ranges from maximums of 10–32 km. Also the northern rim of Clavius may be offset as much as 30 km. The sense of movement along these faults is consistent with a medianal compressive stress in the moon's crust, e.g., right-lateral movement along the NW-SE faults and left-lateral movement along the NE-SW faults.

This isolated evidence for strike-slip movement is still not strong enough to definitely prove that extensive wrench faulting has occurred on the moon. The vast majority of lineaments give no indication of the type of movement which may have occurred. However, the faults along which Fielder has found evidence of horizontal displacement are all very long (220–360 km). The majority of lineaments are short (5–40 km), and would be expected to have horizontal offsets of no more than a few kilometers. Such small offsets could hardly be recognized from earth-based photography. If such small offsets occurred on these lineaments the cumulative amount of horizontal displacement would be thousands of kilometers. This may be one reason why there are no major wrench faults comparable to the San Andreas or Great Glen faults. Small increments of strain would have been relieved along a great many small faults rather than great increments of strain being relieved along several large faults.

The north-south compressive stresses to which the moon's crust has been subjected were probably active primarily from the moon's beginnings through the formation of the maria, after which they gradually subsided to the present time. Recent observations of reddish spots near Aristarchus (Greenacre, 1963) and the Kosyrev (1962) observation of emmissions from the central peak of Alphonsus may indicate slight present-day tectonic activity.

The primary problem is to establish a cause of the north-south compression. Fielder (1963) has also concluded that the nonradial lineament systems are the result of a medianal pressure in the moon's crust and favors Runcorn's (1963) hypothesis of convection currents in the lunar mantle as the cause of this pressure. This hypothesis is attractive from a tectonic viewpoint because Runcorn's calculated distribution of horizontal velocity components (Fig. 9) would impart compressive stresses to the moon's crust which would act from the equator toward the north and south poles. However, we have seen that the spatial relationships of the lineaments require the stresses to have been relatively uniform in magnitude and direction. Figure 9 shows that the stresses would be oriented in an east-west direction near the equatorial region and that the speed of the horizontal velocity components, and therefore the magnitude of the stresses, increases toward the north and south poles. This should produce a broad zone of tension in the equatorial region, but to date there is no surface evidence for such a zone of tension. The hypothesis of lunar convection currents is highly speculative and requires much further study before it can be accepted or rejected. This is especially true since terrestrial convection currents are as yet unproven.

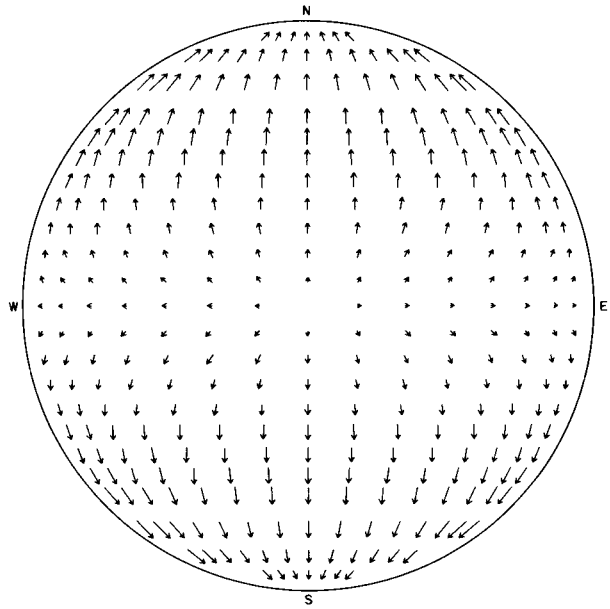


Fig. 9. Distribution of horizontal velocity components produced by Runcorn's hypothetical convection currents in the moon. Lengths of arrows are proportional to flow speeds. (After Runcorn with modifications.)

Other possible causes of a north-south compression are *(a)* the gradual subsidence of the "tidal bulge" as the moon recedes from the earth, *(b)* expansion and contraction of the moon, *(c)* a change in the possible axis of flattening due to a shift of the moon's axis of rotation, and *(d)* lunar body tides due to librations in longitude and latitude, and the changing distance between the earth and moon. All of these factors may have played a part in producing the nonradial lineament systems of the moon. It remains for subsequent investigations to determine which factor was dominant.

Acknowledgments. The author wishes to thank Mr. Ewen Whitaker and Mr. William Hartmann for their verifications of lineaments and their many helpful suggestions. Mr. Paul Masser's help in programming lineament length and azimuth equations for the IBM 7072 computer is also gratefully acknowledged. The work reported here was supported by the National Aeronautics and Space Administration through Grant NsG 161-61.

REFERENCES

Anderson, E. M. 1951, *The Dynamics of Faulting* (Edinburgh: Oliver and Boyd).

Billings, M. P. 1954, *Structural Geology* (New York: Prentice-Hall, Inc.).

Darling, James A. 1948, *Crater Tests in Basalt.* Dept. of Operations and Maintenance, Spec. Eng. Div. Panama Canal Zone, ICS Memo 284-P.

de Sitter, L. U. 1956, *Structural Geology* (New York: McGraw-Hill.).

Fielder, G. 1963 "Lunar Tectonics," *Quart. Jour. Geol. Soc. London, 119,* 65–94.

————. 1963, "Four Major Strike-Slip Faults on the Moon," *Geophys. Journ. of The Roy. Astron. Soc., 8,* 2, 187–195.

————. 1964, "Strike-Slip Faulting in the Vaporum Region of the Moon," *Quart. Jour. Geol. Soc. London, 120,* 275–281.

Fullmer, C. V. and Roberts, W. A. 1963, "Rock Induration and Crater Shape," *Icarus, 2,* 5–6, 452–465.

Greenacre, J. A. 1963, "A Recent Observation of Lunar Color Phenomena," *Sky and Telescope, 26,* 6, 316–317.

Haites, T. B. 1960, "Transcurrent Faults in Western Canada," *Journ. Alberta Soc. Petro. Geologists, 8,* 33–78.

Hartmann, W. K. 1963, "Radial Structures Surrounding Lunar Basins, I: The Imbrium System," *Comm. L.P.L., 2,* 24, 1–15.

————. 1964, "Radial Structures Surrounding Lunar Basins, II: Oriental and Other Systems; Conclusions, *"Comm. L.P.L., 2,* 36, 175.

Hartmann, W. K. and Kuiper, G. P. 1962, "Concentric Structures Surrounding Lunar Basins," *Comm. L.P.L., 1,* 12, pp. 51–66.

Runcorn, S. K. 1963. *The Interior of the Moon,* Jet Propulsion Laboratory, Pasadena, TR 32-529.

Shoemaker, E. M. 1959, *Impact Mechanics of Meteor Crater, Arizona,* Open File Report, U.S. Atomic Energy Comm.

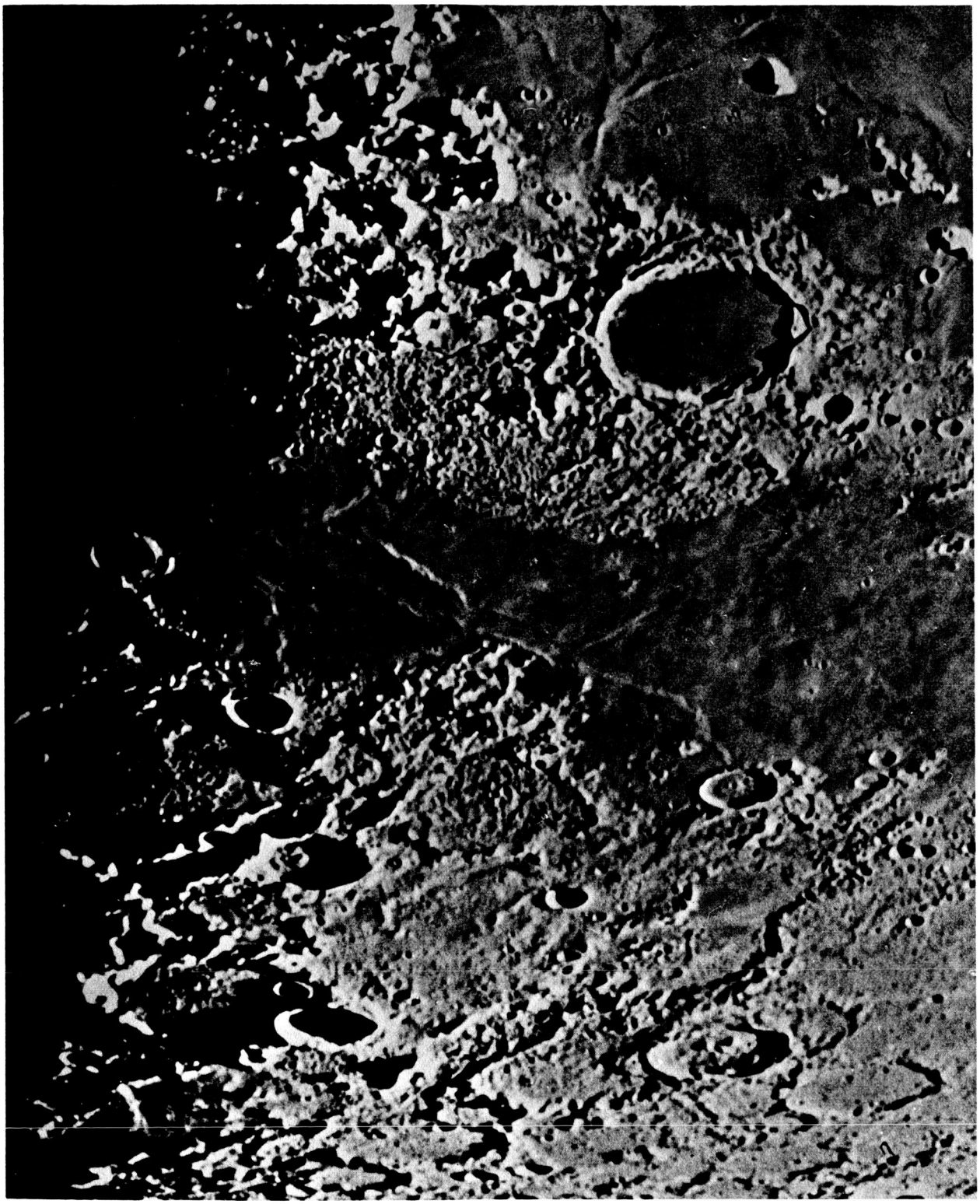


Plate 1a. Linear mare ridges in Mare Frigoris which coincide with the directions of lineaments in the adjacent terrae.

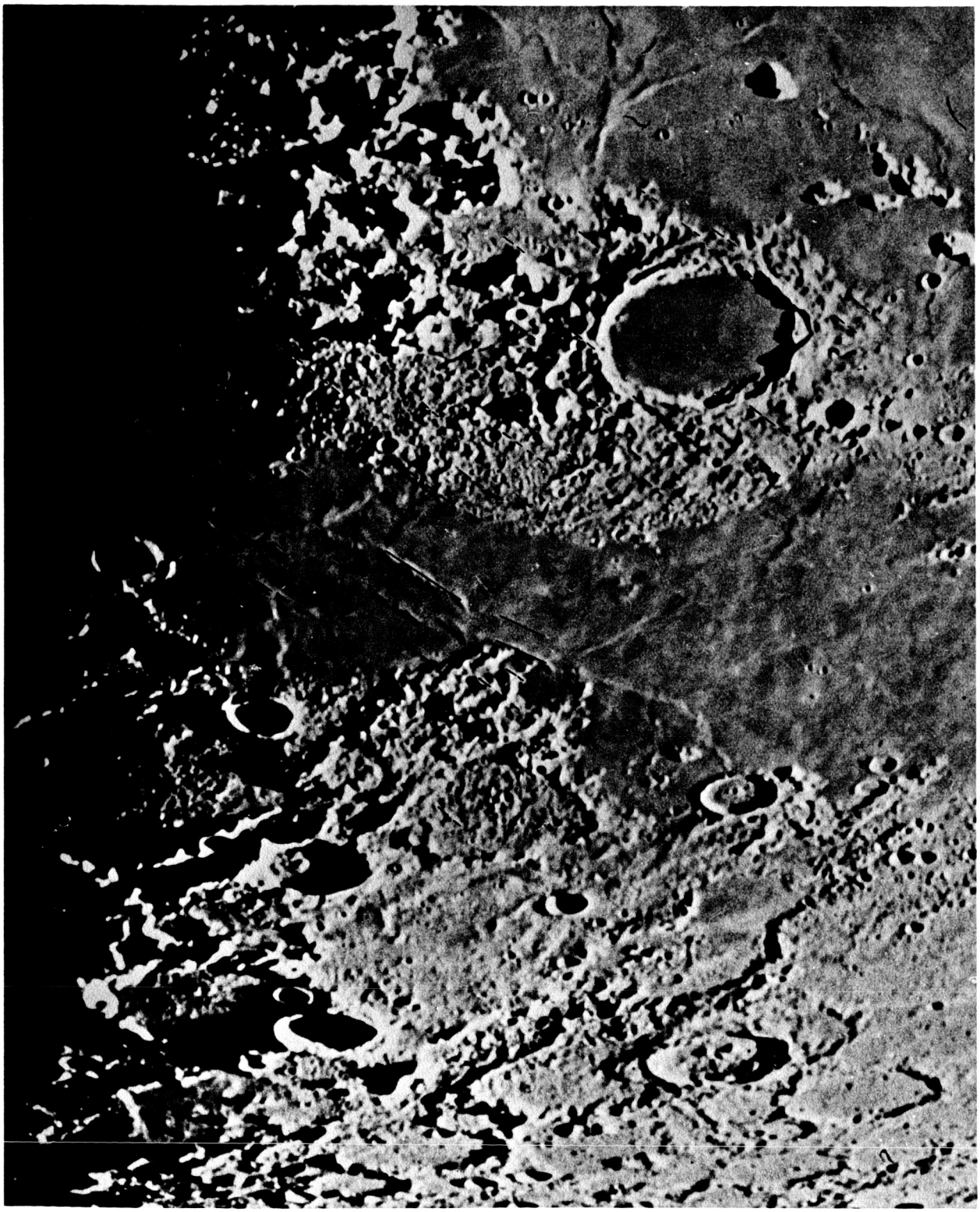


Plate 1b. Same as *1a*, with overlay marking parallelism between ridges and lineaments.

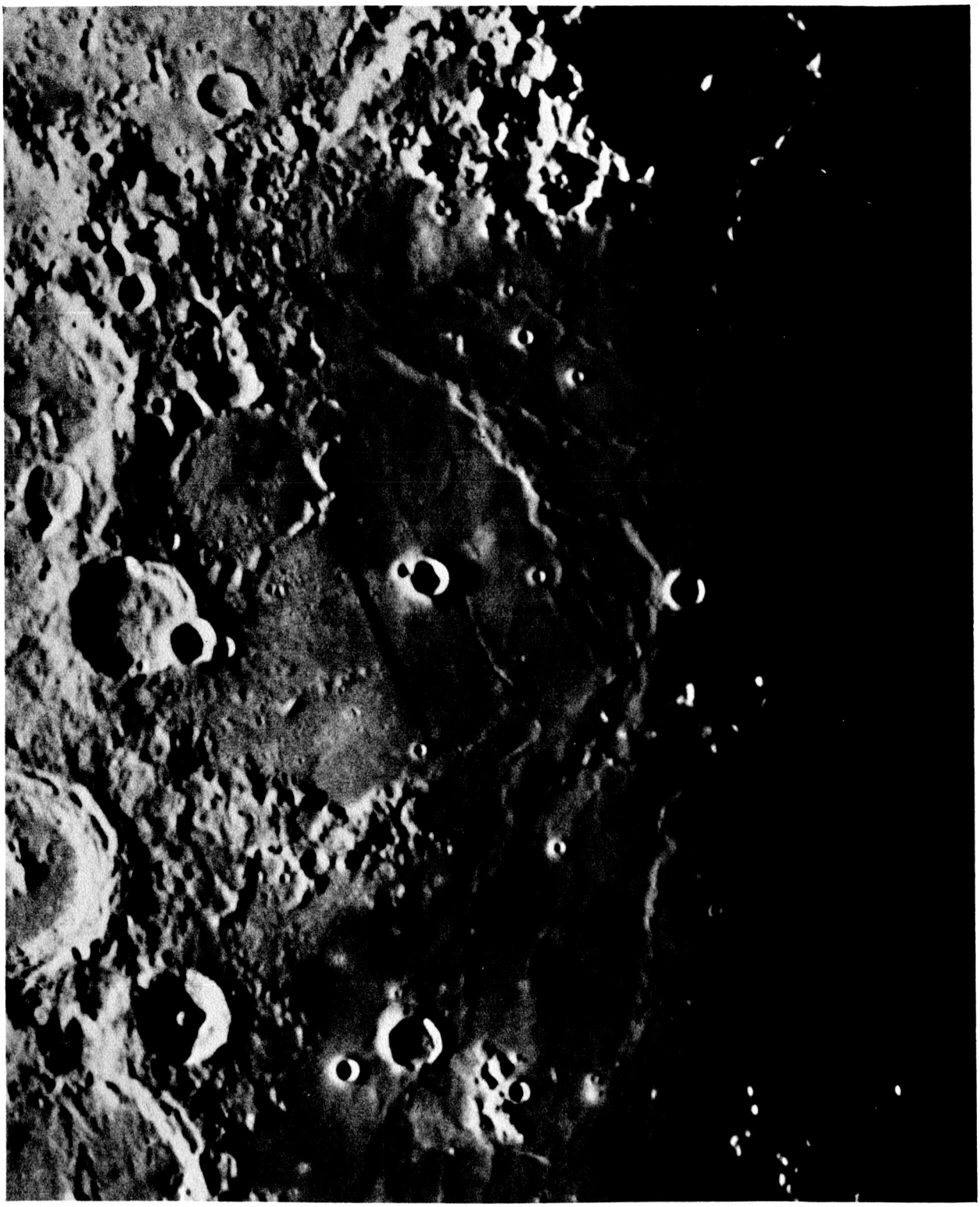


Plate 2a. Linear mare ridges in Mare Nubium which coincide with the direction of lineaments in the adjacent terrae.



Plate 2b. Same as *2a*, with overlay marking parallelism between ridges and lineaments.